Stony Brook University

GATING AND BLOCK MECHANISMS IN AMPA RECEPTORS

A Dissertation Presented

by

Martin Loynaz Prieto

to

The Graduate School

in Partial Fulfillment of the

Requirements

for the Degree of

Doctor of Philosophy

in

Neuroscience

Stony Brook University

December 2009

Stony Brook University

The Graduate School

Martin Loynaz Prieto

We, the dissertation committee for the above candidate for the

Doctor of Philosophy degree, hereby recommend

acceptance of this dissertation.

Lonnie P. Wollmuth – Dissertation Advisor

Professor, Department of Neurobiology and Behavior

Gary G. Matthews – Chairperson of Defense

Professor, Department of Neurobiology and Behavior

Peter R. Brink

Professor, Department of Physiology and Biophysics

James P. Dilger

Professor, Department of Anesthesiology

This dissertation is accepted by the Graduate School

Lawrence Martin

Dean of the Graduate School

Abstract of the Dissertation

GATING AND BLOCK MECHANISMS IN AMPA RECEPTORS

by

Martin Loynaz Prieto

Doctor of Philosophy

in

Neuroscience

Stony Brook University

2009

AMPA receptors are ligand-gated ion channels that mediate excitatory synaptic transmission throughout the central nervous system. Two mechanisms regulating the activity of AMPA receptors are state-dependent channel block by intracellular polyamines and subunit-independent gating.

Polyamine block of Ca^{2+}-permeable AMPA receptors is state-dependent, resulting in activity-dependent synaptic facilitation. To understand the mechanism of this phenomenon, I studied the dependence of the kinetics of spermine block on the state of the channel, and on neutralization of a negatively charged aspartate residue (D590) in the pore loop, using macroscopic current recording. In open channels, the kinetics of spermine dissociation were the same for internally and externally applied spermine, and charge neutralization decreased the rate of dissociation to the internal solution and increased the rate of dissociation to the external solution in a manner consistent with a D590 acting through a surface charge mechanism. In closed channels, charge neutralization increased the rate of dissociation to either solution. Based on these results, I propose that channel gating involves a reorientation of D590, such that its carboxyl group influences polyamine dissociation through a strictly electrostatic mechanism in open channels, but interacts directly with polyamines bound to closed channels.

AMPA receptors show multiple conductance levels, indicating that gating of individual AMPA receptor subunits is to some extent independent of the other subunits. To study AMPA receptor subunit interactions during activation gating, I recorded from single channels in the absence of channel block and desensitization at negative and positive membrane potentials. In saturating glutamate, the relative occupancies of the various conductance levels were consistent with complete subunit independence. In contrast, the relative occupancies in subsaturating glutamate indicate that the channel switches between a low-affinity gating mode and a high-affinity gating mode in which the subunit open probability is equal to that in saturating glutamate. These gating modes occur at both negative and positive potentials, with the high-affinity mode becoming more prominent at positive potentials. The switch between low- and high-affinity modes,

and its modulation by voltage and other factors, may constitute a novel mechanism regulating AMPA receptor mediated synaptic activity.

TABLE OF CONTENTS

LIST OF FIGURES

LIST OF TABLES

LIST OF EQUATIONS

GATING AND BLOCK MECHANISMS IN AMPA RECEPTORS

CHAPTER 1: GENERAL INTRODUCTION

Ion channels are molecular pores made of protein that allow ions to cross the otherwise impermeable phospholipid membranes of cells, and ionic currents through these pores are the source of all biological electrical activity, in the brain and elsewhere. This class of proteins has been the subject of intense experimental investigation by physiologists for many years. Ion channel physiologists speak of "studying the structure and function of ion channels" or "performing structure/function studies." Although neuroscientists with other specializations recognize that ion channels are central to all aspects of neuroscience, they sometimes seem to consider structure/function studies an esoteric corner of the field. This is unnecessary because the goals of ion channel physiologists studying structure and function are the same as those of other neuroscientists, and indeed of all biologists. In general, biologists have limited information about the structure and function of the extraordinarily complex living systems that they study, and they attempt to develop insight into the relationship between structure and function based on this information. In other words they attempt to say something about "how the system works." In doing so, they develop models that are inevitably incredibly simplified but hopefully are a valid representation of some important aspect of the system under consideration.

In studying ion channels, it is helpful to view structure and function not as distinct categories of information but as intertwined aspects of a single concept—thus, "structure/function." In the era of molecular cloning, amino acid sequences are available for almost all intensely studied proteins, so the goal of structure/function studies is

sometimes conceptualized as "determining how the amino acid sequence of a protein (i.e., its structure) allows it to perform its function." The detailed molecular structures of certain ion channels provided by X-ray crystallography and other high-resolution techniques also encourage the view that function is mapped onto structure. Throughout most of the history of the scientific investigation of ion channels, however, "structural" information actually consisted of inferences drawn from input-output relations—in other words, from functional information. For example, the dependence of ionic flux and conductance in the squid giant axon on K^+ concentration led to the conclusion that K^+ ions cross the membrane through a narrow pore in single file, and that this pore is long enough to contain four ions simultaneously (Hodgkin and Keynes, 1955; Hille and Schwarz, 1978). Many years later, precisely this type of pore was seen in the crystal structure of the KcsA K^+ channel (Doyle et al., 1998).

I have studied the structure and function of one particular ion channel, the AMPA receptor channel. As stated above, the goal of structure/function studies of ion channels is to develop a model of certain aspects of the channel based on limited information regarding its structure and function. In what way is our knowledge of AMPA receptors limited? Knowledge of the function of AMPA receptors is limited in the sense that they function in the context of an incredibly complex living system, the brain. The activity of AMPA receptors ultimately contributes to such phenomena as vision, learning and memory, and according to materialist theories of mind, the entirety of the thoughts, experience, and personality of an individual. Clearly, our understanding of how AMPA receptors "function" in this context is extremely limited. On a somewhat less grandiose level, the function of AMPA receptors is to regulate the flow of ionic current in response

to release of the neurotransmitter glutamate at a synapse. Even at this level, AMPA receptors are part of an immensely complicated structure known as the postsynaptic density consisting of hundreds of closely associated proteins (Sheng and Hoogenraad, 2007). Structure/function studies of AMPA receptors in heterologous expression systems obviously cannot replicate this complex synaptic environment, so the behavior of AMPA receptors in these systems may differ from their behavior at synapses. For example, the recent discovery that the interaction of AMPA receptors with the postsynaptic density protein stargazin alters many of their functional properties (Priel et al., 2005; Tomita et al., 2005) has caused much excitement and consternation among physiologists studying these receptors. Rather than attempting to describe the precise functioning of AMPA receptors in the context of the postsynaptic density, it is therefore preferable to sharpen our focus further still and subdivide the function of AMPA receptors into two general tasks: the binding of glutamate, and the regulation of ionic current. These two functions are associated with distinct structural modules of the protein, the ligand-binding domain and the ion channel. Our knowledge of the structure of AMPA receptors is limited by the fact that, at the time of this writing, there are no high-resolution molecular structures of the intact AMPA receptor. Nonetheless there is a great deal of information on the structure of AMPA receptors derived from functional studies, as well as crystal structures of the isolated ligand-binding domain.

STRUCTURE AND FUNCTION OF AMPA RECEPTORS

General structure.

AMPA receptors are tetramers of structurally similar subunits. There are four different subunit types, known as GluA1, -2, -3, and -4 (Collingridge et al., 2009). Physiologically, AMPA receptors are generally heterotetramers containing two each of two different subunit types, but homotetramers can assemble and are functional in heterologous expression systems. The tertiary structure of an AMPA receptor subunit is illustrated in Figure 1.1. Each subunit has three α-helical transmembrane segments, known as M1, M3, and M4, and a partially α-helical segment, known as the M2 loop or the pore loop, that enters and exits the membrane from the intracellular side. Additionally, there are extensive extracellular regions of partly α-helical and partly irregular secondary structure at the amino-terminus of the subunit and between the M3 and M4 segments, as well as shorter intracellular regions of irregular secondary structure at the C-terminus and linking M2 with M1 and M3.

The ligand-binding domain.

The ligand-binding domain is formed by part of the amino-terminus proximal to M1, known as S1, and by part of the region linking M3 and M4, known as S2 (Figure 1.1). Thus AMPA receptors have four glutamate binding sites, one for each subunit. Molecular structures of the ligand-binding domain in glutamate-bound and unbound states have been obtained from X-ray crystallography of an artificial soluble protein consisting of the S1 and S2 domains separated from the ion channel and linked by a series of glycine residues (Armstrong and Gouaux, 2000) (for a review see Mayer, 2006). The ligand- →

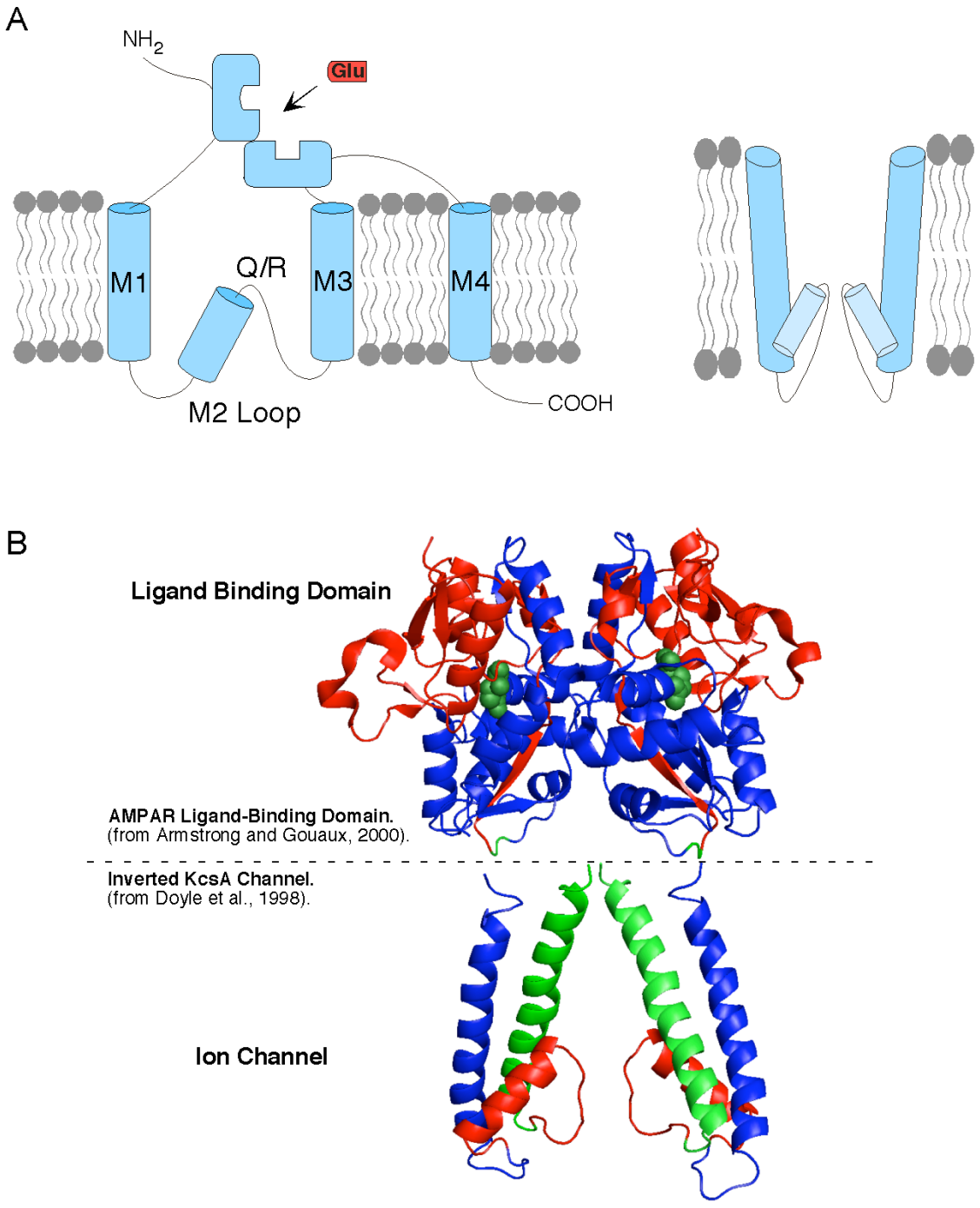

Figure 1.1. Models of AMPA receptor structure.

(A) Cartoon models of AMPA receptor structure. *Left:* Transmembrane topology of an individual AMPA receptor subunit. *Right:* Side view of two pairs of pore-forming domains. **(B)** Molecular models of AMPA receptor structure. *Top:* Crystal structure of an AMPA receptor ligand-binding domain dimer. S1 is in blue and S2 in red, with glutamate and the artificial linker region in green. *Bottom:* Inverted KcsA K^+ channel, representing the approximate structure of AMPA receptor pores. Two subunits are shown. M1 is in blue, M2 in red, and M3 in green.

→binding domain is made of two distinct lobes forming a structure that some have compared to a clamshell or Venus's fly-trap. These two lobes are not to be confused with the S1 and S2 domains; different parts of S1 and S2 contribute to both lobes. Glutamate binds inside the cleft between the lobes, causing the clamshell to "close," and subsequently inducing conformational changes in the ion channel. The upper lobe of each ligand-binding domain dimerizes with that of an adjacent ligand-binding domain, so the mobility of the upper lobes is limited and closing of the clamshell consists mainly of movement of the lower lobe. Glutamate binding destabilizes the upper lobe dimers, leading to de-dimerization, which is coupled to entry of the ion channel into a long-lived non-conducting state, a process known as desensitizaiton (Sun et al., 2002). A point mutation in the dimer interface strengthens the interaction between upper lobe pairs, preventing desensitization (Stern-Bach et al., 1998; Partin, 2001), as does the drug cyclothiazide, which binds at the dimer interface (Sun et al., 2002; Jin et al., 2005).

The ion channel.

The three transmembrane segements and the M2 loop form the ion channel. The four subunits are arranged around the axis of an aqueous pore, with M2 and M3 forming the pore walls. The pore consists of two wide vestibules on either side of a narrow region known as the selectivity filter, with M3 forming the walls of the external vestibule and M2 forming the walls of the internal vestibule and the selectivity filter (Wollmuth and Sobolevsky, 2004). The selectivity filter is, by definition, the region of the pore where ions interact most directly with the channel and as such is the primary determinant of the channel's ion selectivity and permeability. AMPA receptors are selective for cations over

anions, but are not selective among monovalent cations, and are also permeable to many large organic cations. The permeability of AMPA receptors to large cations indicates that the diameter of the selectivity filter is no smaller than ~0.78 nm (Burnashev et al., 1996). The permeation properties of AMPA receptor channels are strongly influenced by the residue at a position in the selectivity filter known as the Q/R site. All AMPA receptor subtypes except GluA2 have glutamine at this position; RNA editing substitutes arginine for glutamine in GluA2 subunits in physiological situations (Sommer et al., 1991). Channels lacking the edited GluA2 subunit are permeable to Ca^{2+}, with the permeability of Ca^{2+} approximately equal to that of monovalent ions (Burnashev et al., 1992; Burnashev et al., 1995), and are blocked by intracellular polyamines in a voltage-dependent manner (Bowie and Mayer, 1995). The conductance of AMPA receptor ion channels is highly variable but is small relative to most other ion channels: ~10-30 pS for Ca^{2+}-permeable channels, and less than 1 pS for Ca^{2+}-impermeable channels (Smith et al., 2000).

The AMPA receptor ion channel is able to switch between conducting (open) and non-conducting (closed or desensitized) conformations. The nature of the structure that controls the flow of ionic current, known as the activation gate, is controversial. Various lines of evidence suggest that the activation gate is formed either by the M3 helices at the external entrance to the pore (Antonov et al., 1995; Blanpied et al., 1997; Qian and Johnson, 2002; Chang and Kuo, 2008), or by the selectivity filter (Sobolevsky et al., 2002; Sobolevsky et al., 2003; Wollmuth and Sobolevsky, 2004).

Coupling of ligand binding and channel gating.

Structural changes in the ligand-binding domain induced by glutamate binding must somehow be coupled to the switch between conducting and non-conducting conformations of the ion channel. The mechanisms coupling ligand-binding domain closure to channel opening, and ligand-binding domain de-dimerization to channel desensitization, are unknown, but probably involve the region linking M3 and S2.

KINETIC MODELS OF AMPA RECEPTORS

A common technique in ion channel physiology is the use of Markov chain kinetic models, in which the behavior of ion channels is described by discrete transitions between states. The parameters of kinetic models are the conductances of the various states and a set of rate constants describing the probability, per unit time, of all possible transitions between pairs of states (Colquhoun and Hawkes, 1995b). These parameters can be used to fit the time course of macroscopic currents, or distributions of the conductances and open and closed event lifetimes of microscopic (single channel) currents (Colquhoun and Hawkes, 1995a).

The development of accurate kinetic models of AMPA receptors is essential to understanding the function of synapses and designing effective therapeutic drugs that target these receptors. The simplest kinetic model of AMPA receptors that provides a useful description of their function is Model 1 in Figure 1.2. The model has only four states: an agonist unbound closed state (C), an agonist bound closed state (CA), an agonist bound open state (O), and an agonist bound non-conducting desensitized state (D). Model 1 is obviously simplified because four glutamate binding steps are condensed into a single step, but it is useful because it describes the behavior of AMPA receptors in response to certain experimental manipulations. According to the model, the channel can transition to either the open or desensitized state from the agonist-bound closed state, but the rate constant for the closed to open transition is much faster than the rate constant for the closed to desensitized transition (Raman and Trussell, 1995a). Thus in response to a brief (<1 ms) pulse of saturating glutamate, AMPA receptors will not desensitize significantly. In the continuous presence of glutamate, however, channels will, on →

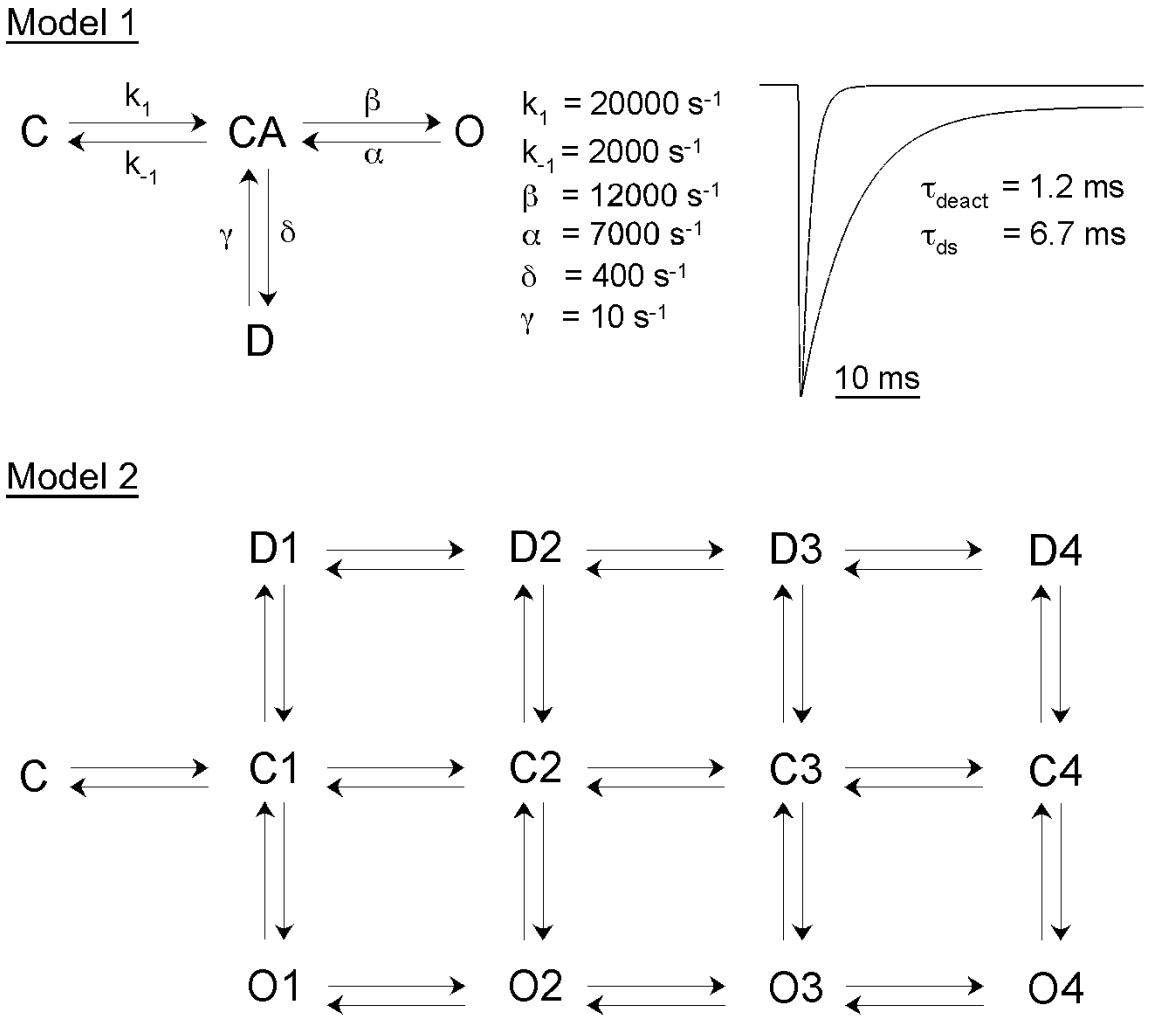

Figure 1.2. Kinetic models of AMPA receptor function.

Model 1: Simplified model of AMPA receptor function. The rate constants listed reproduce the approximate macroscopic response of AMPA receptors to saturating concentrations of glutamate. The current traces are simulated responses to 0.5 ms and continuous applications of saturating glutamate. The macroscopic time constants of deactivation (τ_{deact}) for the 0.5 ms application and desensitization (τ_{ds}) for the continuous application are listed below the current traces. **Model 2:** A more elaborate model of AMPA receptor function. The numbers to the right of the states labeled O, C, and D correspond to the number of agonist-bound subunits. The model is not quantified but illustrates the level of complexity necessary to describe macroscopic responses to a wide range of glutamate concentrations.

→average, cycle back and forth between the open and closed state several times before eventually entering the desensitized state. The rate of transition out of the desensitized state is slow relative to the rate of transition into it, so most channels will be desensitized at steady-state in the presence of saturating glutamate. This model predicts that drugs that increase the stability of the open state relative to closed agonist-bound state (increasing the ratio β/α) will slow the macroscopic time course of desensitization, without actually altering the rate constants for entry into or exit from the desensitized state. This is thought to be the mechanism of the desensitization-blocking drug cyclothiazide (Partin et al., 1996).

As seen in Model 2 in Figure 1.2, kinetic models of AMPA receptors require many additional states if the behavior of individual subunits is explicitly included in the model. The individual subunits of the channel can transition from closed to open conformations in a manner at least to some extent independent of the conformation of the other subunits. The channel conductance is determined by the number of subunits in the open conformation, such that AMPA receptors have up to four open channel conductance levels associated with partial gating of the channel (Rosenmund et al., 1998; Smith and Howe, 2000), as represented by the O1, O2, O3, and O4 states in Model 2. The number of occupied glutamate binding sites determines the probability that a ligand-binding domain pair will de-dimerize, so the rate of transition from the open state O1 to the desensitized state D1 is slower than the rate of transition from O4 to D4. Kinetic models as elaborate as Model 2 or even more so are necessary to accurately describe the behavior of AMPA receptors in response to a wide range of glutamate concentrations (e.g., Robert and Howe, 2003).

Concerted versus independent subunit gating.

Historically, conformational transitions in the individual subunits of multimeric proteins have been described by either concerted or independent models of subunit gating. In concerted models, all of the subunits in the protein must change conformation simultaneously (Figure 1.3 *A*). In independent models, subunits can change conformation individually, and the rate constants for conformational transitions in individual subunits are not influenced by the conformation of the other subunits (Figure 1.3 *B*). Intermediate between these two paradigms are models with subunit interactions, in which subunits can change conformation individually, but transitions in one subunit change the rate constants for transitions in the other subunits. In fact, concerted and independent gating can be seen as two extremes at either end of a continuum of varying degrees of subunit interactivity. If an initial transition in one subunit increases the rate constants for the same transition in the remaining subunits by several orders of magnitude, subunit gating will appear concerted unless temporal resolution is extremely high. For example, K^+ channel subunits are usually regarded as gating in a concerted manner, but very brief events of intermediate conductance can occasionally be seen at the start of K^+ openings (Chapman and VanDongen, 2005). Similarly, if transitions in each subunit change the rate constants for transitions in the remaining subunits by small amounts, subunit gating will appear to be independent unless the rate constants are measured very accurately.

Models with completely independent subunit gating can accurately describe many aspects of AMPA receptor behavior (Rosenmund et al., 1998; Jin et al., 2003; Robert and Howe, 2003). However, I will demonstrate in Chapter 4 that there are actually significant interactions between AMPA receptor subunits.

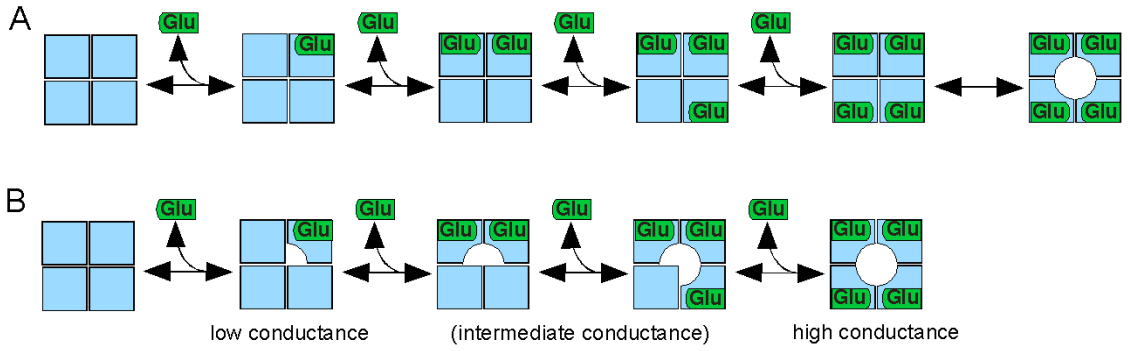

Figure 1.3. Concerted, independent, and interactive ion channel gating.

(A) Cartoon illustrating concerted subunit gating in a hypothetical glutamate-activated channel. **(B)** Cartoon illustrating independent or interactive subunit gating. The intermediate glutamate binding steps are not included in the illustration. For independent subunit gating, the rate constants for the binding and gating steps in each subunit are independent of the binding site occupancy or ion channel conformation of the other subunits.

RELATIVES OF AMPA RECEPTORS

The glutamate receptor family.

Glutamate and GABA are the major neurotransmitters in the mammalian brain. Other neurotransmitters, such as dopamine and serotonin, are selectively involved in well characterized neural circuits with specialized function (Kandel et al., 2000), but glutamate and GABA are the "workhorses" among neurotransmitters, with glutamate responsible for most excitatory (depolarizing) and GABA responsible for most inhibitory (hyperpolarizing) synaptic transmission. Glutamate activates three major classes of ionotropic receptors, known as the glutamate receptor ion channels, as well the otherwise unrelated metabotropic glutamate receptors. All glutamate receptor ion channels are tetramers with the general structure shown in Figure 1.1.

The three members of the glutamate receptor family, named after the agonists with which they were originally distinguished pharmacologically, are: N-methyl-D-aspartate receptors (NMDA receptors), α-amino-3-hydroxy-5-methyl-4-isoxazole propionate receptors (AMPA receptors), and kainate receptors (kainate receptors) (Dingledine et al., 1999). NMDA receptors and AMPA receptors are found on the postsynaptic membranes of most excitatory synapses, while kainate receptors are found on the membranes of presynatic terminals. The function of presynaptic kainate receptors is not well understood. AMPA receptors and kainate receptors are much more similar to one another than they are to NMDA receptors, in terms of both amino acid sequence and functional properties, so they are referred to collectively as non-NMDA receptors. Glutamate receptors vary considerably in their affinity for glutamate, kinetic behavior, and other properties:

1. NMDA receptors require the binding of the co-agonist glycine, in addition to glutamate, to activate. NMDA receptors are heteromers composed of two GluN1 subunits, which bind glycine, and two GluN2 or two GluN3 subunits, which bind glutamate and may be any of several subtypes, either GluN2A, -B, -C, and –D, or GluN3A and -B. Their affinity for glutamate, as measured by the EC_{50} in the presence of saturating glycine, is ~1 μM. NMDA receptors are highly Ca^{2+} permeable (Ca^{2+} permeability ~3-4 times that of monovalent cations), but are blocked by extracellular Mg^{2+} in a voltage-dependent manner. They activate and deactivate slowly, show weak desensitization, and have high conductance (~50 pS), relative to non-NMDA receptors.

2. AMPA receptors have intermediate affinity for glutamate, with an EC_{50} of ~500 μM. As discussed above, they may be Ca^{2+}-permeable or impermeable, and if Ca^{2+}-permeable, are blocked by intracellular polyamines in a voltage-dependent manner. They activate and deactivate rapidly and show strong desensitization, relative to NMDA receptors.

3. Kainate receptors can be homomers or heteromers of GluK1, -2, or -3 subunits, and may also contain GluK4 or -5 subunits, which do not form functional channels on their own. They have intermediate to low affinity for glutamate (EC_{50} ranges from ~0.5 to 5 mM), depending on subunit composition. Their kinetics and conductance vary significantly with subunit composition, but are generally comparable to those of AMPA receptors.

The P-loop channels.

Glutamate receptors are part of a large family of structurally homologous ion channels, known as the pore-loop, or P-loop, channels. The P-loop channel family is functionally diverse and includes the cation selective K^+, Na^+, Ca^{2+} channels and the cation non-selective cyclic-nucleotide-gated (CNG) and transient receptor potential (TRP) channels, among others (Catterall, 2000; Yellen, 2002; Matulef and Zagotta, 2003; Venkatachalam and Montell, 2007). All P-loop channels are tetrameric ion channels characterized by reentrant loops (pore loops) structurally homologous to the M2 segment loop of AMPA receptors. Interestingly, glutamate receptors are inverted within the membrane relative to other P-loop channels, since all other members of the family have pore loops entering and exiting the membrane from the extracellular rather than the intracellular side. The pores of P-loop channels are formed by the pore loop and an adjacent transmembrane segment (homologous to M3 in AMPA receptors). Only one additional transmembrane segment seems to be necessary to form functional channels, since the KcsA K^+ channel is functional with just a pore loop and two transmembrane domains, but most family members have additional functional elements that regulate channel function in response to stimuli such as membrane voltage, ligand binding, and temperature. Despite this diversity of regulatory elements, mechanisms of gating may be conserved at the level of the ion channel itself.

AMPA RECEPTORS IN SYNAPTIC PHYSIOLOGY

A typical glutamatergic synapse contains AMPA receptors and NMDA receptors in combination with various auxiliary proteins. The auxiliary proteins form a dense, cytoskeleton-associated intracellular matrix that is thought to stabilize glutamate receptors at the synapse. Among other auxiliary proteins, synaptic AMPA receptors may be associated with transmembrane AMPA receptor regulatory proteins (TARPs), which in addition to regulating trafficking of AMPA receptors can also alter their kinetics, conductance and other properties (e.g., Priel et al., 2005; Tomita et al., 2005). In addition to synaptic receptors, there are substantial numbers of extra-synaptic AMPA receptors found on dendrites adjacent to synapses, and in clusters of intracellular vesicles associated with synapses. The number of AMPA receptors at the synapse is dynamic and highly regulated, with constant exchange between extra-synaptic, synaptic, and intracellular vesicle populations (Derkach et al., 2007). Extrasynaptic AMPA receptors are highly mobile, but mobility is reduced at synapses, presumably due to interactions with intracellular matrix proteins (Ehlers et al., 2007).

Various mechanisms regulate the amplitude of the response to presynaptic glutamate release, referred to as synaptic strength (Citri and Malenka, 2008). Changes in synaptic strength are categorized as either short-term or long-term plasticity, depending on the duration of the change, with short-term plasticity encompassing changes lasting from milliseconds to minutes and long-term plasticity encompassing changes lasting from hours to days. Long-term plasticity is primarily dependent on NMDA receptor activity. At resting membrane potentials (approximately –80 mV) NMDA receptors are blocked by extracellular Mg^{2+} and therefore unresponsive to glutamate release. AMPA receptors

are active at resting potential and current flowing through AMPA receptor channels in response to glutamate release depolarizes the membrane. Activation of AMPA receptors at multiple synapses can depolarize the membrane beyond the threshold for action potential initiation, activating voltage-gated Na^+ channels and causing the cell to rapidly depolarize towards the Nernst potential for Na^+ (~ +60 mV) and thereby relieving NMDA receptors of Mg^{2+} block (Mayer et al., 1984; Nowak et al., 1984). This creates a brief window in which NMDA receptors are available to be activated by glutamate release. Thus activation of NMDA receptors depends on coincident action potentials in presynaptic (in order to trigger glutamate release) and postsynaptic (in order to relieve NMDA receptors of Mg^{2+} block) cells. Ca^{2+} influx through NMDA receptors triggers a series of intracellular events that culminates in the addition of AMPA receptors to the postsynaptic membrane, strengthening the AMPA receptor-mediated synaptic response. This NMDA receptor-dependent increase in synaptic strength is widely believed to be the mechanism of associative learning (Citri and Malenka, 2008).

An interesting variation on the theme of LTP is the concept of "silent synapses" (Liao et al., 1995). Some synapses have only NMDA receptors and are therefore "silent" at resting membrane potential because of Mg^{2+} block. Activity at AMPA receptor-containing synapses of the same neuron can initiate action potentials, allowing Ca^{2+} influx through NMDA receptors at silent synapses, thereby causing insertion of AMPA receptors into the membrane and "unsilencing" the synapse.

Ca^{2+} influx through NMDA receptors also leads to long-term depression (LTD) of glutamatergic synapses. The mechanisms determining whether the response to NMDA receptor-mediated Ca^{2+} influx is potentiating or depressing are complex, but the

difference is thought to depend on the location and subtype of the NMDA receptors, and the timing of the postsynaptic action potential relative to synaptic activity (Sheng and Kim, 2002).

The changes in synaptic response associated with LTP and LTD are thought to be primarily due to changes in the number of receptors at the synapse. The intracellular and extrasynaptic receptor populations are sources for the additional receptors inserted into synapses during LTP, and receptors internalized during LTD are returned to the intracellular vesicle pool. Long-term plasticity may also involve exchange between receptors of different subunit composition. In particular, receptors containing edited GluA2 channels may replace Ca^{2+} permeable channels during LTP (Liu and Cull-Candy, 2000; Plant et al., 2006). The properties of receptors already present at the synapse may also be modified during LTP; for example, Ca^{2+} influx may trigger phosphorylation of AMPA receptors, increasing their conductance (Benke et al., 1998).

Although Ca^{2+} influx through NMDA receptors is thought to be the major factor contributing to long-term plasticity at most synapses, AMPA receptor-mediated Ca^{2+} influx can also cause long-term changes in synaptic strength in some neurons (Mahanty and Sah, 1998; Lamsa et al., 2007). The role of AMPA receptors in short-term synaptic plasticity, however, is much more pronounced.

Short-term synaptic plasticity encompasses a broad range of phenomena that increase or decrease the synaptic strength on a time scale of milliseconds to minutes. In addition to a variety of presynaptic mechanism that change the probability, time course, or amount of transmitter release (Zucker and Regehr, 2002), there are several postsynaptic mechanisms that depend on the properties of AMPA receptors.

Desensitization provides one such mechanism. If receptors desensitize in response to an initial release event, the response to a subsequent release event occurring before the receptors have recovered from desensitization will be depressed. However, desensitization is counteracted by another form of short-term synaptic plasticity, activity-dependent relief of polyamine block of AMPA receptors (Rozov and Burnashev, 1999). Polyamines are molecules that contain several positively charged amine groups at intracellular pH and play a regulatory role in a wide variety of cellular processes. The affinity of AMPA receptors for polyamines is much greater in the closed state than in the open state, so synaptic activity causes relief from polyamine block. The mechanistic basis for this phenomenon is the subject of Chapter 3.

Two less prominent mechanisms of short-term synaptic plasticity that are nonetheless important at certain synapses are receptor saturation and "spillover." In general AMPA receptors are not saturated during synaptic activity because of their low affinity for glutamate; however, AMPA receptor currents can become saturated at certain synapses (e.g., Foster et al., 2005). Finally, when large amounts of transmitter are released, glutamate can diffuse from an active synapse to a neighboring synapse, a phenomenon known as "spillover" (e.g., Diamond, 2005).

CHAPTER 2: STATE-DEPENDENT POLYAMINE BLOCK OF AMPA RECEPTORS AND FREQUENCY-DEPENDENT SYNAPTIC FACILITATION

INTRODUCTION

Before I discuss the mechanistic basis of state-dependent polyamine block in Chapter 3, I would like to briefly discuss its contribution to frequency-dependent synaptic plasticity. Frequency-dependent synaptic plasticity covers a broad range of phenomena in which the amplitude of the postsynaptic response is increased (facilitation) or decreased (depression) depending on the frequency of action potential firing in the presynaptic cell. Frequency-dependent plasticity is central to theoretical and experimental investigations of information processing in the central nervous system. Frequency-dependent synaptic plasticity is appealing as a mechanism of information processing for at least two reasons. First, different types of cortical neurons exhibit distinct patterns of action potential firing in response to sustained current input, and, as scientists, our instinctive reaction to these patterns is a conviction that they must be functionally important. Second, action potential firing is in a sense binary, since currents depolarizing a cell beyond the threshold for action potential initiation will reliably elicit action potentials with identical amplitude and time course. Digital computers demonstrate that binary elements can combine to perform extremely complex calculations.

Although action potential firing is binary, release of neurotransmitter vesicles in response to action potentials is stochastic. The postsynaptic response therefore cannot represent the binary pattern of action potential firing with absolute fidelity, and the analogy between the brain and digital computers breaks down. Nonetheless, it is easy to

imagine that groups of neurons with different action potential firing patterns could be arranged into circuits of feedback and feed-forward interactions that perform simple calculations, and that large numbers of these circuits could be combined to enable complex information processing. However, it is doubtful that this could be accomplished if all of the postsynaptic targets of a single neuron responded to its pattern of action potential firing in the same way. Thus in addition to a variety of cells with distinct action potential firing properties, cortical information processing requires different synaptic mechanisms for discriminating between firing patterns in the presyanptic cell. This is the role of frequency-dependent synaptic plasticity. I will now use a simple model to describe how state-dependent polyamine block can result in postsynaptic discrimination between different frequencies of action potential firing.

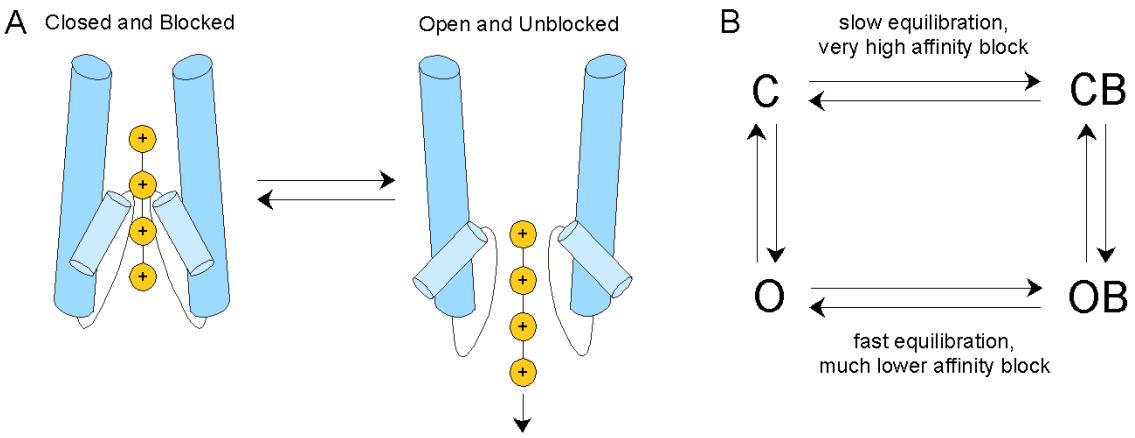

Figure 2.1. State-dependent polyamine block of AMPA receptors.

(A) Cartoon illustrating state-dependent polyamine block of AMPA receptors. Under physiological conditions, polyamines bind to closed AMPA receptor channels with high affinity, but rapidly dissociate from open channels. **(B)** Kinetic model of state-dependent polyamine block. The slow equilibration of polyamine block of closed channels (C, closed unblocked channel; CB, closed blocked channel) is described by $\tau_{reblock}$ in Figures 2.2-4. The rapid equilibration of polyamine block of open channels (O, open unblocked channel; OB, open blocked channel) is described by $\tau_{unblock}$ in Figures 2.2-4.

MODEL

The affinity of AMPA receptor channels for polyamines is much higher in closed than in open channels, but the kinetics of polyamine block are much slower in closed channels (Figure 2.1) (Bowie et al., 1998; Rozov et al., 1998). As a result, synaptic AMPA receptors are constitutively blocked by polyamines at inactive synapses. Synaptic activity partially relieves the channels of polyamine block, and block recovers slowly, so that the response to subsequent synaptic events may be potentiated (Rozov and Burnashev, 1999; Shin et al., 2005; Soto et al., 2007). As a result, state-dependent polyamine block acts as a high-pass filter for the frequency of action potential firing in the presynaptic cell. The frequency response is dependent on the precise balance between the rate of relief from block in open channels, and the rate of recovery of block in closed channels, and these in turn are dependent on the microscopic kinetics of the interactions of polyamines with AMPA receptors.

The simple model in Figure 2.2 illustrates frequency-dependent facilitation of excitatory postsynaptic potentials due to activity dependent relief from polyamine block. The model has four parameters, the macroscopic time constant for relief from polyamine block in open channels ($\tau_{unblock}$), the macroscopic time constant for recovery of polyamine block in closed channels ($\tau_{reblock}$), the frequency of presynaptic action potential firing, and the pulse length, which is the amount of time the receptors are exposed to a high concentration of glutamate. The values of $\tau_{unblock}$, $\tau_{reblock}$, and the pulse length, as listed in Figure 2.2, are chosen to be in reasonable agreement with results from synaptic physiology and kinetic investigations of AMPA receptors, as well as the kinetics of polyamine block as determined in Chapter 3, and to qualitatively reproduce the →

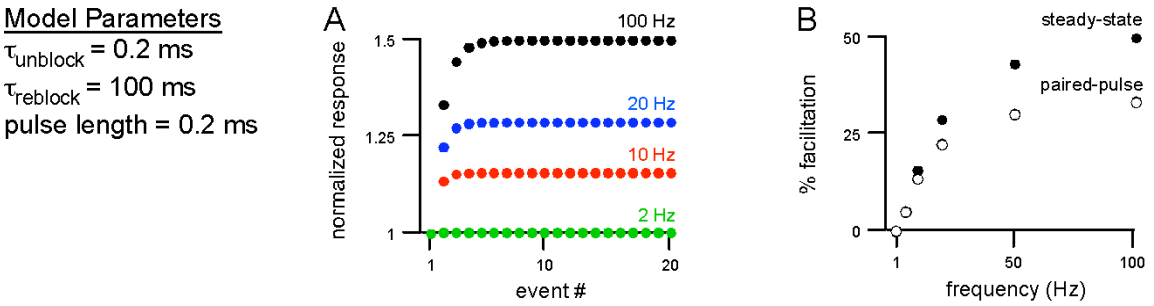

Figure 2.2. A model of frequency-dependent synaptic facilitation due to state-dependent polyamine block.

(A) Normalized excitatory postsynaptic response as a function of synaptic event number at various event frequencies. **(B)** Percent steady-state and paired-pulse facilitation as a function of event frequency.

→frequency-dependent facilitation seen experimentally. At resting membrane potential (approximately –80 mV), the microscopic rate of dissociation from AMPA receptors for the most common polyamine, spermine, is predicted to be very fast (~50,000 s^{-1}) (see Chapter 3, Figure 3.2 and Table 3.1), so relief from polyamine block is limited by the rate of AMPA receptor activation, and the value of $\tau_{unblock}$ (0.2 ms) is based on this rate. In the closed state, $\tau_{reblock}$ is dominated by the microscopic rate of spermine association with closed AMPA receptors, which was estimated as 6.2 $s^{-1}\mu M^{-1}$ (see Chapter 3, Supplemental Figure S3.2), giving $\tau_{reblock}$ of 100 ms for low micromolar concentrations of spermine. The pulse length (0.2 ms) condenses the kinetics of glutamate release, diffusion, and uptake into a single parameter. (The lifetime of glutamate in the synaptic cleft is notoriously difficult to estimate, but is probably on the order of a few hundred microseconds.)

The model makes the simplifying assumption that each action potential leads to release of a single vesicle of glutamate, ignoring various presynaptic factors leading to variability in synaptic response, and also ignores AMPA receptor desensitization. Obviously, it is not intended as a realistic model of any actual synapse but is rather meant to illustrate how state-dependent polyamine block can give rise to frequency-response characteristics that may be functionally important in neurons.

Figure 2.2 *A* illustrates the postsynaptic response of the model synapse to a series of presynaptic release events occurring at various frequencies, normalized to the amplitude of the response to the initial event. Two useful measures of synaptic facilitation are paired-pulse facilitation and steady-state facilitation. Paired-pulse facilitation is the amplitude of the response to the second synaptic event normalized to

that of the inital event, and steady-state facilitation is the amplitude of the response once the response to synaptic events has stopped changing, normalized to the amplitude of the response to the initial event. The amounts of paired-pulse and steady-state facilitation are plotted as a function of the frequency of synaptic events in Figure 2.2 *B*. The reason for the frequency dependence of facilitation seen in Figure 2.2 *B* is clear. If the interval between events is short relative to $\tau_{reblock}$, significant reblock of closed channels does not occur between events and the relief from block occurring with each event adds to that of the previous events. As the interval increases, so does the amount of reblock between pulses, and the additive unblocking effect is diminished until facilitation no longer occurs.

The effects of changing $\tau_{reblock}$ on the frequency dependence of facilitation are illustrated in Figure 2.3. Figure 2.3 *A* shows the response of the model synapse to repetitive synaptic events at 100 Hz, for several values of $\tau_{reblock}$. In addition to decreasing the overall amount of paired-pulse and steady-state facilitation, decreasing $\tau_{reblock}$ shifts the cut-off frequency of the high-pass filter to higher frequencies, and decreases the steepness of the filter roll-off, as shown for steady-state facilitation in Figure 2.3 *B*. The effects of changing $\tau_{unblock}$ are illustrated in Figure 2.4. Figure 2.4 *A* shows the response to repetitive synaptic events at 100 Hz for several values of $\tau_{unblock}$. If $\tau_{unblock}$ is very small, relief from block is nearly complete after the first the event and significant facilitation does not occur. Large values of $\tau_{unblock}$ allow for large amounts of facilitation, as seen in Figure 2.4 *B* for paired-pulse facilitation, but many events are required for facilitation to reach steady-state.

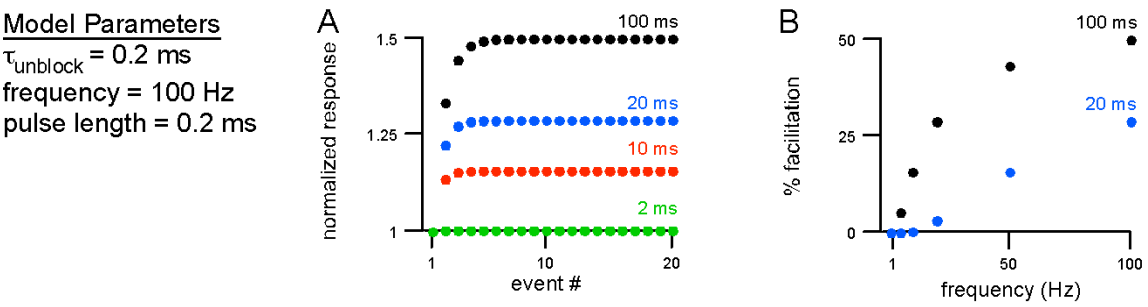

Figure 2.3. Dependence of synaptic facilitation on $\tau_{reblock}$.

(A) Normalized excitatory postsynaptic response as a function of synaptic event number at an event frequency of 100 Hz for various values of $\tau_{reblock}$. **(B)** Percent steady-state facilitation as a function of event frequency for $\tau_{reblock}$ = 100 ms and $\tau_{reblock}$ = 20 ms.

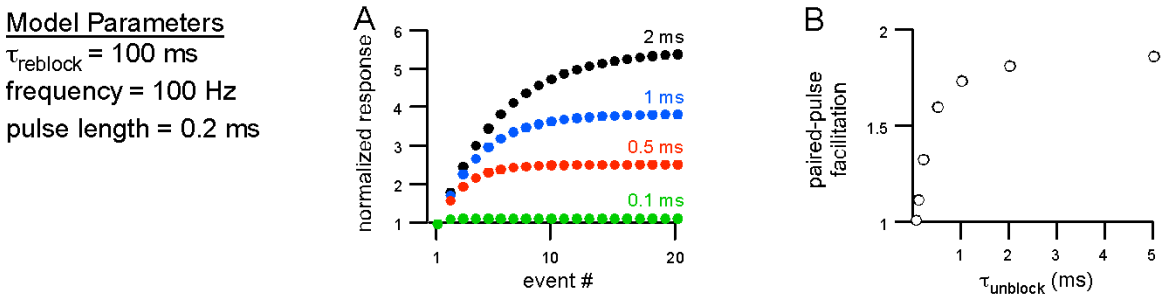

Figure 2.4. Dependence of synaptic facilitation on $\tau_{unblock}$.

(A) Normalized excitatory postsynaptic response as a function of synaptic event number at an event frequency of 100 Hz for various values of $\tau_{unblock}$. **(B)** Paired-pulse facilitation at an event frequency of 100 Hz as a function of $\tau_{unblock}$.

POTENTIAL FUNCTIONAL IMPORTANCE

The model illustrates that state-dependent polyamine block can cause short-term frequency-dependent synaptic plasticity, but numerous other presynaptic and postsynaptic factors are involved in short-term synaptic plasticity, and amidst these other factors state-dependent polyamine block may be of relatively minor functional significance. However, it has been demonstrated that polyamine block can convert paired-pulse depression to paired-pulse facilitation at some pyramidal-to-multipolar cell synapses and reduce the degree of paired-pulse depression at others (Rozov and Burnashev, 1999), so short-term synaptic plasticity due to polyamine block is not just a theoretical possibility. Additionally, if the values of $\tau_{reblock}$ or $\tau_{unblock}$ were altered at a synapse, the frequency response characteristics of the synapse would also be changed, resulting in metaplasticity or "plasticity of plasticity." There are several mechanisms by which the values of these time constants could be altered at a synapse, and although it has not been demonstrated that these mechanisms result in functionally important changes in short-term synaptic plasticity, they provide an intersting opportunity for speculation. For example, it has been shown that the concentration of intracellular polyamines is higher in developing than in mature neocortical neurons (Shin et al., 2005). Polyamines perform many regulatory functions in cells, so changes in synaptic properties resulting from elevated polyamine concentrations during development may be a functionally unimportant, incidental effect of some other regulatory process; nevertheless, increasing intracellular polyamine concentration would increase $\tau_{reblock}$. Perhaps patterns of action potential firing during development require synapses with different frequency response characteristics than those of mature neurons. Association of AMPA receptors with

stargazin reduces $\tau_{unblock}$ such that complete relief from polyamine block occurs in response to a single brief glutamate application and frequency-dependent facilitation is eliminated (Soto et al., 2007). This effect was demonstrated using recombinant AMPA receptors in HEK cells, but exchanging synaptic AMPA receptors associated with stargazin for receptors lacking stargazin could "switch on" the high pass filter due to state-dependent polyamine block. It has also been shown that, in certain forms of LTP, Ca^{2+}-permeable AMPA receptors are replaced by Ca^{2+}-impermeable receptors (which are not blocked by polyamines) (Liu and Cull-Candy, 2000; Plant et al., 2006). This would have the effect of switching off the high-pass filter. The ability to switch on or off a high-pass filter at a key synapse in a neural circuit might allow for plasticity of circuit function. These are all interesting possibilities to consider, but it is time to proceed to actual experimental results.

CHAPTER 3: GATING-DEPENDENT REARRANGEMENTS IN THE SELECTIVITY FILTER UNDERLIE STATE-DEPENDENT POLYAMINE BLOCK OF AMPA RECEPTORS

INTRODUCTION

Ca^{2+}-permeable non-NMDA receptors are blocked by internal polyamines, such as spermine, in a state-dependent manner. The affinity of non-NMDA receptor channels for polyamines is higher for closed than for open channels, but the kinetics of polyamine block are much slower for closed channels (Bowie et al., 1998; Rozov et al., 1998). The state-dependence of block results in frequency-dependent synaptic potentiation of synaptic AMPA receptor responses, and as discussed in Chapter 2, this potentiation depends on a precise balance between the rates at which polyamines associate with and dissociate from open and closed AMPA receptor channels. The structural mechanisms underlying this critical balance are not well understood.

Polyamine block is also dependent on membrane potential (Bowie and Mayer, 1995; Kamboj et al., 1995; Koh et al., 1995). Polyamines block non-NMDA receptors at a site that, at least in open channels, is exposed to the transmembrane electric field, so the rates at which polyamines associate with and dissociate from the channel are exponentially related to membrane voltage. Polyamines can dissociate from open channels to either the internal or external solution (and thus can permeate the channel), so under physiological conditions non-NMDA receptors have doubly rectifying current voltage (I-V) relations. The rate at which polyamines associate with closed non-NMDA receptors is voltage-independent (Bowie et al., 1998), suggesting that the polyamine

blocking site may not be exposed to the transmembrane electric field in closed channels. Thus the voltage dependence of polyamine block, as well as the zero-potential rates of association and dissociation, is different in open and closed channels.

State-dependent interactions between AMPA receptors and polyamines probably reflect differences in the structure of open and closed channels, so understanding their structural basis may provide insight into glutamate receptor channel gating. To define the structural basis for the state-dependent interactions between AMPA receptors and polyamines, I compared the kinetics of block of open and closed channels by internally and externally applied spermine using fast agonist application. I also compared the kinetics of block in wild-type channels and in mutant channels in which a conserved negatively charged residue (D590) critical for internal polyamine block has been neutralized. I propose that reorientation of this residue underlies the state-dependence of polyamine block.

MATERIALS AND METHODS

Molecular biology and heterologous expression.

All experiments were performed with previously described expression constructs for the wild-type rat GluA2(Q) subunit (Collingridge et al., 2009), where i indicates the flip splice variant and Q indicates the residue occupying the Q/R editing site (Sommer et al., 1991). Numbering of amino acids is for the mature protein.

Channels were transiently expressed in human embryonic kidney 293 (HEK 293) cells. HEK 293 cells were transfected with glutamate receptor subunits using FuGene 6 (Roche, Indianapolis, IN). A vector for enhanced green fluorescent protein (pEGFP-C1, Clontech, Palo Alto, CA) was co-transfected at a ratio of 1:9 (pEGFP-C1:subunit). Recordings were made one to three days after transfection.

The D590N mutant was generated using the QuickChange site-directed mutagenesis kit (Stratagene, La Jolla, CA). The mutation was initially made in a pSP64T-derived vector because of its smaller size. After the introduction of the mutation, a fragment encompassing it was subcloned back into a wild-type template contained in pRK eukaryotic expression vector. The construct was sequenced over the entire length of the subcloned fragment.

Current recording.

Macroscopic currents in outside-out patches, isolated from HEK 293 cells, were recorded at room temperature (20-23°C) using an EPC-9 (HEKA Elektronik, Lambrecht, Germany) or Axopatch 200B (Molecular Devices, Sunnyvale, CA) amplifier with PULSE or Patchmaster software (HEKA Elektronik), low-pass filtered at 2.8 or 10 kHz (-

3 dB) using an 8 pole low pass Bessel filter and digitized at 50 or 100 kHz. An additional 2 kHz digital Gaussian filter was sometimes applied before analysis. For display, currents were digitally filtered with a 1 kHz Gaussian filter and resampled at 3-5 kHz. Pipettes had resistances of 2-10 MΩ when filled with the pipette solution and measured in the standard external solution. I did not use series resistance compensation or correct for junction potentials. In most patches, experiments were performed several times and the results of at least three trials were averaged.

External solutions were applied using a piezo-driven double barrel application system made from theta glass. One barrel contained the external solution; the other contained the same solution with added glutamate (5-10 mM). The tip of the theta glass application pipette was treated with hydrofluoric acid to reduce the thickness of the septum. At the end of experiments where solution exchange rates were critical, the outside-out patch was removed by applying positive pressure to the patch pipette, and the open tip response was recorded. Where appropriate, I included in the final analysis only those patches where the 10-90% rise time was <350 μs.

Solutions.

The standard internal (pipette) solution consisted of (mM): 110 NaCl, 20 Na_2ATP, 5 Hepes, and 1 Bapta, pH 7.2 (NaOH). Based on the high estimated binding constant between spermine and ATP (Watanabe et al., 1991), internal solutions with high concentrations of free ATP have been used to achieve "polyamine free conditions", and I-V relations for Ca^{2+}- permeable AMPA receptors do not show double rectification with this solution (e.g., Rozov et al., 1998). Spermine (5 μM or 1 mM) was added to this

solution, yielding approximate free spermine concentrations of 0.4 or 81 μM, based on the estimated binding constant between spermine and ATP. The standard external solution consisted of (mM): 140 NaCl and 10 HEPES, pH 7.2 (NaOH) with 30 μM cyclothiazide (CTZ) (from 10 mM stock solution in 100 mM NaOH) to prevent desensitization (Partin et al., 1993). Spermine was added to this solution without correcting for concentration. For experiments involving extreme membrane potentials (Figures 3.4 and 3.5), $CaCl_2$ (0.2-1 mM) was sometimes added to the external solution to help stabilize the patches. All chemicals were obtained from Sigma (St. Louis, MO) or J.T. Baker (Phillipsburg, NJ).

Data analysis and experimental protocols.

Currents were analyzed using Igor Pro (WaveMetrics, Inc., Lake Oswego, OR). Current-voltage (I-V) relations were derived either from peak or steady-state current amplitudes. I-V relations were fit with 4^{th} or 5^{th} order polynomial functions, and the x-intercepts of the fits were taken to be the zero-current or reversal potentials. Two patches were excluded from the final analysis because their reversal potentials were <-5 mV or >+5 mV from 0 mV.

Removal of spermine block with conditioning glutamate applications. Polyamines have a higher affinity for the closed than for the open state of AMPA receptor channels (Rozov et al., 1998). Thus polyamine block is state-dependent and can be relieved by activity. I therefore preceded test glutamate applications with conditioning glutamate applications to ensure that spermine was not bound to the channels at the start of the test glutamate application. Conditioning glutamate applications, referred to as “conditioning prepulses”

throughout the text, consisted of a 10-20 ms application of glutamate at a holding potential of either -100 mV or +100 mV. Examples of conditioning prepulses are seen in the left half of Figure 3.1 *A*. The membrane potential was switched to the test potential 10-20 ms after the conclusion of the conditioning prepulse. The rate at which spermine associates with closed AMPA receptor channels is ~3 s^{-1} for the concentration of internal spermine used here, and external spermine associates with closed channels very slowly or not at all, so significant recovery of block does not occur during the interval between the end of the conditioning prepulse and the start of the test glutamate application. Indeed, nearly all channels are unblocked at the start of the test glutamate application (Supplemental Figure S3.1).

Subtraction of capacity currents. Transient capacitive currents occur when the holding potential is switched from the ±100 mV prepulse potential to the test potential. To remove capacitive currents from the records, currents in response to the switch in holding potential were recorded in the absence of conditioning and test glutamate applications, and these baseline currents were subtracted from the experimental records.

Quantification of block. The fraction of channels blocked by spermine at steady state was determined by:

$$\%\text{Block} = (I_{control} - I_{block})/I_{control} \qquad (3.1)$$

where I_{block} and $I_{control}$ correspond to currents with and without spermine block. $I_{control}$ was obtained from the peak response to glutamate applications after conditioning prepulses, as indicated in Figure 4.1 *A*. I_{block} was obtained from steady-state responses after conditioning prepulses, or from peak current responses without conditioning prepulses. As a control for the effectiveness of the conditioning prepulses for removing external

spermine block, %Block was also determined by comparing current amplitudes recorded without conditioning prepulses in the absence of internal or external spermine ($I_{control}$), and after washing in external spermine (I_{block}) (Supplemental Figure S3.1 *B*).

Internal polyamines permeate open glutamate receptors at sufficiently positive, and external polyamines at sufficiently negative, potentials (Bahring et al., 1997) resulting in doubly rectifying I-V plots and the corresponding bell-shaped plots of steady-state block versus voltage. A minimal kinetic scheme for permeant block by internal spermine is:

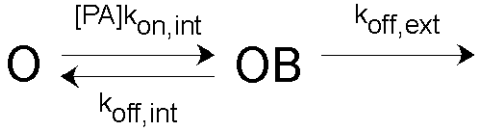

where [PA] is the spermine concentration; $k_{on,int}$ is the second-order rate constant of association with the pore for internal spermine; and $k_{off,int}$ and $k_{off,ext}$ are the rate constants of spermine dissociation to the internal and external solutions. In the absence of external spermine, $k_{on,ext}$, the second-order rate constant of association with the pore for external spermine, is omitted from the reaction scheme. Dissociation of spermine by the $k_{off,ext}$ pathway returns the channel to the O state.

For permeant block by external spermine, the kinetic scheme is similar, but $k_{on,int}$ is omitted because my recording conditions are free of internal spermine:

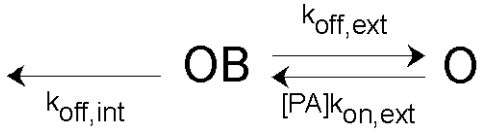

Dissociation of spermine by the $k_{off,int}$ pathway returns the channel to the O state.

Assuming these kinetic schemes, expressions for the steady-state voltage dependendence of block by internal and external spermine are given by:

$$\%\text{Block(internal)} = \frac{[\text{PA}]k_{on,int}(0)\exp(z\delta_{on,int}\text{V}^*)}{[\text{PA}]k_{on,int}(0)\exp(z\delta_{on,int}\text{V}^*) + k_{off,int}(0)\exp(-z\delta_{off,int}\text{V}^*) + k_{off,ext}(0)\exp(z\delta_{off,ext}\text{V}^*)} \quad (3.2\text{A})$$

and

$$\%\text{Block(external)} = \frac{[\text{PA}]k_{on,ext}(0)\exp(-z\delta_{on,ext}\text{V}^*)}{[\text{PA}]k_{on,ext}(0)\exp(-z\delta_{on,ext}\text{V}^*) + k_{off,int}(0)\exp(-z\delta_{off,int}\text{V}^*) + k_{off,ext}(0)\exp(z\delta_{off,ext}\text{V}^*)} \quad (3.2\text{B})$$

where $k_{on,int}(0)$, $k_{on,ext}(0)$, $k_{off,int}(0)$, and $k_{off,ext}(0)$ are the zero-potential rate constants of spermine association and dissociation in the kinetic schemes given above, and $z\delta_{on,int}$, $z\delta_{on,ext}$, $z\delta_{off,int}$, and $z\delta_{off,ext}$ are their voltage dependences, [PA] is the concentration of internal or external spermine, and V^* is $\text{V}F/RT$ with F, R, and T having their usual thermodynamic meanings.

If the kinetics of block are ignored, a simplified, steady-state description of block by internal spermine is given by:

$$\%\text{Block(internal)} = \frac{1}{1 + \frac{K_b}{[\text{PA}]\exp\left(z\delta_b\text{V}^*\right)} + \frac{K_p}{[\text{PA}]\exp\left(-z\delta_p\text{V}^*\right)}} \quad (3.3\text{A})$$

Here, K_b is the equilibrium binding constant for a hypothetical channel that is impermeable to internal spermine but otherwise identical to the channel being studied; similarly, K_p is the steady-state binding constant for another hypothetical channel: this channel is permeable to spermine, but spermine cannot dissociate from the channel to the internal solution once it is bound; $z\delta_b$ and $z\delta_p$ describe the voltage dependence of steady-

state block for these hypothetical channels. For internal spermine, K_b and K_p are defined in terms of the microscopic rate constants in the kinetic scheme above as $k_{off,int}(0)/k_{on,int}(0)$ and $k_{off,ext}(0)/k_{on,int}(0)$, respectively, and $z\delta_b$ and $z\delta_p$ are defined as $z\delta_{off,int} + z\delta_{on,int}$ and $z\delta_{off,ext} - z\delta_{on,int}$, respectively.

For external spermine block, the signs on $z\delta_b$, and $z\delta_p$ are reversed, the interpretations of K_b and K_p are adjusted accordingly, and the steady-state equation for block is:

$$\%\text{Block(external)} = \frac{1}{1 + \frac{K_b}{[\text{PA}]\exp\left(-z\delta_b \text{V}^*\right)} + \frac{K_p}{[\text{PA}]\exp\left(z\delta_p \text{V}^*\right)}} \qquad (3.3\text{B})$$

Here, K_b and K_p are defined as $k_{off,ext}(0)/k_{on,ext}(0)$ and $k_{off,int}(0)/k_{on,ext}(0)$, respectively, and $z\delta_b$ and $z\delta_p$ are defined as $z\delta_{off,ext} + z\delta_{on,ext}$ and $z\delta_{off,int} - z\delta_{on,ext}$ respectively. The definitions of these steady-state parameters are not the same as for internal spermine. Note that there are six kinetic parameters describing block by internal and external spermine, four of which ($k_{off,int}$ & $z\delta_{off,int}$ and $k_{off,ext}$ & $z\delta_{off,ext}$) are shared between the equations for internal and external block.

Voltage dependence and zero-potential rate constants of block. Macroscopic time constants for the equilibration of block (τ_{block}) were obtained from single exponential fits to the decay of glutamate-activated current after a conditioning prepulse. According to the kinetic schemes above, these time constants are the inverse of the sum of three microscopic rate constants. For internal and external spermine, respectively:

$$\tau_{block}(\text{internal}) = \frac{1}{[\text{PA}]k_{on,int} + k_{off,int} + k_{off,ext}} \qquad (3.4\text{A})$$

and

$$\tau_{block}(\text{external}) = \frac{1}{[\text{PA}]k_{on,ext} + k_{off,int} + k_{off,ext}} \qquad (3.4B)$$

For internal spermine, $k_{off,int}(0)$ can be expressed in terms of K_b and $k_{on,int}(0)$; $z\delta_{off,int}$ in terms of $z\delta_b$, and $z\delta_{on,int}$; $k_{off,ext}(0)$ in terms of K_p and $k_{on,int}(0)$; and $z\delta_{off,ext}$ in terms of $z\delta_p$ and $z\delta_{on,ext}$:

$$k_{off,int}(0) = K_b k_{on,int}(0), \qquad (3.5A)$$

$$z\delta_{off,int} = z\delta_b - z\delta_{on,int},$$

$$k_{off,ext}(0) = K_p k_{on,int}(0),$$

$$\text{and } z\delta_{off,ext} = z\delta_p + z\delta_{on,int}$$

Similarly, for external spermine:

$$k_{off,int}(0) = K_p k_{on,ext}(0), \qquad (3.5B)$$

$$z\delta_{off,int} = z\delta_p + z\delta_{on,ext},$$

$$k_{off,ext}(0) = K_b k_{on,ext}(0),$$

$$\text{and } z\delta_{off,ext} = z\delta_b - z\delta_{on,ext}$$

Thus, if K_b & $z\delta_b$ and K_p & $z\delta_p$ have been obtained from steady-state data, substituting Equations 3.5A into Equation 3.4A gives an equation for the voltage dependence of $1/\tau_{block}$ for internal spermine with $k_{on,int}$ and $z\delta_{on,int}$ as the only free variables:

$$\frac{1}{\tau_{block}(\text{V})} =$$
$$k_{on,int}(0)([\text{PA}]\exp\left(z\delta_{on,int}\text{V}^*\right) + K_b \exp(-(z\delta_b - z\delta_{on,int})\text{V}^*) + K_p \exp((z\delta_p + z\delta_{on,int})\text{V}^*))$$

(3.6A)

Likewise, substituting Equations 3.5B into Equation 3.4B gives an equation for the voltage dependence of $1/\tau_{block}$ for external spermine with $k_{on,ext}$ and $z\delta_{on,ext}$ as the only free variables:

$$\frac{1}{\tau_{block}(\mathrm{V})} = k_{on,external}(0)([\mathrm{PA}]\exp\left(-z\delta_{on,ext}\mathrm{V}^*\right) + K_b\exp((z\delta_b - z\delta_{on,ext})\mathrm{V}^*) + K_p\exp(-(z\delta_p + z\delta_{on,ext})\mathrm{V}^*))$$

(3.6B)

Single channel recordings indicate that open probability in the absence of polyamines is >90% under my recording conditions (see Chapter 4), so my estimates of the kinetic parameters of open channel block are unlikely to be affected by long closings of individual channels during nominal open periods.

"Escape" of trapped polyamines from closed channels. For the experiments in Figures 3.4 and 3.5, recovery from block in closed channels at extreme potentials was quantified using ratios of peak to steady-state current, after holding at extreme potentials in the absence of glutamate. For these experiments, it was necessary to distinguish between small peaks occurring after relief from spermine block and random current noise. To do so, I measured the peak current during the first 3 ms of the test glutamate application (40 ms at +20 mV). The peak current during this 3 ms window was considered significant if it was greater than the mean ± 2SD of the steady-state current (as measured using the last 20 ms of the test application). Otherwise, the mean current value of the window was substituted for the peak current for the purpose of calculating peak to steady-state current ratios, yielding ratios of ~1.

The dependence of I_{peak}/I_{ss} on the voltage during the holding period (V_h) was used to calculate the zero-potential rate constants ($k_{off,closed,int}(0)$ and $k_{off,closed,ext}(0)$) and voltage

dependences ($z\delta_{off,closed,int}$ and $z\delta_{off,closed,ext}$) of external spermine dissociation from closed channels. External spermine associates with closed channels at a rate that is very slow relative to the rates of dissociation (Supplemental Figure S3.3), so the dependence of I_{peak}/I_{ss} on V_h is given by:

$$I_{peak}/I_{ss}(V_h),\ \text{external} = \frac{1 - \%\text{Block}_{open}(V_{test})\exp(-tk_{off,closed}(V_h))}{1 - \%\text{Block}_{open}(V_{test})} \qquad (3.7)$$

where t is the length of the holding period (1 s), $k_{off,closed}(V_h)$ is the rate constant of spermine dissociation from closed channels to the internal (at extreme negative potentials) or the external (at extreme positive potentials) solution, and $\%\text{Block}_{open}(V_{test})$ is the steady-state percentage of open channels blocked by spermine at the test potential, chosen to be near the potential for maximal block. Internal spermine associates with closed channels at a voltage independent rate (Supplemental Figure S3.2, Bowie et al., 1998), so the dependence of I_{peak}/I_{ss} on V_h is more complicated, and was not investigated in detail.

Statistical analysis.

For statistical analysis, I used Igor Pro (WaveMetrics, Inc.) and Microsoft Excel (Redmond, WA). Results are shown graphically as mean ± SEM. Equations were fit to the entire data set using non-linear least squares fitting in Igor Pro. For kinetic analysis, certain parameters were determined as products or sums of pairs of parameters obtained from these fits (Equations 3.5A and 3.5B). The standard deviations for such parameters were determined from the square roots of the summed squares of the relative errors (for

products of rates) or absolute errors (for sums of $z\delta$ values) of the parameters from which they were derived.

An ANOVA or a Student's *t*-test was used to define statistical differences. The Tukey test was used for multiple comparisons. Significance was assumed if $P < 0.05$.

RESULTS

To characterize the mechanism of state-dependent polyamine block, I compared the interactions of internal and external spermine with open and closed channels. As a first step, I compared the voltage dependence and kinetics of block of open channels by internal and external spermine.

Steady-state block of open AMPA receptor channels by internal and external spermine.

Figure 3.1 *A* shows the protocol I used to measure the voltage dependence of block of AMPA receptors by internal and external spermine. Glutamate-activated currents were recorded from outside-out patches containing GluA2(Q) receptors at test potentials ranging from –100 mV to +100 mV in 10 mV intervals, in the presence of 0.4 μM internal (shown) or 5 μM external spermine. As explained in the Materials and Methods section, the test glutamate applications were preceded by conditioning glutamate applications, or prepulses, at –100 mV (as shown for internal spermine) or +100 mV (for external spermine). The effect of the prepulses is illustrated in Figure 3.1 *B*, which shows glutamate-activated currents at +20 mV obtained after holding the membrane at –100 mV either with (arrow) or without the conditioning prepulse. The prepulse potentiates the current amplitude by relieving the channels of spermine block; the rapidly decaying peak current is due to reequilibration of block. Similar results are seen for external spermine (Figure 3.1 *C*).

Figure 3.1 *D* shows I-V relations for peak (*open circles*) and steady-state (*triangles*) currents measured at the points indicated in Figure 3.1 *A*. The steady-state →

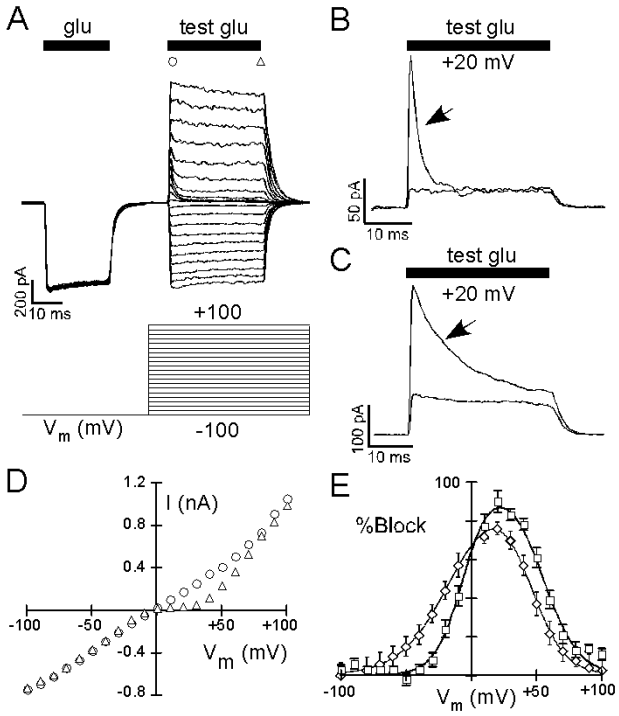

Figure 3.1. Steady-state block of open AMPA receptor channels by internal and external spermine.

(A) Protocol to measure block of AMPA receptors by spermine. Recordings are from outside-out patches isolated from HEK 293 cells expressing GluA2(Q) channels with 0.4 μM internal spermine. Currents (*middle traces*) were generated by a combination of glutamate applications (*upper thick bars*, 5 mM) and voltage steps (*lower traces*). The initial glutamate application ("conditioning prepulse", 20 msecs) at –100 mV relieves channels of spermine block. 10 ms after the end of the conditioning prepulse, the membrane potential is stepped to various test potentials from –100 to +100 mV in 10 mV increments. A test glutamate application (30 ms) is made 5 ms after the voltage step. **(B) and (C)** Example glutamate-activated currents in response to test glutamate applications either with (*arrow*) or without a conditioning prepulses. (B) Currents at +20 mV with 0.4 μM internal spermine. (C) Currents at +20 mV with 5 μM external spermine. **(D)** I-V relations for peak (*open circles*) and steady-state (*open triangles*) currents measured at the points indicated in (A). **(E)** Mean %Block ($100(I_{control} - I_{block})/I_{control}$), as determined for 0.4 μM internal spermine from peak currents ($I_{control}$) after conditioning prepulses and steady-state currents (I_{block}) (*open squares, n* = 7); and as determined for 5 μM external spermine from peak currents ($I_{control}$) after conditioning prepulses and steady-state currents (I_{block}), or from steady-state currents in the absence of spermine ($I_{control}$) and after washing in spermine (I_{block}) (*open diamonds*, *n* = 13). The continuous lines are fits of Equations 3.3A and 3.3B, yielding parameters (mean ± SD): K_b = 0.22 ± 0.03 μM, $z\delta_b$ = 2.31 ± 0.22, K_p = 0.0068 ± 0.0024 μM, and $z\delta_p$ = 1.84 ± 0.15 for internal spermine; and K_b = 0.18 ± 0.06 μM, $z\delta_b$ = 1.87 ± 0.15, K_p = 2.27 ± 0.26 μM, and $z\delta_p$ = 1.29 ± 0.09 for external spermine.

→I-V relation shows the familiar double rectification resulting from voltage-dependent block and permeation of Ca^{2+}-permeable AMPA receptor channels by spermine. Peak current I-V relations obtained after conditioning prepulses are indistinguishable from I-V relations obtained in the absence of polyamines for the concentrations of internal and external spermine used in my experiments (Supplemental Figure S3.1). Therefore, the percentage of current blocked by spermine at steady-state (%Block) can be calculated from the amplitudes of the peak currents relative to either subsequent steady-state currents, or steady-state currents not preceded by prepulses. The voltage dependence of %Block obtained in this manner is shown in Figure 3.1 *E* for 0.4 μM internal (*open squares*) and 5 μM external (*open diamonds*) spermine. The solid lines in Figure 3.1 *E* are fits of Equations 3.3A and 3.3B with K_b = 0.22 ± 0.03 μM, $z\delta_b$ = 2.31 ± 0.22, K_p = 0.0068 ± 0.0024 μM, and $z\delta_p$ = 1.84 ± 0.15 for internal spermine; and K_b = 0.18 ± 0.06 μM, $z\delta_b$ = 1.87 ± 0.15, K_p = 2.27 ± 0.26 μM, and $z\delta_p$ = 1.29 ± 0.09 for external spermine (mean ± SD).

Kinetics of block of open channels by internal and external spermine.

In addition to %Block, the protocol illustrated in Figure 3.1 *A* provides the macroscopic rate of equilibration of spermine block of open AMPA receptor channels ($1/\tau_{block}$). As shown in Figure 3.2 *A* (internal spermine, +20 mV) and *C* (external spermine, –20 mV), the differences between currents with and without prepulses are well fit by single exponentials. The macroscopic rate of current decay, $1/\tau_{block}$, is the sum of at minimum three microscopic rates: the rate at which spermine dissociates from the channel to the internal solution ($k_{off,int}$), the rate at which it dissociates from the channel to the →

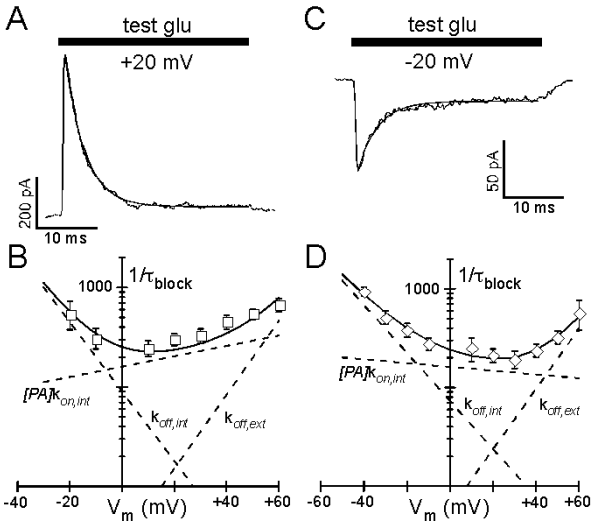

Figure 3.2. Steady-state block of open AMPA receptor channels by internal and external spermine.

(A) and (C) Difference currents obtained at +20 mV in the presence of 0.4 μM internal spermine (A) and at –20 mV in the presence 5 μM external spermine (C). The currents are the difference between currents recorded with and without a conditioning prepulse. The solid lines are single exponentials fits (τ_{block} = 3.02 ms, internal; and 3.32 ms, external). **(B) and (D)** Kinetics and voltage dependence of block by 0.4 μM internal (B) and 5 mM external (D) spermine. Inverse of the mean τ_{block} values as a function of membrane potential (V_m) ($n \geq 5$ at each potential). The solid lines through the data points are fits derived from Equations 3.6A (internal) and 3.6B (external). Estimates of $k_{on,int}(0)$ & $z\delta_{on,int}$ and $k_{on,ext}(0)$ & $z\delta_{on,ext}$ obtained from these fits are 400.6 ± 32.5 $s^{-1}\mu M^{-1}$ & 0.30 ± 0.05 (internal), and 32.4 ± 1.5 $s^{-1}\mu M^{-1}$ & 0.11 ± 0.03 (external) (mean ± SD). The dashed lines are the voltage dependences of $k_{off,int}$, $k_{off,ext}$, and [PA]$k_{on,int}$ or [PA]$k_{on,ext}$ (see Table 3.1).

Table 3.1. Steady-state and kinetic parameters describing block of open wild-type AMPA receptor channels by internal and external spermine.

	Internal Spermine	External Spermine
K_b (μM)	0.22 ± 0.03	0.18 ± 0.06
$z\delta_b$	2.31 ± 0.22	1.87 ± 0.15
K_p (μM)	0.0068 ± 0.0024	2.27 ± 0.26
$z\delta_p$	1.84 ± 0.15	1.29 ± 0.09
$k_{on,int}(0)$ ($s^{-1}\mu M^{-1}$)	400.6 ± 32.5	--
$z\delta_{on,int}$	0.30 ± 0.05	--
$k_{on,ext}(0)$ ($s^{-1}\mu M^{-1}$)	--	32.4 ± 1.5
$z\delta_{on,ext}$	--	0.11 ± 0.03
$k_{off,int}(0)$ (s^{-1})	90.1 ± 15.0	73.5 ± 9.0
$z\delta_{off,int}$	2.01 ± 0.22	1.40 ± 0.10
$k_{off,ext}(0)$ (s^{-1})	2.73 ± 0.97	5.94 ± 1.84
$z\delta_{off,ext}$	2.14 ± 0.15	1.76 ± 0.15

The values of K_b & $z\delta_b$ and K_p & $z\delta_p$ were determined for homomeric GluA2(Q) channels by fitting Equations 3.3A and 3.3B to the voltage dependence of steady-state block by 0.4 μM internal and 5 μM external spermine, respectively (Figure 3.1 *E*). The values of $k_{on,int}(0)$ and $z\delta_{on,int}$ were determined from the voltage dependence of the decay rates of glutamate activated currents after conditioning prepulses (Figure 3.2 *B*) using Equation 3.6A with K_b & $z\delta_b$, and K_p & $z\delta_p$ held constant at the values determined from the steady-state block data. $k_{on,ext}(0)$ and $z\delta_{on,ext}$ were determined from the voltage dependence of the decay rates of glutamate activated currents after conditioning prepulses (Figure 3.2 *D*) using Equation 3.6B with K_b & $z\delta_b$, and K_p & $z\delta_p$ held constant at the values determined from the steady-state block data. The remaining parameters were determined using Equations 3.5A for internal spermine and Equations 3.5B for external spermine. Values are shown ± SD.

→external solution ($k_{off,ext}$), and the rate at which it associates with the channel from the internal or external solution ($k_{on,int}$ or $k_{on,ext}$). The rate of spermine association and its voltage dependence ($z\delta_{on,int}$ or $z\delta_{on,int}$) can be determined from the voltage dependence of $1/\tau_{block}$ using Equation 3.6A or 3.6B with K_b & $z\delta_b$ and K_p & $z\delta_p$ held constant at the values obtained from the voltage dependence of steady-state block (Figure 3.1 *E*). Figures 3.3 *B* and *D* show $1/\tau_{block}$ plotted versus voltage for internal and external spermine, along with the fitted voltage dependences obtained in this manner (*solid lines*). These fits provide the values of $k_{on,int}$ & $z\delta_{on,int}$ and $k_{on,ext}$ & $z\delta_{on,ext}$; the remaining kinetic parameters of block follow from the definitions of K_b & $z\delta_b$ and K_p & $z\delta_p$ (Equations 3.5A and 3.5B; see Table 3.1). The voltage dependences of the microscopic components of $1/\tau_{block}$ are shown in Figures 3.3 *B* and *D* as dashed lines.

As seen in Table 3.1, the rate at which spermine associates with open AMPA receptor channels is ~20 faster from the internal solution than from the external solution, whereas the values of the parameters for dissociation shared between Equations 3.6A and 3.6B ($k_{off,int}(0)$ & $z\delta_{koff,int}$ and $k_{off,ext}(0)$ & $z\delta_{koff,ext}$) are very similar for internally and externally applied spermine. This indicates that spermine block of open channels can be described by a model with a single binding site, with the ~10-fold difference in apparent affinity between internal and external spermine determined by differences in association rates. This simple model, however, obviously cannot account for all of the interactions between the pore and a large multivalent blocker like spermine (see Discussion). I therefore refer to the general region of the pore where spermine binds as the blocking site.

A negative charge at position 590 affects internal and external spermine block of open channels in part through a surface charge mechanism.

A negatively charged residue, conserved in non-NMDA receptors (aspartate (D) in AMPA receptors, glutamate (E) in kainate receptors), is critical for internal polyamine block in AMPA receptors (Dingledine et al., 1992) and kainate receptors, with charge neutralization increasing the equilibrium dissociation constant for spermine by two to three orders of magnitude (Panchenko et al., 1999). I hypothesized that D590 might play a key role in the state dependence of polyamine block, so I wanted to establish a mechanistic basis for its effects in open channels. For these experiments, I replaced the negatively charged aspartate with the neutral but similarly sized asparagine (D590N).

Figure 3.3 *A* shows glutamate-activated currents for D590N channels using the prepulse protocol, with the polyamine free internal solution and 5 μM external spermine. The peak current I-V relation for this patch, measured at the point indicated by the open circle in Figure 3.3 *A*, is shown in Figure 3.3 *B* (*open circles*), along with the I-V relation from the same patch recorded without conditioning prepulses (*concentric circles*). Figures 3.3 *C* and *D* compare %Block derived from such pairs of I-V relations for block of D590N channels by 5 μM external (Figure 3.3 *C*, *solid squares*) and 81 μM (Figure 3.3 *D*, *solid circles*) spermine with %Block for block of wild-type channels by 5 μM external (Figure 3.3 *C*, *open diamonds*) and 0.4 μM (Figure 3.3 *D*, *open squares*) spermine. The values of the steady-state parameters of block are listed in Table 3.2. D590N reduces the peak value of %Block for 5 μM external spermine, but the reduction in block is small compared to the orders of magnitude reduction in apparent affinity for internal spermine. The location of the peak value of %Block, however, is shifted by →

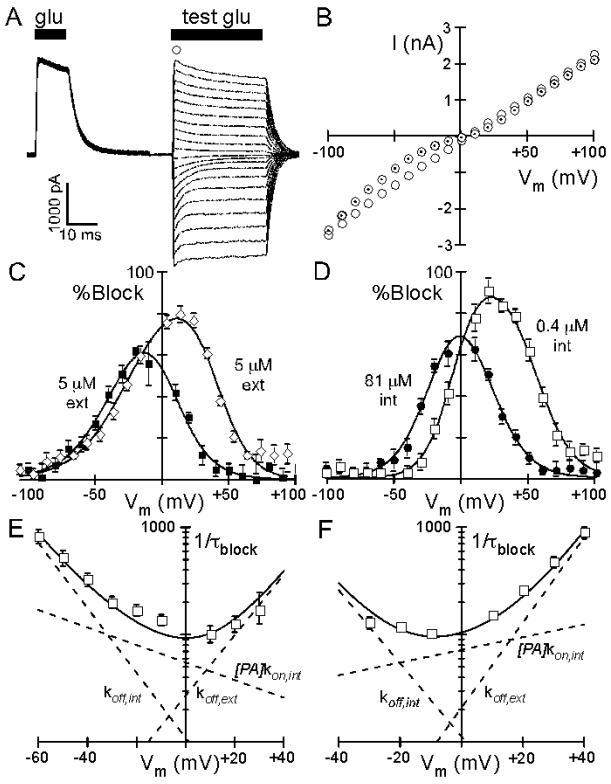

Figure 3.3. Block of D590N channels by internal and external spermine.

(A) Block of D590N mutant channels by external spermine measured using the prepulse protocol. Recordings are from outside-out patches isolated from HEK 293 cells expressing GluA2(Q) D590N channels, with the external solution containing 5 μM spermine and the internal solution polyamine free. **(B)** I-V relations for peak glutamate-activated currents for the patch in (A) recorded with (*open circles*) or without (*concentric circles*) conditioning prepulses. **(C)** Mean %Block by 5 μM external spermine, as determined from peak currents with ($I_{control}$) or without (I_{block}) conditioning prepulses for D590N (*solid squares*, $n = 6$) or wild-type channels (*open diamonds*, from Figure 3.1 *E*). The continuous lines are fits of Equation 3.3B to the data points. The parameters for D590N are: $K_b = 2.46 \pm 0.47$ μM, $z\delta_b = 2.09 \pm 0.24$, $K_p = 1.00 \pm 0.18$ μM, and $z\delta_p = 1.27 \pm 0.10$ (mean ± SD). **(D)** Same as in (C), but for block of D590N channels by 81 μM internal spermine using peak currents with and without conditioning prepulses (*solid circles*, $n = 5$) and block of wild-type by 0.4 μM spermine (*open squares*, from Figure 3.1 *E*). The continuous lines are fits of Equation 3.3A to the data points.The parameters for D590N are : $K_b = 12.8 \pm 3.8$ μM, $z\delta_b = 2.28 \pm 0.27$, $K_p = 23.2 \pm 5.4$ μM, and $z\delta_p = 1.92 \pm 0.22$. **(E) and (F)** Kinetics and voltage dependence of block of D590N channels by 5 μM external spermine (E) and 81 μM internal spermine (F). Inverse of the mean τ_{block} values as a function of membrane potential (V_m) ($n \geq 6$). The solid lines through the data points are fits derived from Equations 3.6B and 3.6A. Estimates of $k_{on,ext}(0)$ and $z\delta_{on,ext}$ obtained from this fit are 11.0 ± 1.2 $s^{-1}\mu M^{-1}$ and 0.47 ± 0.05 (external); and 0.90 ± 0.12 $s^{-1}\mu M^{-1}$ and 0.35 ± 0.09 (internal) (mean ± SD). The dashed lines are the voltage dependences of $k_{off,int}$, $k_{off,ext}$, and [PA]$k_{on,ext}$ or [PA]$k_{on,int}$ (see Table 3.2).

Table 3.2. Steady-state and kinetic parameters describing block of open D590N AMPA receptor channels by internal and external spermine.

	Internal Spermine	External Spermine
K_b (μM)	12.8 ± 3.8	2.46 ± 0.47
$z\delta_b$	2.28 ± 0.27	2.09 ± 0.24
K_p (μM)	23.2 ± 5.4	1.00 ± 0.18
$z\delta_p$	1.92 ± 0.22	1.27 ± 0.10
$k_{on,int}(0)$ ($s^{-1}\mu M^{-1}$)	0.90 ± 0.12	--
$z\delta_{on,int}$	0.35 ± 0.09	--
$k_{on,ext}(0)$ ($s^{-1}\mu M^{-1}$)	--	11.0 ± 1.2
$z\delta_{on,ext}$	--	0.47 ± 0.05
$k_{off,int}(0)$ (s^{-1})	11.5 ± 3.7	11.0 ± 2.3
$z\delta_{off,int}$	1.93 ± 0.29	1.74 ± 0.11
$k_{off,ext}(0)$ (s^{-1})	20.8 ± 5.6	27.1 ± 5.9
$z\delta_{off,ext}$	2.27 ± 0.24	1.62 ± 0.24

Parameters were determined for homomeric GluA2(Q) D590N channels from block by 81 μM internal and 5 μM external spermine as described in the legend for Table 3.1. Values are shown ± SD.

→approximately the same amount for internal and external spermine (~25 mV and ~28 mV), suggesting that D590N may affect internal and external spermine block through a common mechanism.

To further resolve the effects of D590N on spermine block, I analyzed the kinetics of spermine block using Equations 3.6A and 3.6B as for wild-type channels (Figures 3.3 *E* and *F* for external and internal spermine, respectively, with the kinetic parameters listed in Table 3.2). Kinetically, the most dramatic effect of D590N is an ~400-fold reduction in $k_{on}(0)$ for internal spermine. For external spermine, $k_{on}(0)$ was reduced only ~3-fold and its voltage dependence was increased. In contrast, D590N changed $k_{off,int}(0)$ and $k_{off,ext}(0)$, parameters common to both internal and external block, by similar amounts for internal and external spermine, and did not affect their voltage dependences.

D590 is located at the internal entrance to the selectivity filter (Kuner et al., 2001), and has been proposed to affect polyamine block through a surface charge mechanism (Panchenko et al., 2001), consistent with the large reduction in $k_{on,int}(0)$ and the leftward shift in the voltage dependence of steady-state block for D590N channels. An internal negative surface charge would increase the concentration of spermine at the internal entrance to the channel, elevating the apparent value of $k_{on,int}(0)$ and thereby accounting for the greatly reduced value of $k_{on,int}(0)$ in D590N channels, and would also shift the transmembrane potential in the vicinity of the channel away from the holding potential toward negative potentials, accounting for the shift in the potential for maximal block (Green and Andersen, 1991). However, the selectivity filter is probably the location of the spermine blocking site (Panchenko et al., 1999), and thus D590 could also interact directly with spermine as part of the blocking site.

Elimination of a pure surface charge effect should not affect the voltage dependence of spermine association and dissociation and should decrease the apparent zero potential values of $k_{off,int}$ and $k_{on,ext}$, and increase the apparent zero potential value of $k_{off,ext}$, by amounts exponentially related to their voltage dependences and the surface potential (V_S), according to:

$$k(0),\mathrm{WT}/k(0),\mathrm{D590N} = \exp(\pm z\delta V_s F/RT) \qquad (3.8)$$

For $k_{on,int}$, the local shift in potential due to D590N is counteracted by the decrease in the effective spermine concentration. Assuming that the effective spermine concentration due to the surface potential is $[\mathrm{PA}]\exp(-4V_s F/RT)$, where 4 is the valence of spermine, the apparent value of $k_{on,int}(0)$ should be changed by elimination of a pure surface charge effect according to:

$$k_{on,int}(0),\mathrm{WT}/k_{on,int}(0),\mathrm{D590N} = \exp((z\delta-4)V_s F/RT) \qquad (3.9)$$

Solving Equation 3.8 for V_s gives values of ~-25 mV based on the WT/D590N ratios of $k_{off,int}(0)$ and $k_{off,ext}(0)$, suggesting that the effects of D590N on spermine dissociation are purely electrostatic in origin. However, solving Equation 3.9 for V_s based on the WT/D590N ratio of $k_{on,int}(0)$ gives a much larger value of –42 mV. This disparity may reflect the complex pore structure of AMPA receptors, in which wide aqueous vestibutles surround the narrow selectivity filter. It may be that the concentrating effect of the internal surface charge is enhanced within the small volume of the internal vestibule, resulting in a greater increase in the rate of spermine association than expected for a transfer from the bulk solution to the binding site. Nonetheless, the change in $z\delta_{on,ext}$ indicates that D590N does not affect spermine association from the external solution by a pure surface charge effect.

These results suggest that D590N affects spermine block through electrostatic and additional undefined mechanisms. The value of the surface potential due to D590 cannot be ascertained from these experiments, so the relative contributions of electrostatic and other mechanisms to the changes in rates cannot be determined. However, the similar values of V_S obtained from the ratios of the wild-type and mutant values of $k_{off,int}(0)$ and $k_{off,ext}(0)$ are unlikely to be the result of coincidence, and provide strong evidence that D590N affects spermine dissociation through an electrostatic mechanism without changing the intrinsic strength of spermine binding at the blocking site.

Recovery from spermine block at extreme negative but not extreme positive potentials suggests that spermine cannot dissociate from closed channels to the external solution.

In open channels, D590 seems to affect spermine dissociation through electrostatic interactions only. To see if this is true of closed channels as well, I wanted to measure the zero-potential rate constants ($k_{off,closed,int}$ and $k_{off,closed,ext}$) and voltage dependences ($z\delta_{off,closed,int}$ and $z\delta_{off,closed,ext}$) of spermine dissociation in closed channels. The affinity of closed AMPA receptors for internal spermine is apparently very high, despite a very slow rate of spermine association with closed channels from the internal solution (Supplementary Figure S3.1, Rozov et al., 1998). I therefore used extreme potentials to measure these parameters.

The experimental protocol used to measure the kinetic parameters of spermine dissociation in closed channels is illustrated in Figure 3.4 *A*. An initial glutamate application at the test potential (+20 mV) is made to block the channels. The membrane is

then held at various extreme potentials (–160 mV and +160 mV are shown in the figure) in the absence of glutamate for 1 s. Next, the membrane is returned to the test potential and the amount of recovery from block during the holding period is assayed by a test glutamate application.

As seen in the inset of Figure 3.4 *A*, the test current after the –160 mV holding period shows a small, rapidly decaying peak (*arrow*), approximately 3 times the amplitude of the steady-state current. A similar peak does not appear in the test current after the +160 mV holding period. This indicates that a small fraction of closed channels are relieved of spermine block during the –160 mV, but not during the +160 mV, holding period. I refer to recovery from block in closed channels at extreme potentials as "escape" of spermine from closed channels. Thus, spermine can escape from closed channels to the internal solution at –160 mV, but apparently not to the external solution at +160 mV.

The ratio of the peak to the steady-state test current (I_{peak}/I_{ss}) is plotted versus the holding potential (V_h) in Figure 3.4 *B* and *C* for 0.4 μM internal and 5 μM external spermine. These results indicate that spermine can dissociate from closed channels to the internal solution in a voltage-dependent manner, and thus that the spermine blocking site is located within the transmembrane electric field in closed channels. In contrast, there is no indication that spermine can dissociate from closed channels to the external solution. For internally applied spermine, the voltage-independent rate of association from the internal solution contributes to the macroscopic time course of recovery from block, making it difficult to quantify the voltage dependence of escape. However, the similar →

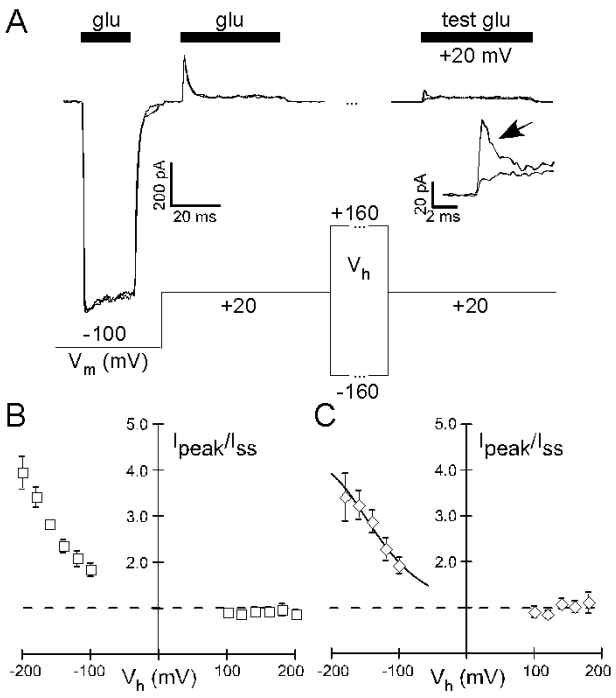

Figure 3.4. Dissociation of internally and externally applied spermine from closed AMPA receptor channels.

(A) Protocol to test for escape of spermine from closed channels. Recording conditions are the same as in Figure 3.1, with 0.4 μM internal spermine. The voltage protocol is shown below the current traces, and glutamate (5 mM) was applied as indictated by the thick lines. A conditioning prepulse of glutamate (20 ms) was applied at –100 mV to relieve the channels of spermine block. The membrane potential was then stepped to +20 mV and glutamate was applied (40 ms). Next, the membrane potential was stepped to a variety of extreme negative (-100 to -200 mV, -160 mV in the example shown) or positive (+100 to +200 mV, +160 in the example shown) test holding potentials in ±20 mV increments for 1 s (indicated by the dashed lines, raw currents not shown). Subsequently, a test glutamate pulse (40 ms) was given at +20 mV. The current records shown are approximately overlapping, except at the beginning of the test glutamate application, as shown on an expanded scale in the inset. The arrow indicates the current trace after holding at –160 mV. In this example, the ratios of peak current to steady-state current in response to the test application (I_{peak}/I_{ss}) were 3.1 for -160 mV and 0.70 for +160 mV. **(B) and (C)** Dependence of I_{peak}/I_{ss} on V_h for 0.4 μM internal (A) and 5 μM external (B) spermine. The line through the points in (C) is a fit of Equation 3.7 giving $k_{off,int,closed} = 0.055 \pm 0.036$ and $z\delta_{off,int,closed} = 0.48 \pm 0.12$ (external) (mean ± SD).

→values of the kinetic parameters describing dissociation, and the similar effects of D590N on dissociation, for internally and externally applied spermine (Table 3.1) indicate that the blocking site for spermine is the same whether it is applied internally or externally. I therefore assume that conclusions obtained with external spermine (which does not associate with closed channels at a significant rate relative to the time scale of my experiments—see Supplemental Figure S3.3) are also valid for the more physiologically relevant internal spermine. A fit of Equation 3.7 to the dependence of I_{peak}/I_{ss} on V_h for externally applied spermine (Figure 3.4 *C*, *solid line*), gives $k_{off,closed,int}(0) = 0.055 \pm 0.036$ and $z\delta_{off,closed,int} = 0.48 \pm 0.12$ (mean ± SD). The rate of dissociation to the internal solution for externally applied is ~1300 times smaller in closed channels than in open channels, and is much less voltage-dependent (cf. Table 3.1). Dissociation to the external solution is obviously strongly state-dependent as well, although I was unable to measure its rate or voltage dependence in closed channels.

D590N affects spermine block of closed and open channels by different mechanisms. Spermine is apparently unable to escape from closed AMPA receptor channels to the external solution at positive membrane potentials up to +200 mV (Figure 3.4). The state dependence of spermine dissociation to the external solution (and of association from the external solution), is probably due in part to state-dependent conformational changes at the external entrance to the pore that regulate access to the blocking site (Antonov et al., 1995; Blanpied et al., 1997; Sobolevsky et al., 1999; Jones et al., 2002; Qian and Johnson, 2002; Sobolevsky et al., 2002; Sobolevsky et al., 2003; Chang and Kuo, 2008). However, the state-dependence of dissociation to the internal solution suggests that the

intrinsic strength of binding at the spermine blocking site is increased by channel closing, which would also decrease the rate of dissociation to the external solution. It is therefore difficult to distinguish the relative contributions of the spermine blocking site and more external structural elements of the pore to the state dependence of $k_{off,ext}(0)$. D590N reduces the apparent affinity of open AMPA receptor channels for externally applied spermine at positive potentials (Figure 3.3, Table 3.2) and if it has a similar effect on affinity in closed channels could provide an opportunity to resolve this issue.

I tested for escape of externally applied spermine from closed D590N channels using the same protocol as for wild-type channels (Figure 3.4), with –20 mV as the test potential. Unlike wild-type channels, spermine could escape from closed D590N channels to the external (Figure 3.5 *A*, *upper current traces*) as well as the internal (Figure 3.5 *A*, *lower current traces*) solution with I_{peak}/I_{ss} dependent on V_h at both positive and negative potentials (Figure 3.5 *B*). This result indicates that the rate of spermine dissociation is strongly dependent on the negative charge at position 590.

The solid lines in Figure 3.5 *B* are fits of Equation 3.7 giving $k_{off,int,closed}(0) = 0.16 \pm 0.06$ s^{-1} and $z\delta_{off,int,closed} = 0.25 \pm 0.06$ (negative potentials); and $k_{off,ext,closed}(0) = 0.017 \pm 0.010$ s^{-1} and $z\delta_{off,ext,closed} = 0.54 \pm 0.09$ (positive potentials) (mean ± SD). The value of $k_{off,int}(0)$ for open D590N channels (11.0 s^{-1}) is only ~70 times the value of $k_{off,int}(0)$ for closed channels, compared with the ~1300-fold difference seen for wild-type channels. This result indicates that the charge on D590 plays a larger role in determining the rate of spermine dissociation to the internal solution in closed channels than in open channels. Thus channel closing seems to involve changes in the position of D590 that affect its →

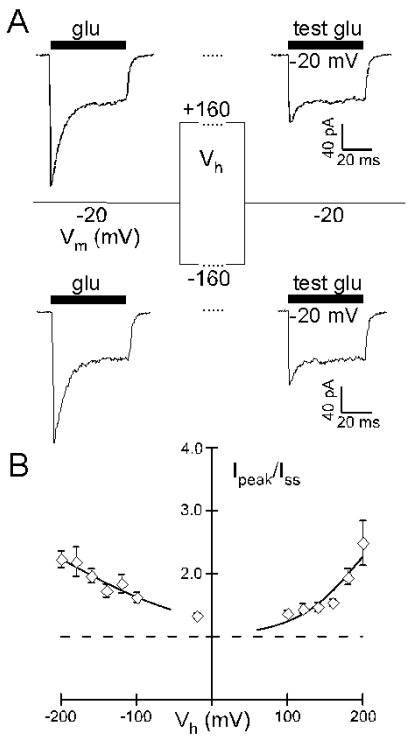

Figure 3.5. Dissociation of externally applied spermine from closed D590N channels.
(A) Example currents showing escape of externally applied spermine (5 μM) from closed channels. The voltage protocol was identical to that used in Figure 3.4, except that –20 mV was the test potential. Part of the voltage protocol is shown between the two pairs of current traces. The currents were preceded by a conditioning prepulse at –100 mV (not shown). Test currents in response to 5 mM glutamate show decaying peaks after holding at +160 mV (*top*) or –160 mV (*bottom*) for 1 s as indicated by the three dots. The peak to steady-state current ratios (I_{peak}/I_{ss}) of the test currents shown are 1.49 (+160 mV) and 1.54 (-160 mV). **(B)** Dependence of of I_{peak}/I_{ss} on V_h. The lines through the points are fits of Equation 3.7 giving $k_{off,int,closed}$ = 0.16 ± 0.06 s^{-1} and $z\delta_{off,int,closed}$ = 0.25 ± 0.06 at negative potentials; and $k_{off,ext,closed}$ = 0.017 ± 0.010 s^{-1} and $z\delta_{off,ext,closed}$ = 0.54 ± 0.09 at positive potentials (mean ± SD).

→ interactions with spermine. I was not able to measure $k_{off,ext,closed}(0)$ in wild-type channels, but assuming similar values of $z\delta_{off,ext,closed}$ in mutant and wild-type channels, this must be at least two orders of magnitude lower in wild-type than in D590N channels for escape of externally applied spermine not to have occured at +180 mV (Figure 3.4 *C*).

In contrast with its effect in open channels, the effects of D590N on spermine dissociation from closed channels do not appear electrostatic in origin. Whereas neutralization of a surface charge should alter $k_{off,int}(0)$ and $k_{off,ext}(0)$ in opposite directions without affecting their voltage dependences, as seen for open channels, D590N increased the rates of dissociation to both the internal and external solutions in closed channels and decreased $z\delta_{off,int,closed}$ from 0.48 to 0.25. The increases in both $k_{off,int}(0)$ and $k_{off,ext}(0)$ seen with D590N for closed channels suggest that, unlike in open channels, the side chain of D590 is part of the spermine binding site in closed channels. Thus D590 seems to affect spermine block through different mechanisms in open and closed channels.

DISCUSSION

I have characterized the state-dependent kinetics of spermine block of AMPA receptor channels, in wild-type channels and in mutant channels in which a conserved negatively charged residue in the pore loop has been neutralized. Comparison of kinetic parameters suggests that this residue is involved in gating-dependent rearrangements in the selectivity filter that underlie the state-dependence of block.

The spermine blocking site in AMPA receptor pores.

Spermine is a relatively long, multivalent blocker containing four amine groups, with each pair of positive charges separated by three or four carbon atoms. It is therefore likely that the different sets of amine groups interact sequentially with several electrostatically favorable locations as spermine moves through the channel. Hydrophobic interactions (Cu et al., 1998), and competitive or repulsive interactions with permeating ions (Bahring et al., 1997; Bowie et al., 1998) are additional important determinants of spermine block. Thus the "microscopic" rate constants measured in Figures 3.2 and 3.3 may actually represent the aggregate of several kinetic processes occurring below the resolution of my experiments. Nonetheless, the kinetic parameters obtained for dissociation of internal and external spermine (Table 3.1) indicate that the complex process of spermine dissociation is well approximated by a single binding site model, and that this model is appropriate for investigating the effects of the D590N mutation.

Although my goal is not to define the mechanism of spermine block at the molecular level, it is useful to know the approximate location of the blocking site when interpreting changes in the kinetics of spermine block in terms of specific structural

changes in the pore. Previous work has shown that the size of the residue at the Q/R site, as well as its charge, is critical for block by internal polyamines (Panchenko et al., 1999). This site is located four residues upstream of D590, and based on the accessibility of substituted cysteines to internal and external methanethiosulfonate reagents, the Q/R site and D590 are located at the external and internal entrances, respectively, to the selectivity filter (Kuner et al., 2001), and interactions with permeant ions are most likely to occur in this narrow region. Based on these considerations, it seems likely that the spermine blocking sites is located within a limited region of the pore encompassing D590 and the Q/R site.

The role of D590 in the state-dependence of spermine block.

My results suggest that D590 affects spermine block through different mechanisms in open and closed channels: in open channels, it acts primarily through a surface charge mechanism, but in closed channels it interacts directly with spermine as part of the blocking site. The conformational changes that determine the state dependence of the channel's affinity for spermine could be quite subtle and need not involve significant changes in the diameter of the selectivity filter. Indeed, ion channel function is in general dependent on the precise molecular structure of selectivity filters, and can be regulated by small changes in the position of just a few selectivity filter residues (e.g. , Dutzler et al., 2003; Berneche and Roux, 2005; Cordero-Morales et al., 2006a; Cordero-Morales et al., 2006b). Obviously it is not possible to define structural changes at the molecular level from the experiments described here, but one possibility is that the carboxyl group of D590 does not face the ion permeation pathway in open channels and therefore affects

spermine block through electrostatic interactions only, but upon channel closure the carboxyl group reorients to face the permeation pathway and interacts directly with spermine.

D590 clearly has a major role in determining the state dependence of spermine block, but spermine dissociation is still state-dependent in D590N channels, indicating that additional factors contribute to the state dependence of block. These additional factors probably include rearrangements at the external entrance to the pore (Antonov et al., 1995; Blanpied et al., 1997; Sobolevsky et al., 1999; Jones et al., 2002; Qian and Johnson, 2002; Sobolevsky et al., 2002; Sobolevsky et al., 2003; Chang and Kuo, 2008), and the interaction of spermine with permeant ions (Bahring et al., 1997; Bowie et al., 1998), which would be expected to occur in open but not in closed channels. One caveat to the interpretation of experiments on D590N channels, however, is that this mutation may cause unanticipated changes in channel structure extending beyond its immediate vicinity. For example, the pore-lining helices could adjust their position to accommodate structural changes in the pore loop due to D590N. However, the kinetics of deactivation and desensitization were identical in wild-type (τ_{deact}, 0.56 ± 0.04 ms; τ_{deact}, 6.26 ± 0.25 ms (n = 11)) and D590N channels (τ_{deact}, 0.56 ± 0.11 ms; τ_{ds}, 6.11 ± 0.21 ms (n = 6)), suggesting that D590N does not disrupt normal channel function (data not shown).

In conclusion, I propose that gating-dependent structural rearrangements in the selectivity filter, critically including movement of D590, are a major determinant of the state dependence of polyamine block in AMPA receptors. Rearrangements in the selectivity filter of K^+ channels underlying inactivation have been characterized at the molecular level (Berneche and Roux, 2005; Cordero-Morales et al., 2006a; Cordero-

Morales et al., 2006b), so it is interesting to speculate that homologous rearrangements occur in glutamate receptors. Additionally, polyamine block of AMPA receptors is regulated by interaction with stargazin (Soto et al., 2007), but whether this regulation involves rearrangements of the selectivity filter is unknown.

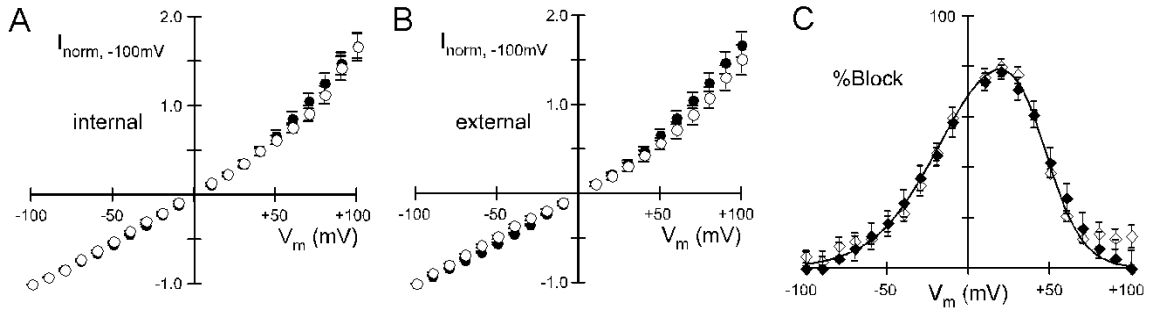

Supplemental Figure S3.1. Conditioning prepulses are effective at relieving AMPA receptor channels of internal and external spermine block.

(A) I-V relations, normalized to the current at –100 mV ($I_{norm, -100mV}$) for peak glutamate-activated currents following conditioning prepulses in the presence of 0.4 μM internal spermine (*open circles*, $n = 7$) or steady-state currents in the absence of polyamines (*solid circles*, $n = 9$). At any potential, none of the normalized values were significantly different. Some error bars are smaller than the symbol size. **(B)** Same as in (A), except peak currents are in the presence of 5 μM external spermine (*open circles*, $n = 5$). **(C)** Mean %Block, as determined from peak currents with ($I_{control}$) and without (I_{block}) conditioning prepulses preceding the test application (%Block = $100(I_{control} - I_{block})/I_{control}$) (*open diamonds*, $n = 5$). Also shown is the mean %Block determined from steady-state currents recorded in outside-out patches with the standard high-ATP internal solution before ($I_{control}$) and after (I_{block}) washing in 5 μM external spermine (*solids diamonds, n* = 8). At any one potential, values of %Block determined by either method were not significantly different. The continuous line is a fit of Equation 3.3B to the combined data sets for the prepulse and wash-in protocols (n =13), yielding parameters (mean ± SD): K_b = 0.18 ± 0.06 μM, $z\delta_b$ = 1.87 ± 0.15, K_p = 2.27 ± 0.26 μM, and $z\delta_p$ = 1.29 ± 0.09.

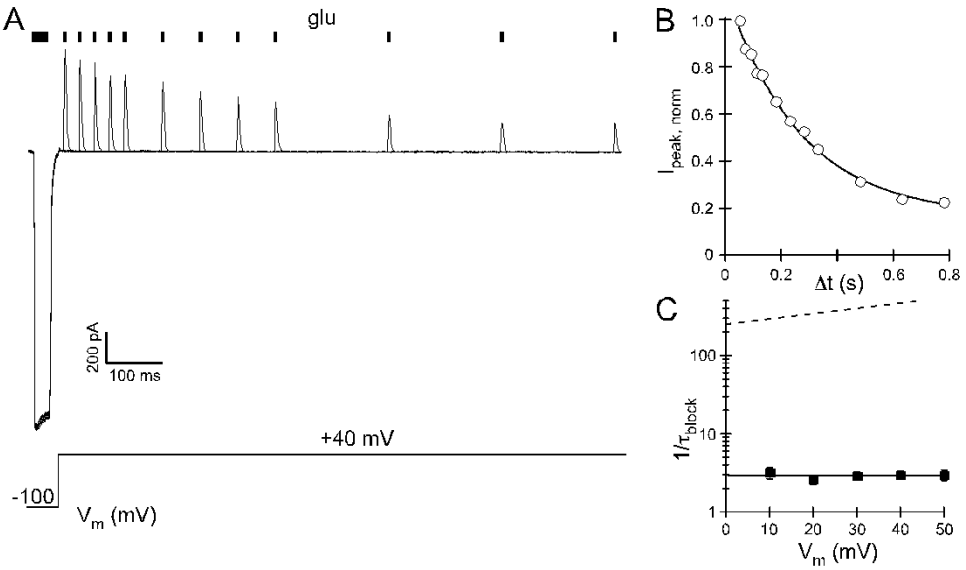

Supplemental Figure S3.2. Voltage-independent block of closed AMPA receptor channels by internal spermine.

(A) Protocol to measure block of closed AMPA receptors by internal spermine. The internal solution contained 0.4 μM spermine. The voltage protocol is shown below the current traces, and glutamate (5 mM) was applied as indictated by the thick lines. While holding the membrane at –100 mV, a conditioning glutamate prepulse (20 ms) was applied to relieve the channels from spermine block. At various time intervals (Δt) after stepping to the test potential (+40 mV in the example shown), brief test pulses of glutamate (5 ms) were applied. The initial Δt was 10 ms. **(B)** Peak current amplitudes during the test glutamate application, normalized to that at Δt = 10 ms, plotted as a function of Δt. The solid line is a single exponential fit yielding τ_{block} = 268 ms. **(C)** Voltage dependence of block of closed AMPA receptor channels. Inverse of the mean τ_{block} values for block of closed channels by 0.4 μM internal spermine (*solid squares*, $n \geq 4$), as determined using the protocol in (A), plotted as a function of membrane potential (V_m). The straight line through the data points is a fit of $1/\tau_{on}(V_m) = [PA]k_{on,int,closed}(0)\exp(z\delta V_m F/RT)$. Estimates of $k_{on,int,closed}(0)$ and $z\delta_{on,int,closed}$ obtained from this fit are 6.17 ± 1.09 $s^{-1}\mu M^{-1}$ and 0.00002 ± 0.0002 (mean ± SD). Some error bars are smaller than the symbol size. The dashed lines is the estimated voltage dependence of $[PA]k_{on,int}$ for open channels from Figure 3.2.

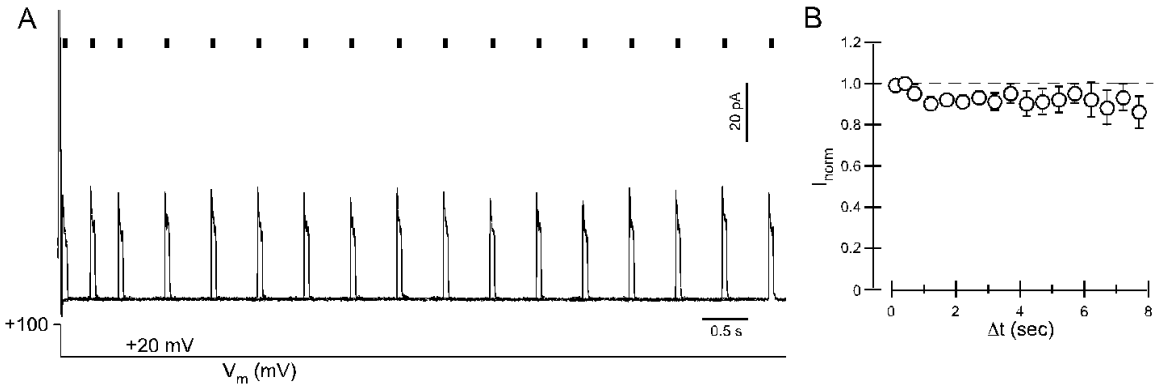

Supplemental Figure S3.3. External spermine block does not recover in closed channels.

(A) Protocol to test for block of closed AMPA receptors by external spermine (5 μM). The voltage protocol is shown below the current traces, and glutamate (5 mM) was applied as indictated by the thick lines. While holding the membrane at +100 mV, a conditioning glutamate prepulse (10 ms) was applied to relieve the channels from spermine block. At various time intervals (Δt) after stepping to the test potential (+20 mV in the example shown) test pulses of glutamate (50 ms) were applied as indicated by the thick black bars. The initial Δt was 20 ms. **(B)** Mean peak current amplitudes after the conditioning prepulse, plotted as function of Δt and normalized to the peak current amplitude at Δt = 20 ms (n = 7). None of the values were significantly different from the control value. Similar results were obtained at –20 mV and in D590N channels. These results indicate that external spermine cannot associate with closed channels or does so at a rate that is very slow relative to the rates of dissociation from closed channels.

CHAPTER 4: LOW- AND HIGH-AFFINITY GATING MODES IN AMPA RECEPTORS

INTRODUCTION

The most fundamental aspect of ligand-gated ion channel function is the relationship between ligand binding and opening/closing of the ion channel. Within the glutamate receptor family of ligand-gated ion channels, NMDA receptors and AMPA receptors both have four subunit-associated ligand-binding sites, but beyond this basic similarity of binding site stoichiometry, they differ strikingly in terms of the relationship between ligand binding and ion channel opening. NMDA receptors undergo concerted gating in which all four subunits must bind agonists for the channel to open, with the open-to-closed transition occuring essentially simultaneously in all subunits (Banke and Traynelis, 2003; Erreger et al., 2004; Kussius and Popescu, 2009). Thus, at the level of the individual NMDA receptor subunit, ligand binding and channel opening/closing are not strongly correlated. In contrast, AMPA receptor subunits that have bound glutamate can apparently transition between open and closed ion channel conformations independently of the ion channel conformation or binding site occupancy of the other subunits (Rosenmund et al., 1998; Smith and Howe, 2000), resulting in the multiple conductance levels that are a prominent feature of native and recombinant microscopic AMPA receptor currents (Howe et al., 1991; Wyllie et al., 1993; Swanson et al., 1997; Derkach et al., 1999; Banke et al., 2000; Smith et al., 2000; Jin et al., 2003; Tomita et al., 2005; Gebhardt and Cull-Candy, 2006; Zhang et al., 2008). Independent subunit gating

allows for a much stronger correlation between agonist binding and ion channel opening/closing than concerted gating.

NMDA and AMPA receptors also show dramatically different maximal open probabilities. Although NMDA receptor current amplitudes in glycine saturate at glutamate concentrations (~100 μM) an order of magnitude lower than those required to saturate AMPA receptor currents (~1 mM), the maximal open probability (in the absence of desensitization) for NMDA receptors is ~50% or less under most conditions (Erreger et al., 2004), while that for AMPA receptors is ~90-100% (Rosenmund et al., 1998; Smith and Howe, 2000; Smith et al., 2000). The shut time distributions for NMDA receptors show several exponential components associated with conformational changes preceding the concerted opening transition in the ion channel (Banke and Traynelis, 2003; Popescu and Auerbach, 2003; Auerbach and Zhou, 2005; Kussius and Popescu, 2009). Thus the relatively low maximal open probability of NMDA receptors may in part reflect the fact that separate conformational changes must occur either simultaneously or sequentially in all four subunits before the ion channel can open. In AMPA receptors, however, the high maximal open probability is the result of independent subunit gating. In saturating glutamate, and in the absence of desensitization, the probability that an individual subunit is in the open conformation has been estimated as 67% (Jin et al., 2003), so while each individual subunit may be closed approximately one third of the time, all four subunits are rarely closed simultaneously.

The differences between NMDA and AMPA receptor gating no doubt reflect their distinct synaptic roles, but are also remarkable with regard to the structural similarities between NMDA and AMPA receptors (Furukawa et al., 2005; Mayer, 2006; Oswald et

al., 2007). How do two such closely related ion channels display such disparate behavior? A logical first step in understanding the function of ligand-gated ion channels is to study their single-channel behavior in saturating agonist concentrations, and in the absence of additional gating processes such as channel block and desensitization, allowing opening and closing to be observed in isolation from other gating processes. Here, I compare the behavior of non-desensitizing AMPA receptors in saturating and subsaturating glutamate, and at negative and positive membrane potentials, with an emphasis on the relative occupancy of the various conductance levels. In agreement with the prevailing model of independent subunit gating in AMPA receptors, I find that the relative occupancies of the conductance levels follow a binomial distribution in saturating glutamate. In subsaturating glutamate, however, the relative occupancies diverge dramatically from a binomial distribution, with openings to the higher conductance levels occurring much more often than predicted. Surprisingly, channel activity in subsaturating glutamate was identical to that in saturating glutamate during periods lasting several milliseconds. I propose that the affinity of AMPA receptors for glutamate is regulated by previously unknown subunit interactions, such that affinity is greatly increased by the binding of multiple agonist molecules.

MATERIALS AND METHODS

Molecular biology and heterologous expression.

All experiments were performed with previously described expression constructs for the wild-type rat, "flip" splice-variant GluA1, GluA2(Q), or GluA4 subunits (Collingridge et al., 2009) where Q indicates the residue occupying the Q/R editing site (Sommer et al., 1991).

Channels were transiently expressed in human embryonic kidney 293 (HEK 293) cells. HEK 293 cells were transfected with glutamate receptor subunits using FuGene 6 (Roche, Indianapolis, IN). A vector for enhanced green fluorescent protein (pEGFP-C1, Clontech, Palo Alto, CA) was co-transfected at a ratio of 1:9 (pEGFP-C1:subunit). Recordings were made one to three days after transfection.

Current recording.

Currents in outside-out patches, isolated from HEK 293 cells, were recorded at room temperature (20-23°C). External solutions were applied using a piezo-driven double barrel application system made from theta glass. One barrel contained the external solution; the other contained the same solution with added glutamate (0.06-10 mM). For experiments involving desensitizing channels, I measured the solution exchange rate using the 10-90% rise time when switching between the standard external solution and a 10% dilution of that solution. Patches were not included in the analysis if the rise time was >300 μs. I did not use series resistance compensation or correct for junction potentials.

Macroscopic currents. Macroscopic currents were recorded using an EPC-9 amplifier (HEKA Elektronik, Lambrecht, Germany) with PULSE or PatchMaster software (HEKA Elektronik), low-pass filtered at 2.8 kHz (-3 dB) using an 8 pole low-pass Bessel filter and digitized at 50 or 100 kHz. Pipettes had resistances of 2-10 MΩ when filled with the pipette solution and measured in the external solution.

Microscopic currents. Microscopic currents were recorded using an Axopatch 200B amplifier (Molecular Devices, Sunnyvale, CA) with PatchMaster software and were initially filtered at 10 kHz using a 4 pole low-pass Bessel filter and digitized at 50 kHz. Pipettes were pulled from thick-walled borosilicate glass and fire polished immediately before recording and had resistances of 10-40 MΩ when filled with the pipette solution and measured in the external solution. To reduce noise during microscopic recordings, currents were recorded with the headstage set to capacitive feedback mode, pipettes were coated three times with Sylgard (Dow Corning, Midland, MI), the pipette holder was cleaned daily with 70% ethanol and stored in Drierite overnight, and care was taken to keep the level of the bath solution as low as possible. To eliminate noise resulting from oscillation of the piezo device at the start of the glutamate application, voltage steps to the piezo device were filtered at 20 kHz using an 8 pole Bessel filter.

Solutions. For macroscopic and microscopic recordings, the internal (pipette) solution contained (in mM): 110 NaCl, 20 Na_2ATP (to chelate endogenous polyamines (Rozov et al., 1998)), 5 Hepes, and 1 Bapta, pH 7.2 (NaOH). The external solution contained (in mM): 140 NaCl, and10 Hepes, ph 7.2 (NaOH). Unless otherwise indicated, cyclothiazide (CTZ, 30 μM) was included to prevent desensitization (Partin et al., 1993). For microscopic and in some instances macroscopic recordings, 1 mM $CaCl_2$ was included.

Analysis and idealization of single-channel currents.

Current records were exported from PatchMaster to Igor Pro (WaveMetrics, Inc., Lake Oswego, OR) for initial processing (subtraction of the mean baseline current, resampling, and additional filtering) and characterization. Records with sufficiently low baseline noise (see below) were exported from Igor Pro to QuB (www.qub.buffalo.edu) for idealization, and idealized records were then exported back to Igor Pro, Mathematica (Wolfram Research, Inc., Champaign, IL), or ChannelLab (Synaptosoft, Inc., Decatur, GA) for additional analysis.

A typical single-channel experiment consisted of 200 ms applications of saturating (5 mM) or subsaturating (0.06 mM) glutamate at membrane potentials alternating between –80 and +80 mV. Although these recording times are much briefer than those of typical single-channel experiments, this was necessary to prevent the patches from becoming unstable as a result of prolonged depolarization to +80 mV. However, the open probability of AMPA receptors in the presence of CTZ is very high in saturating and relatively high in subsaturating glutamate, and the mean lifetimes of each of the four AMPA receptor conductance levels are on the order of 100-200 μs, so the idealized record for a single 200 ms glutamate application typically contained ~1000 events for saturating glutamate and ~100 events for subsaturating glutamate, and at least 1 second of channel activity was recorded for each experimental condition analyzed.

Patches with baseline root mean squared (rms) noise less than 500 fA after additional filtering at 5 kHz with a digital Gaussian filter (for a final filter frequency of ~4.5 kHz), and with similar baseline noise at –80 mV and +80 mV, were used for initial analysis of the rectification and concentration response properties of microscopic currents

(Supplemental Figure S4.2). Only patches with baseline rms noise ≤ 300 fA after filtering at 4 kHz (final frequency ~3.7 kHz) were used for analysis of the variance of microscopic glutamate-activated currents (Supplemental Figure S4.3) and idealization in QuB (Figures 4.1 and 4.4).

Idealization of single-channel records using QuB. Idealization was performed after filtering at a final frequency of ~3.7 kHz and resampling at 25 kHz, with a dead time of 40 or 80 μs. Both values of the dead time gave essentially identical results (Supplemental Table S4.2), but results are reported and the idealizations pictured are for 40 μs. Records were idealized using the segmental k-means algorithm (SKM) (Qin, 2004), which requires a kinetic model of the data as an initial input. The models I used for idealization had four open classes that were all connected to one another and to a closed class. This closed class was connected to one additional closed class, or two additional closed classes in series; the additional closed classes were not connected to the open classes. In my preliminary attempts at idealization using SKM, I estimated the mean current levels and standard deviations of the open classes using the Grab Amplitudes feature of QuB and allowed the mean current levels and standard deviations to be reestimated during optimization of the model, but I found that this often resulted, illogically, in open classes with standard deviations less than the baseline rms noise. I therefore set the standard deviation of all classes equal to the baseline rms noise and fixed the standard deviations during the idealization. In doing so, I assume that all of the variance of microscopic AMPA receptor currents is due to transitions between conductance levels, and that the conductance levels do not display significant open channel noise. For idealization of currents activated by saturating glutamate, I set the initial current amplitudes of the four

open classes to ±0.6, 1.2, 1.8, and 2.9 pA and allowed the current levels to be reestimated during the idealization. The initial values were based on previously published values of the single channel conductance levels for recombinant homomeric GluA2(Q) channels (Zhang et al., 2008), assuming Ohmic conductance. For idealization of currents recorded at –80 mV, the final current levels were only slightly different than the initial estimates; for currents recorded at +80 mV, the final current levels were generally larger than the initial estimates (Figure 4.5 *B*).

For idealization of currents activated by subsaturating glutamate, the current levels were fixed to the levels obtained for saturating glutamate in the same patch and their standard deviations were fixed to the baseline rms noise. In order to control for false events (i.e., variations in baseline noise interpreted as openings to the lowest conductance level) in the idealization of the relatively low open probability channel activity occuring in subsaturating glutamate, I idealized the adjacent baseline segments along with the glutamate-activated current. In all patches idealized, false openings to the lowest conductance level constituted ≤1% of the total time for the idealized baseline records. Although the relative occupancies of O3 and O4 in subsaturating glutamate at –80 mV are similar to the proportion of false events, all of the false events were O1 events, so the occurrence of these conductance levels cannot be accounted for by false events. It is therefore unlikely that false events significantly bias my estimation of the relative occupancy of the current levels in subsaturating glutamate.

Statistical analysis.

For statistical analysis, I used Microsoft Excel (Redmond, WA). A Student's *t*-test was used to define statistical differences. Significance was assumed if $P < 0.05$. Results are

shown graphically as mean ± SEM. Curve fitting was performed using non-linar least squares fitting in IgorPro. Distributions of events were fit with probability density functions using the Maximum Likelihood method.

RESULTS

To study activation gating in AMPA receptors, I recorded the activity of individual GluA2(Q) channels in outside-out patches under conditions designed to minimize channel block and desensitization. Specifically, ATP was included in the internal solution to eliminate polyamine block, and glutamate was applied in brief (200 ms) pulses with cyclothiazide (CTZ, 30 μM) included in the external solution to minimize desensitization. These brief glutamate pulses also allowed me to monitor the baseline current level, which would otherwise have been difficult in saturating glutamate due to the high open probability.

AMPA receptor subunit interactions are apparent in subsaturating but not saturating glutamate.

Figure 4.1 shows single-channel AMPA receptor currents in response to 200 ms applications of saturating (5 mM, Figure 4.1 *A*) and subsaturating (0.06 mM, Figure 4.1 *B*) glutamate at –80 mV. For macroscopic currents, 0.06 mM glutamate gave current amplitudes that were ~10% of the maximal response at –80 mV. The current records are shown overlaid with the idealization of the current obtained using the segmental k-means (SKM) algorithm of QuB (Qin, 2004). The algorithm gave subjectively plausible idealizations, although there were inevitable ambiguities in the classification of events (see enlarged portions of the records in Figure 4.1 *A*-*B*). At –80 mV, the estimated conductances of the four open levels (O1-O4) were highly reproducible (mean ± SEM: O1, 7.6 ± 0.2 pS; O2, 15.4 ± 0.2, pS; O3, 22.8 ± 0.3 pS; O4, 30.8 ± 0.5 pS; n = 6) and were consistent with previously reported values (Supplemental Table S4.1), although →

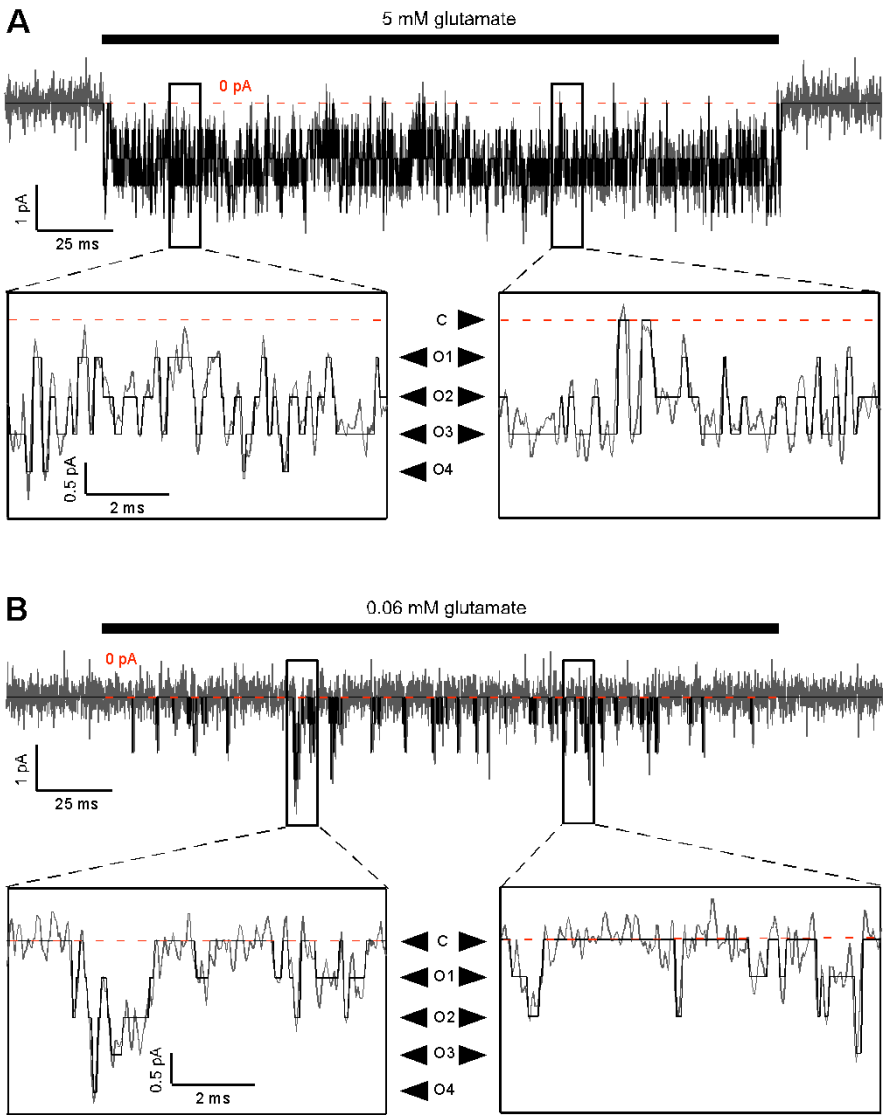

Figure 4.1. AMPA receptor single-channel currents in the absence of polyamine block and desensitization, in saturating and subsaturating glutamate at –80 mV.

(A) Current from an outside-out patch containing a single GluA2(Q) channel in response to a 200 ms application of 5 mM glutamate, recorded at –80 mV, along with the idealization of the record generated by the SKM algorithm of QuB. The current was recorded in the presence of CTZ (30 μM) to block desensitization and in the absence of polyamines. The record is shown sampled at 25 kHz and filtered at ~3.7 kHz, the same sampling and filter frequencies used for idealization. The four open current levels at –80 mV in this patch were –0.60 (O1), –1.24 (O2), –1.84 (O3), and –2.45 (O4) pA, as seen more clearly in the expanded sections of the records. **(B)** Same as in (A), but showing current from the same patch in 0.06 mM glutamate.

→four conductance levels have not been detected in all studies. In saturating glutamate, the channel occupied primarily intermediate conductance levels (Figure 4.2), with openings to O2 and O3 accounting for the majority of the total occupancy (O2, 33 ± 4%; O3, 36 ± 7%). Closings (C, 6 ± 3%) and openings to the remaining conductance levels were also detected (O1, 18 ± 5%; O4, 7 ± 2%; n = 6). The relative occupancy in saturating glutamate at –80 mV thus resembles a binomial distribution for four independent trials, with the conductance level determined by the number of successes (i.e., the number of subunits in the open conformation) (Figure 4.2 *B*). The probability of success that gave the best fit to the combined data set was 58 ± 3%. This result is consistent with the idea that AMPA receptor subunits gate independently (Rosenmund et al., 1998), and is similar to the previously estimated individual subunit open probability of 67% (Jin et al., 2003).

In subsaturating glutamate, the opening reaction is more complicated than in saturating glutamate, involving a glutamate-binding step followed by an ion channel gating step. Still, the steady-state open probability should be the same in all subunits and the relative occupancies should follow a binomial distribution if the subunits are independent—an important, but possibly counter-intuitive point. In subsaturating glutamate at –80 mV, the shut probability was 90 ± 1%, but all conductance levels were represented during the open periods (O1, 4 ± 0.4; O2, 3 ± 0.6; O3, 2 ± 0.4; O4, 0.4 ± 0.2; n = 5) (Figure 4.2). In contrast to saturating glutamate, the binomial distribution fails to describe the relative occupancies in subsaturating glutamate (Figure 4.2 *C*). Here, the best fitting individual subunit open probability, 2 ± 0.2%, predicts the relative occupancies of

C and O1 reasonably accurately (C, 93% predicted versus 90% actual; and O1, 7% predicted versus 4% actual), but predicts that O3 and O4 essentially never occur →

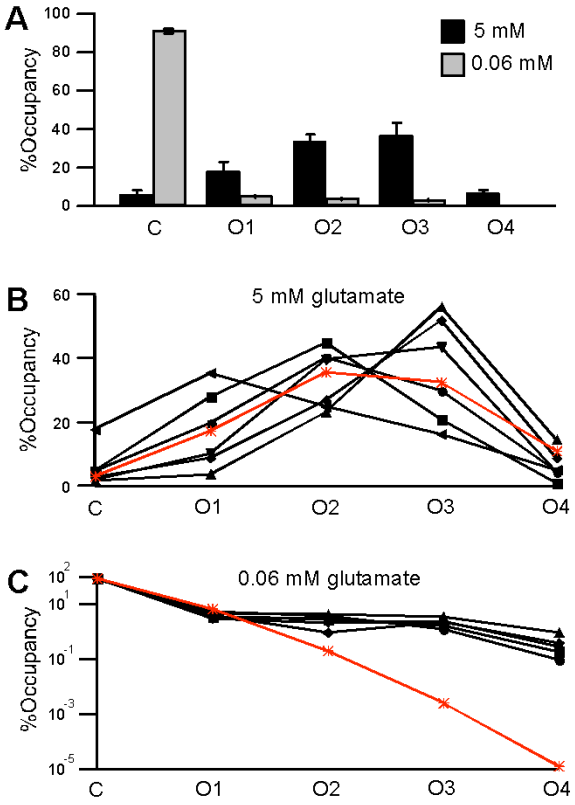

Figure 4.2. The relative occupancies of AMPA receptor conductance levels at –80 mV approximate a binomial distribution in saturating but not subsaturating glutamate.

(A) Mean time spent at each of the open conductance levels (C, O1-O4) at –80 mV, as a fraction of the total time that the channel was exposed to agonist (%Occupancy) for 5 mM (*black*, $n = 6$) and 0.06 mM (*light gray*, $n = 5$) glutamate. **(B)** Relative occupancies of the five conductance levels in 5 mM glutamate at –80 mV for each of the six patches used to determine the mean in (A) (*solid symbols and lines),* along with the relative occupancies predicted by the binomial distribution (**, red line*). The individual subunit open probability that gave the best fit for the binomial distribution (± SD) was 58% (± 3%). **(C)** As in (B), but for currents in 0.06 mM glutamate and excluding one patch for which I did not obtain sufficient data in subsaturating glutamate, plotted on a logarithmic scale. The individual subunit open probability that gave the best fit for the binomial distribution (± SD) was 2% (± 0.2%).

→(O3, $3x10^{-3}$ % predicted versus 2% actual; and O4, $2x10^{-5}$ % predicted versus 0.4% actual). The small amounts of O3 and O4 in the idealized records are unlikely to result from false events (see Materials and Methods), but nonetheless make it problematic to apply least-squares fitting of binomial distributions to the data, since orders of magnitude differences between small numbers will have little influence on the fit. Despite this caveat, this result suggests that, in subsaturating glutamate, AMPA receptor subunits interact in some fashion that causes the relative occupancies to deviate from the predictions of absolute subunit independence.

How can AMPA receptor subunits interact in subsaturating glutamate, while apparently gating independently in saturating glutamate? One explanation is that the apparent independent subunit gating in saturating glutamate is actually the result of an interactive gating process that coincidentally produces binomially distributed occupancies. An alternative explanation that retains the binomial distribution as a physically meaningful description of the data in saturating glutamate is that AMPA receptors display subunit-independent behavior at the level of the ion channel but subunit-interactive behavior at the level of ligand-binding domain. With this idea in mind, I noted that, in subsaturating glutamate, open periods containing O4 events were much longer than open periods containing only lower conductance events (Supplemental Table S4.2). This result suggests that these long open periods result from subunit interactions that only occur when the receptor binds multiple agonist molecules. Because of the rarity of open periods containing O4, however, I was unable to explore this idea further using my data in subsaturating glutamate at –80 mV.

Voltage-dependent gating enhances subunit interactions in subsaturating glutamate. In the absence of block by intracellular polyamines, macroscopic current-voltage (I-V) relations for AMPA receptors are outwardly rectifying with the degree of outward rectification greater in subsaturating than in saturating agonist concentrations (Figure 4.3 *A*-*C*) (Raman and Trussell, 1995b). The effect of agonist concentration on outward rectification is similar for GluA1, GluA2(Q), and GluA4 channels, and also occurs for peak currents when desensitization is intact (Figure 4.3 *D*), suggesting that concentration-dependent outward rectification is a general property of AMPA receptors and not an artifact of conformational restrictions due to the binding of CTZ (Jin et al., 2005). Previously, it was concluded based on macroscopic current variance analysis that in saturating agonist concentrations outward rectification primarily resulted from an increase in single-channel conductance, and that in subsaturating agonist concentrations it also included a voltage-dependent gating component (Raman and Trussell, 1995b). However, this study was done before AMPA receptors were known to have multiple conductance levels, so it is difficult to tell whether the apparent increase in single-channel conductance reflects an actual increase in the conductance of any of the open levels, a change in the relative occupancy of the conductance levels due to voltage dependence of the individual subunit open probability, or some combination thereof. I hypothesized that the increased outward rectification in subsaturating glutamate might reflect a voltage-dependent enhancement of the subunit interactions that I saw at –80 mV but was unable to analyze in detail. I therefore compared single-channel currents in saturating and subsaturating glutamate at +80 mV.

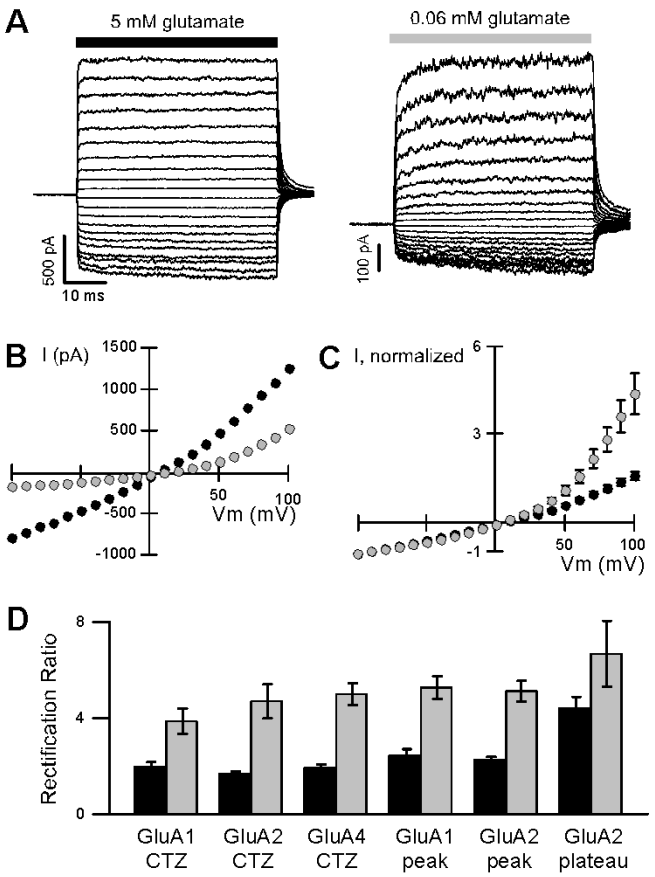

Figure 4.3. Outward rectification of macroscopic AMPA receptor currents in saturating and subsaturating glutamate.

(A) Example glutamate-activated currents in response to 100 ms applications of saturating (5 mM, *left*) or subsaturating (0.06 mM, *right*) glutamate (*bars*). Currents were recorded in outside-out patches obtained from HEK 293 cells expressing GluA2(Q) receptors, in CTZ and in the absence of polyamines, at membrane potentials from –100 to +100 mV (in 10 mV increments). **(B)** Steady-state I-V relations for the patch shown in (A) in saturating (*black*) or subsaturating (*light gray*) glutamate. **(C)** Mean I-V relations, normalized to the current amplitude at –100 mV, for GluA2(Q) receptors in saturating and subsaturating glutamate ($n = 9$). **(D)** Mean ratios of current amplitudes at +100 mV to those at –100 mV (Rectification Ratios) for steady state currents in CTZ or for peak currents (peak) and steady-state currents (plateau) in response to fast agonist application without CTZ, for various homomeric AMPA receptors. Currents were measured either in saturating (5-10 mM) or subsaturating (0.06-0.2 mM) glutamate. Mean values (± SEM) in saturating and subsaturating glutamate were 1.97 ± 0.19 & 3.86 ± 0.53 (GluA1, CTZ, $n = 3$), 1.66 ± 0.13 & 4.70 ± 0.71 (GluA2(Q), CTZ, $n = 9$), 1.92 ± 0.15 & 4.99 ± 0.46 (GluA4, CTZ, $n = 5$), 2.44 ± 0.26 & 5.25 ± 0.47 (GluA1, peak, $n = 7$), 2.27 ± 0.13 & 5.11 ± 0.43 (GluA2(Q), peak, $n = 11$), and 4.40 ± 0.49 & 6.66 ± 1.37 (GluA2(Q), plateau, $n = 6$). The differences in outward rectification in saturating and subsaturating glutamate were statistically significant for all conditions (one-tailed paired *t*-test, $P < 0.05$).

Figure 4.4 shows single-channel AMPA receptor currents in response to 200 ms applications of saturating (Figure 4.4 *A*) and subsaturating (Figure 4.4 *B*) glutamate at +80 mV, from the same patch shown in Figure 4.1 at –80 mV, along with the SKM idealization. The amount of outward rectification in macroscopic and microscopic recordings was similar for both saturating and subsaturating glutamate concentrations (Supplemental Figure S4.2). The open conductance levels at +80 mV were higher than those at –80 mV and more variable (O1, 8.7 ± 0.7 pS1; O2, 19.5 ± 1.1 pS; O3, 29.3 ± 1.6 pS; O4, 38.5 ± 2.4 pS; n = 6) (Figure 4.5 *B*). However, the amount of outward rectification was independent of the conductance level with the mean ratio of the conductance at +80 mV to that at –80 mV being ~1.2 for all levels (1.14 ± 0.9, O1; 1.27 ± 0.07, O2; 1.28 ± 0.06, O3; 1.24 ± 0.06, O4). In saturating glutamate, and in contrast to the results at –80 mV, openings to higher conductance levels predominated at +80 mV, with O3 and O4 accounting for most of the occupancy (47 ± 4%, O3; and 33 ± 5 %, O4), and closings and openings to lower conductance levels occurring rarely (C, 6 ± 2%; O1, 4 ± 1%; O2, 11 ± 2 %; n = 6) (Figure 4.5 *A*; see also Supplemental Figure S4.3). These results indicate that outward rectification in saturating glutamate involves both rectification of the single-channel conductance (Figure 4.5 *B*) and voltage-dependent gating (Figure 4.5 *C*).

The relative occupancies of the conductance levels in saturating glutamate at +80 mV also resemble a binomial distribution (Figure 4.5 *D*). The best fitting individual subunit open probability was 78 ± 2% (compared with 58% at –80 mV). This value predicts a substantially smaller occupancy of the baseline conductance level than →

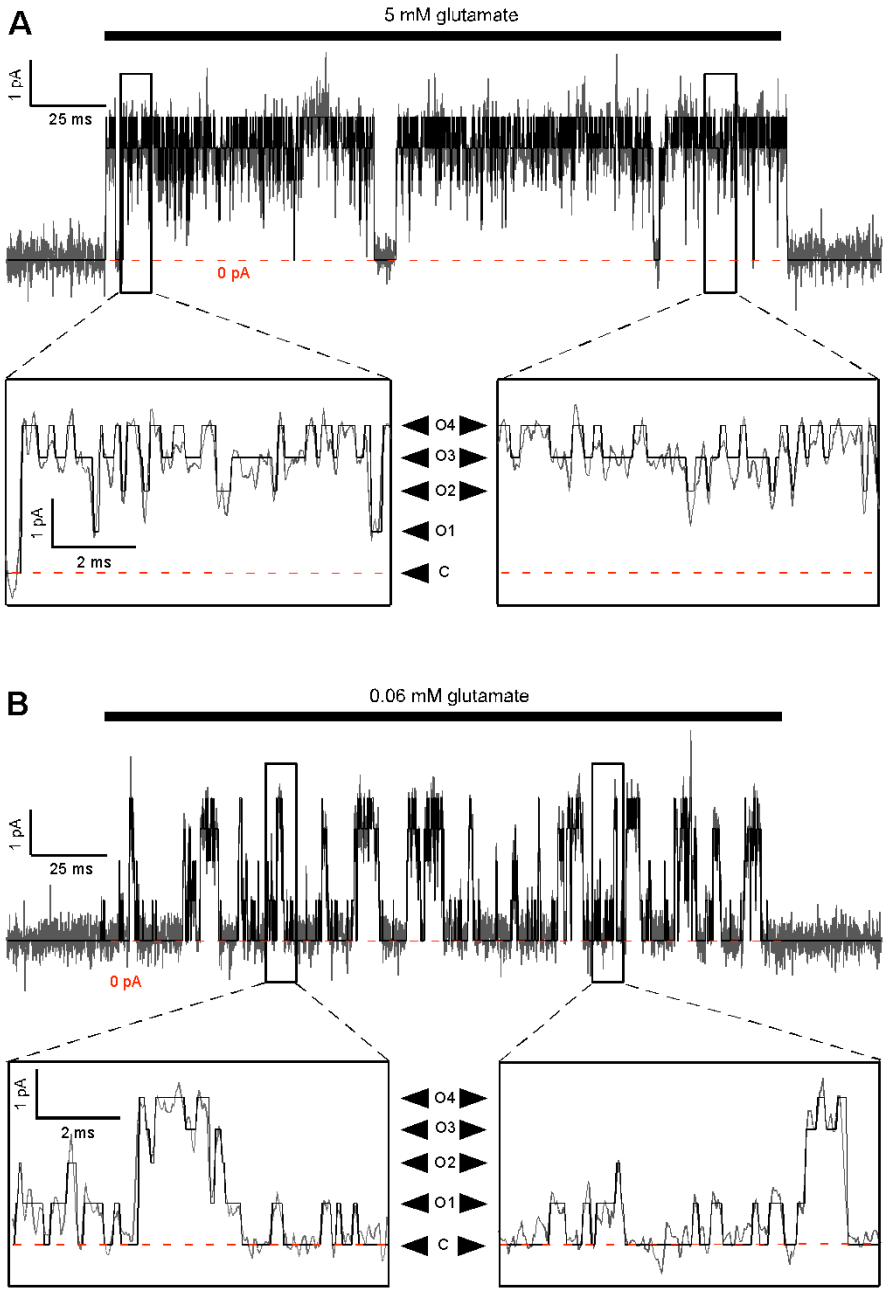

Figure 4.3. AMPA receptor single-channel currents in the absence of polyamine block and desensitization, in saturating and subsaturating glutamate at +80 mV.

(A) Current in 5 mM glutamate from the outside-out patch containing a single GluA2(Q) channel shown in Figure 4.1, recorded at +80 mV, along with the idealization of the record generated by the SKM algorithm of QuB. The record is displayed as in Figure 4.1. The four open current levels at +80 mV in this patch were 0.90 (O1), 1.78 (O2), 2.51 (O3), and 3.20 (O4) pA, as seen more clearly in the expanded sections of the records. **(B)** Same as in (A), but showing current from the same patch in 0.06 mM glutamate.

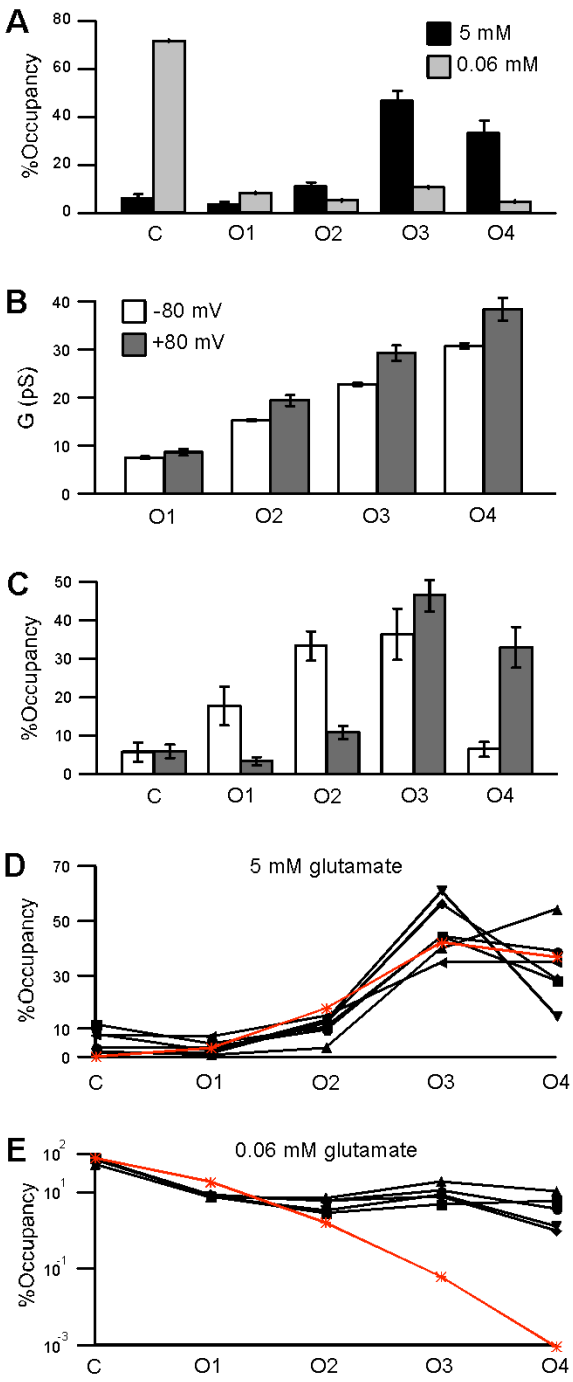

Figure 4.5. The relative occupancies of AMPA receptor conductance levels at +80 mV approximate a binomial distribution in saturating but not subsaturating glutamate.

(A) Mean time spent at each of the five conductance levels (C, O1-O4) at +80 mV, as a fraction of the total time that the channel was exposed to agonist (%Occupancy) for 5 mM (*black*, $n = 6$) and 0.06 mM (*light gray*, $n = 5$) glutamate. **(B)** Comparison of the mean conductance for the four open conductance levels (O1-O4) at –80 (*open*) and +80 (*solid*) mV ($n = 6$). **(C)** Comparison of relative occupancies in saturating glutamate at –80

(*open*) and +80 (*solid*) mV. **(D)** Relative occupancies of each of the five conductance levels (C, O1-O4) in 5 mM glutamate at +80 mV for each of the six patches used to determine the mean in (A) (*solid symbols and lines),* along with the relative occupancies predicted by the binomial distribution (*, *red line*). The individual subunit open probability that gave the best fit for the binomial distribution (± SD) was 78% (± 2%). **(E)** As in (D), but for currents in 0.06 mM glutamate and excluding one patch for which I did not obtain sufficient data in subsaturating glutamate, plotted on a logarithmic scale. The individual subunit open probability that gave the best fit for the binomial distribution (± SD) was 6% (± 1%).

→actually obtained (C, 0.2% predicted versus 6% actual). Indeed, records in saturating glutamate occasionally contained relatively long shut periods that seemed mechanistically unrelated to the predominant mode of fast, subunit-independent gating (for example, Figure 4.4 *A*, Supplemental Figure S4.2 *A*, *top*), though I do not know their functional basis, and they did not occur frequently enough for us to investigate in detail. Nonetheless, the increase in the individual subunit open probability at +80 mV relative to that at –80 mV suggests a small amount of charge associated with each subunit moves through the membrane electric field during the closed to open transition.

In subsaturating glutamate, the relative occupancy of the closed conductance level at +80 mV (C, 71 ± 5%) decreased relative to that at –80 mV (C, 90 ± 1%), consistent with the macroscopic outward rectification in subsaturating glutamate, and the occupancy of the higher conductance levels was surprisingly large (O1, 8 ± 0.2%,; O2, 5 ± 0.8%; O3, 11 ± 3%; O4, 5 ± 2%; n = 5) (Figure 4.5 *A*). At +80 mV, the binomial distribution unambiguously fails to describe the relative occupancies in subsaturating glutamate (Figure 4.5 *E*), with a subunit open probability of 6 ± 1% giving the best fit. As at –80 mV, the greatest deviation occurred for higher conductance levels (O3, 0.06% predicted versus 11% actual; O4, $1x10^{-3}$ % predicted versus 5% actual). The relatively long, high-conductance open periods that I observed in subsaturating glutamate at –80 mV were much more prominent at +80 mV (Figure 4.4 *B*), consistent with my prediction that the apparent subunit interactions at –80 mV would be enhanced by voltage-dependent gating. The duration of open periods depended on the highest conductance level included in the open period (Figure 4.6 *A*-*B*), with open periods including O4 (mean duration 3.35 ± 0.28 ms) lasting on average ~15 times as long as open periods including only O1 (i.e., O1 →

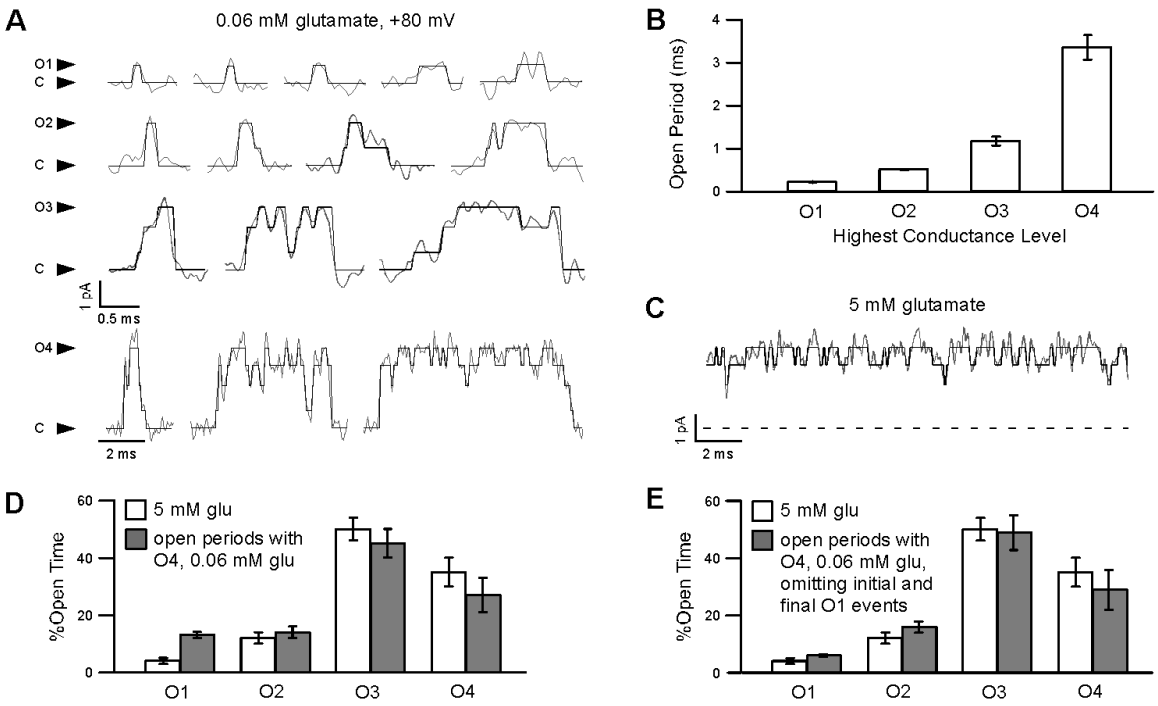

Figure 4.6. AMPA receptors are apparently fully liganded during long open periods in subsaturating glutamate.

(A) Examples of open periods with each of the four open conductance levels (O1-O4) as the highest conductance level reached, with SKM idealization. The highest conductance level and the closed conductance level (C) are indicated (*arrows*). Note the different time scale for open periods reaching O4. The four open current levels in this patch were 0.66 (O1), 1.69 (O2), 2.55 (O3), and 3.19 (O4) pA; and the mean lifetimes of open periods as a function of the highest conductance level reached were 0.206 (O1), 0.522 (O2), 1.23 (O3), and 4.43 (O4) ms. **(B)** Mean values of the mean lifetimes of open periods in 0.06 mM glutamate at +80 mV, as a function of the highest conductance level (Open Period). The mean (± SEM) values were 0.212 ± 0.004 (O1), 0.506 ± 0.017 (O2), 1.17 ± 0.10 (O3), and 3.35 ± 0.28 (O4) ms (n = 5). **(C)** An example of the activity of the patch in (A) in 5 mM glutamate at +80 mV, with SKM idealization. The dashed line indicates the baseline conductance level. **(D)** Comparison of the amount of time spent at each open conductance level at +80 mV, as a fraction of the total open time (%Open Time) for steady-state currents in 5 mM glutamate (*open bars*), and for open periods reaching O4 in 0.06 mM glutamate (*solid bars*). The difference in %Open Time was statistically significant for O1 (unpaired two-tailed t-test, $P < 0.05$), but not for higher conductance levels. **(E)** As in (F), but omitting initial and final O1 events for open periods in 0.06 mM glutamate. The mean values (±SEM) were 4 ± 1% (O1), 12 ± 2% (O2), 50 ± 4% (O3), and 35 ± 5% (O4) in saturating glutamate (n = 6); and 6 ± 0.4% (O1), 16 ± 2% (O2), 49 ± 6% (O3), and 29 ± 7% (O4) in subsaturating glutamate (n = 5). There were no statistically significant differences in %Open Time (unpaired two-tailed t-test).

→events preceded and followed by closed events) (0.212 ± 0.004 ms). (It should be noted, however, that the duration of the open periods is dependent on the resolution of the idealization, since failure to detect brief closed events will increase the apparent duration of open periods).

AMPA receptors switch between low- and high-affinity gating modes in subsaturating glutamate.

To understand the apparent deviations from subunit-independent behavior in subsaturating glutamate at +80 mV, I focused on open periods containing O4 events. Subjectively, the current records during these open periods seemed similar to those in saturating glutamate (compare Figure 4.6 *A*, *bottom* and Figure 4.6 *C*). This resemblance led me to hypothesize that, as in saturating glutamate, the ligand-binding domain might be fully occupied throughout these high-conductance open periods in subsaturating glutamate. To test this hypothesis, I compared the amount of time spent at each open conductance level as a fraction of the total open time (%Open Time) for O4-containing open periods in subsaturating glutamate and for entire current records in saturating glutamate. The values of %Open Time were similar (Figure 4.6 *D*), but, contrary to my expectations, there was a statistically significant excess of O1 for the long open periods relative to saturating glutamate. However, O4-containing open periods frequently began and ended with O1 events (e.g., Figure 4.4 *B*, Figure 4.6 *A*). When these initial and final O1 events were omitted from the calculation of %Open Time, the values were essentially identical to those in saturating glutamate (Figure 4.6 *E*). Thus in subsaturating glutamate,

the receptor appears fully liganded for significant periods of time, despite the low glutamate concentration.

Based on these observations, I developed a kinetic model that qualitatively accounts for my results (Figure 4.7 *A*). In this model, the initial glutamate binding step has low affinity, but binding of two or more glutamate molecules greatly increases the receptor's affinity for glutamate, leading to long open periods in which the receptor is fully liganded. According to this model, AMPA receptors operate in two modes in subsaturating glutamate: a low-affinity mode characterized by short open periods in which zero or one glutamate molecules are bound; and a high-affinity mode characterized by long open periods in which the channel is fully liganded most of the time. Although the model is intended only as a qualitative explanation of certain features of my data, it could serve as the basis of a more quantitative treatment of subunit interactions. However, detailed kinetic models of AMPA receptors have many open states with identical conductance (e.g., Robert and Howe, 2003), making a rigorous quantitative treatment extremely challenging, especially if subunit interactions are included.

Consistent with my model, the distribution of open period durations could be fit with two exponential components (Supplemental Figure S4.4), and the time constant for the fast component (0.151 ± 0.005 ms) was similar to the mean lifetime of open periods with O1 as the highest conductance level (0.212 ± 0.004 ms).

In my model, the open/closed transitions in the ion channel domains of glutamate-occupied subunits are not affected by the ion channel conformation or agonist-binding site occupancy of the other subunits, and the subunit opening and closing rates are identical in both modes. However, the requirement of agonist binding for subunit →

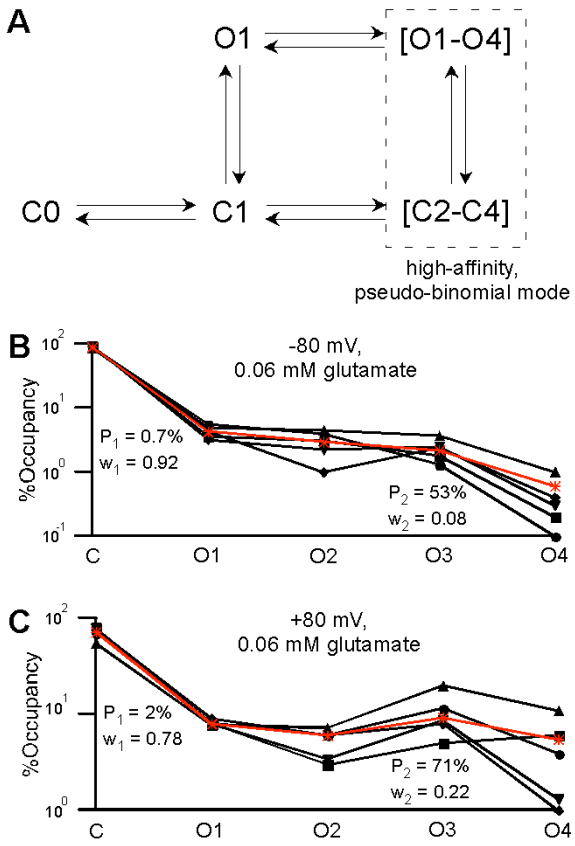

Figure 4.7. AMPA receptors switch between low- and high-affinity gating modes in subsaturating glutamate.

(A) Kinetic model illustrating the switch between low and high-affinity gating modes in subsaturating glutamate. The initial glutamate binding step has low-affinity, but binding of two or more glutamate molecules greatly increases the receptor's affinity for glutamate, leading to long open periods in which channel behavior is very similar to that seen in saturating glutamate and the channel is presumably fully liganded. The relative occupancy of the conductance levels during these long open periods can be approximated by a binomial distribution. **(B)** Fit of the relative occupancies in 0.06 mM glutamate at –80 mV from Figure 4.2 (*solid symbols and lines*) by a weighted sum of two binomial distributions (*, *red line*). The parameters giving the best fit (± SD) were 0.7 ± 0.3 and 53 ± 8% for the low and high subunit open probabilities, with weights of 0.92 and 0.08 (± 1), respectively. **(C)** Fit of the relative occupancies in 0.06 mM glutamate at +80 mV from Figure 4.6 (*solid symbols and lines*) by a weighted sum of two binomial distributions (*, *red line*). The parameters giving the best fit (± SD) were 2 ± 1 and 71 ± 6% for the low and high subunit open probabilities, with weights of 0.78 and 0.22 (± 3), respectively.

→opening, and the dependence of agonist affinity on the number of agonists associated with the receptor, results in a high degree of apparent "cooperativity" in subunit opening. Also, I do not distinguish between a "progressive" model where each glutamate-binding step leads to an increase in affinity (in which case there would be intermediate modes between the low- and high-affinity modes), and a "threshold" model where the binding of two glutamate molecules is sufficient to increase affinity to its maximum level.

The idea of low- and high-affinity modes combined with independent subunit opening/closing suggested that the relative occupancies in subsaturating glutamate could be fit by a weighted sum of two binomial distributions. Indeed this combination of binomial distributions provided an excellent fit to the relative occupancies at both –80 (Figure 4.7 *B*) and +80 (Figure 4.7 *C*) mV. The low-affinity mode had a subunit open probability of 0.7 ± 0.3% at –80 mV and 2 ± 1% at +80 mV, and its weight decreased from 0.92 ± 0.01 at –80 mV to 0.78 ± 0.03 at +80 mV. In my model, this voltage-dependent decrease in the amount of time spent in the low-affinity mode is a consequence of voltage-dependent subunit gating. Because glutamate cannot dissociate from open subunits, and because the subunit open probability is greater at +80 mV than at –80 mV, there is a longer "window of opportunity" at +80 mV in which a second glutamate molecule can bind to a singly liganded channel, sending the channel into the high-affinity mode. Notably, the subunit open probability for the high-affinity mode was similar to that in saturating glutamate at +80 mV (71 ± 6%, high-affinity mode versus 78 ± 2%, saturating glutamate), as expected based on the comparison of %Open Time in Figure 4.6 *E*, and also, at –80 mV (53 ± 8%, high-affinity mode versus 58 ± 3%, saturating glutamate), suggesting that the receptor also becomes fully liganded for extensive periods

of time in subsaturating glutamate at –80 mV. Thus my analysis of AMPA receptor subunit interactions at +80 mV leads to conclusions that are also applicable at more physiological membrane potentials.

DISCUSSION

Dependence of the affinity of AMPA receptors for glutamate on the number of occupied binding sites has not been observed previously, perhaps because it is most apparent at positive membrane potentials not typically used in single-channel recordings of AMPA receptors. However, previous studies of voltage-dependent gating in AMPA receptors are consistent with my results. Wylie et al. (1993) found a voltage-dependent increase in both single-channel conductance and open period length in non-NMDA receptors channels of rat granule cells, while Raman and Trussell (1995a) found an increase in outward rectification in subsaturating agonist concentrations in non-NMDA receptors channels in chick neurons. The latter study also reported that the time-course of deactivation of macroscopic glutamate-activated currents had fast and slow components, with the weight of the components dependent on membrane voltage. The relative amounts of the slow component at negative and positive potentials were practically identical to the relative amounts of the proposed high-affinity mode at –80 and +80 mV (Figure 4.7 *B*). Thus, while my results were obtained using homomeric channels in a heterologous expression system, similar results obtained in two different preparations of native channels suggest that my conclusions are generally applicable to native AMPA receptors that are typically heteromers associated with auxiliary subunits. I also note that these studies of native channels were performed without CTZ. Finally, as shown in Figure 4.3 *D*, the dependence of outward rectification on agonist concentration, which is a manifestation of the switch between low- and high-affinity gating modes, occurs for all AMPA receptor subtypes tested, and in desensitizing channels.

Only three other studies of microscopic AMPA receptor currents have been performed in saturating agonist concentrations with desensitization blocked. Two of these (Smith and Howe, 2000; Smith et al., 2000) were performed on native channels, and did not find binomially distributed relative occupancies. However, native channels are heteromers, so the subunit open probabilities may not be identical for all subunits. The other study used recombinant homomeric channels, but focused on defining glutamate receptor stoichiometry, and did not examine in detail the high frequency changes in conductance for fully liganded channels (Rosenmund et al., 1998) (see Supplemental Discussion for further consideration of this study).

Although I think that the low- and high-affinity mode model with independent subunit opening/closing is the best explanation for my results, I considered several alternative explanations. One possibility is that the apparent low open probability in the low-affinity mode is actually due to the receptor being desensitized for long periods of time in subsaturating glutamate. However, this hypothesis leads to several conclusions that are in conflict with well-established results regarding AMPA receptor desensitization (Supplemental Figure S4.1, Supplemental Table S4.3, Supplemental Discussion). Another alternative, as mentioned previously, is that there is significant interaction between subunits at the level of the ion channel, and that the resemblance between the relative occupancies in saturating glutamate and a binomial distribution is coincidental and not physically meaningful. Although this explanation is not parsimonious, it is plausible based solely on the results at –80 mV. However, that this coincidence would occur once at –80 mV and again +80 mV seems extremely unlikely.

Another consideration is that the current idealizations may not accurately represent the actual transitions between conductance levels, due to an excessively low signal-to-noise ratio, the effects of filtering and sampling, or other issues. There may be three rather than four discrete conductance levels underlying the records, and the fits of binomial distributions to the relative occupancies would in this case not be meaningful. However, the fundamental, novel observation on which my model is based—that, during open periods lasting for several milliseconds, AMPA receptors in subsaturating glutamate behave like fully-liganded channels (Figure 4.6)—is ultimately independent of the accuracy of the SKM algorithm or the appropriateness of the binomial distributions. The combination of relatively brief, low-conductance and relatively long, high-conductance open periods in subsaturating glutamate at +80 mV is apparent upon examination of the raw current records. The SKM idealizations are the output of an algorithm that is highly sensitive to the statistical properties of current records, and these statistical properties are evidently very similar in saturating glutamate and during the long high-conductance open periods in subsaturating glutamate. Nonetheless, the relative occupancies of AMPA receptor conductance levels in saturating glutamate at negative potentials were previously determined to follow a binomial distribution with a subunit open probability (67%) very similar to what I obtain here (Jin et al., 2003), based on idealizations using time-course fitting (Colquhoun and Sigworth, 1995), so I suspect that my idealizations are reasonably accurate.

The occupancy of the proposed high-affinity gating mode is enhanced at positive potentials, due to the increase in subunit open probability. This voltage-dependent enhancement of the high-affinity mode may be a physiologically important mechanism

whereby local synaptic activity and back-propagating action potentials regulate the excitability of glutamatergic synapses. Additionally, I expect that other mechanisms that influence the open probability of AMPA receptors, such as phosphorylation (Benke et al., 1998; Banke et al., 2000) and interaction with the auxiliary subunits stargazin (Priel et al., 2005; Tomita et al., 2005) and cornichon (Schwenk et al., 2009), will influence the equilibrium between low- and high-affinity modes in a manner analogous to membrane voltage. Since the high-affinity mode can be maintained for several milliseconds at a time, it could significantly influence the shape of synaptic responses. For example, desensitization can occur with only one occupied agonist-binding site (Robert and Howe, 2003), while entry into the high-affinity mode requires two occupied binding sites. Thus the opposing influences of these two processes on the spatial extent of AMPA receptor activity may translate graded changes in local agonist concentration into sharply delineated boundaries between inactive and highly active receptors (for example, between perisynaptic and synaptic receptor populations). Additional studies are required to test these possibilities.

I propose that the affinity of AMPA receptors for glutamate is dependent on the number of occupied agonist-binding sites. What is the structural basis for this relationship? A basic structural model of AMPA receptor gating would include three distinct steps in each subunit: a two-step agonist-binding process, made up of an initial agonist association step followed by a conformational change that prevents agonist dissociation (Armstrong et al., 1998; Abele et al., 2000; Armstrong and Gouaux, 2000; Weston et al., 2006), and a conformational change in the ion channel that is tightly coupled to that in the agonist-binding domain (Zhang et al., 2008). Crystallographic

studies indicate that the agonist-binding site is in the cleft of a clamshell-like structure with two distinct lobes (Armstrong et al., 1998; Armstrong and Gouaux, 2000; Mayer, 2006). The first lobe forms an interface between the agonist-binding domains of adjacent subunits, which form dimers, and the second lobe moves upward to "close" the clamshell and prevent glutamate dissociation during the second gating step. Assuming that the initial agonist association step is diffusion-limited, the switch between low- and high-affinity modes probably involves subunit interactions that either stabilize or increase the rate of entry into the closed clamshell conformation. The dimer interface is an obvious possible site for these interactions. Interactions between dimers may also occur, although the structures of isolated dimers do not suggest a mechanism for inter-dimer interactions.

The structural basis of voltage-dependent gating in AMPA receptors is also unknown. Voltage-dependent gating in KcsA channels (which lack the voltage-sensing transmembrane helices of eukaryotic voltage-gated K^+ channels) is determined by a glutamate residue in the extended selectivity filter region of the pore (Cordero-Morales et al., 2006a; Cordero-Morales et al., 2006b). The homologous position in AMPA receptors is occupied by an aspartate residue (D590), but this residue is not responsible for voltage-dependent gating since outward rectification is still dependent on glutamate concentration in D590N channels (not shown). NMDA receptors also show voltage-dependent gating (Nowak and Wright, 1992; Clarke and Johnson, 2008), which influences the voltage-dependence of the rate of Mg^{2+} unblock. Similar structural mechanisms may underlie voltage-dependent gating in both glutamate receptor subtypes, and voltage-dependent gating in AMPA receptors may influence the rate of polyamine unblock, with important physiological consequences (e.g., Rozov and Burnashev, 1999).

During the high-affinity mode, AMPA receptors appear to be saturated by 0.06 mM glutamate, and thus temporarily have an affinity for glutamate comparable to that of NMDA receptors. Because of their uncoordinated subunit activity, however, AMPA receptors only maintain this high-affinity mode for limited periods of time. I speculate that at some point during their evolution, glutamate receptors diverged into high-affinity, slowly activating receptors with, and low-affinity, rapidly activating receptors without coordinated subunit opening—the ancestors of NMDA and AMPA receptors, respectively. Interestingly, an invertebrate glutamate receptor that has relatively high conductance and low maximal open probability comparable to mammalian NMDA receptors lacks multiple open conductance levels but is activated by the AMPA receptor agonist quisqualate (Tour et al., 1998). Finally, cyclic nucleotide gated channels, which have multiple conductance levels like AMPA receptors, also switch between a low overall open probability mode in which one agonist is bound, and a high open probability mode with two or more agonists bound (Biskup et al., 2007). Agonist-binding thresholds for switching between low and high open probability modes may be a common regulatory mechanism for ligand-gated ion channels.

SUPPLEMENTAL MATERIALS AND METHODS

Variance of open channel currents.

The variance of microscopic AMPA receptor currents was determined for currents activated by saturating glutamate. The final filter frequency was ~1 kHz and the sampling frequency was 50 kHz. Although the open channel probability of AMPA receptors in the presence of CTZ and saturating glutamate is close to unity, relatively long resolved closures, which seem to be mechanistically unrelated to the fast gating of individual AMPA receptor subunits, were sometimes apparent at +80 mV (for examples see Supplemental Figure S4.2 *A*, *top*, and Supplemental Figure S4.3 *A*, *left*) and less frequently at –80 mV. To exclude these events, and the initial and final rise times of the current after application and removal of glutamate, from the calculation of the variance, I removed all sample points below a threshold of ±200 fA plus fifteen points (corresponding to 300 μs, i.e., approximately 1 filter rise time) after every positive and before every negative threshold crossing from the records. I assume the baseline current noise and the glutamate-activated current noise are independent, so the baseline rms noise (equal to the variance after subtraction of the mean baseline current) was subtracted from the total variance in glutamate. Since the mean glutamate-activated current amplitude was typically larger at +80 than at –80 mV, I used the coefficient of variation (CV), rather than the absolute variance, to compare the noise at these potentials.

SUPPLEMENTAL RESULTS AND DISCUSSION

How many open conductance levels do AMPA receptors have?

Single-channel studies of recombinant AMPA receptor channels have variously reported three or four open conductance levels. The conductance levels for all previous single-channel studies using recombinant channels are listed in Supplemental Table S4.1. Considering the differences in idealization methods, subunit composition, and ionic content of the internal and external solutions between different experiments, the conductances of the lowest three open levels are quite consistent. The absence of the fourth open conductance level in Swanson et al. (1997), Banke et al. (2000), and Jin et al. (2003) is probably due to its rarity under their experimental conditions(desensitizing channels and subsaturating glutamate in the first two studies, desensitizing channels and saturating glutamate in the latter). The relative occupancy of the highest conductance level was very small (~1-2%) for desensitizing channels in saturating glutamate in Zhang et al. (2008), and in Tomita et al. (2005) when channels were expressed without stargazin. When Tomita et al. (2005) co-expressed channels with stargazin, however, the relative occupancy of the fourth conductance level increased approximately sevenfold. These results are consistent with kinetic models that suggest that AMPA receptors in the absence of stargazin typically desensitize before reaching the fourth conductance level. Even with desensitization blocked by CTZ, I find that the highest conductance level occurs very rarely in subsaturating glutamate.

The absence of a fourth conductance level in Rosenmund et al. (1998) is more puzzling, since their experiments were performed on non-desensitizing channels in saturating glutamate. However, the definition of a conductance level used by the authors

of this study is different from that used in other studies. In their experiments, the transitions between conductance levels are determined by the rate of antagonist dissociation, which is ~2 s^{-1}, orders of magnitude larger than the lifetimes of conductance levels as defined in other studies. Thus the conductance levels of Rosenmund et al. (1998) correspond to the *average* conductance for receptors with different numbers of binding sites available. During the intervals between antagonist dissociations, the channels would be expected to make many transitions between conductance levels as typically defined, and indeed all of the conductance levels identified by Rosenmund et al. (1998) are characterized by high frequency noise. Interestingly, Rosenmund et al. (1998) find that two antagonist molecules must dissociate before any current is detected. Based on this observation, it has been assumed that receptors with only one open ion channel gate have zero or undetectable conductance. This is inconsistent with the observation of four conductance levels in Derkach et al. (1999), Tomita et al. (2005), Zhang et al. (2008), and the present study. An alternative explanation is suggested by the dependence of the receptor's affinity for glutamate on the number of occupied binding sites, as proposed in the present study. A channel with only binding site available would only have access to the low-affinity mode. Thus the agonist concentration used by Rosenmund et al. (1998), which is saturating under normal conditions (and for channels with two or more binding sites available), may be subsaturating for channels with three binding sites occupied by antagonists, explaining the absence of the fourth conductance level.

Desensitization is unlikely to have a significant effect on relative occupancies.

Although desensitization of "flip" splice-variant AMPA receptors is largely blocked by CTZ, a small amount of desensitization (~4%) occurs during prolonged (>1 s) exposure to glutamate (Partin et al., 1993). I therefore considered whether desensitization might influence the relative occupancies of the various conductance levels in my experiments. I was particularly concerned about the effects of desensitization on the relative occupancies in subsaturating glutamate (Figure 4.2 *C*, Figure 4.5 *E*), since the channel spends long periods of time at the baseline conductance level, which I assume to reflect non-desensitized closed states. I considered a model in which the channel can desensitize but otherwise behaves in a subunit independent manner. The model has two parameters, the individual subunit open probability during non-desensitized periods (P_o), and the relative amount of time spent in the desensitized non-conducting state (%Ds). The relative occupancy of the combined non-conducting states is given by:

$$\%C = \%Ds + (1 - \%Ds) * (1 - P_o)^4 \qquad \text{(S4.1)}$$

and the relative occupancy of open level *n* is given by:

$$\%On = (1 - \%Ds) * (24/(n!(4 - n)!)) * (P_o)^n * (1 - P_o)^{4-n} \qquad \text{(S4.2)}$$

Unlike the pure binomial distribution, this model provided a reasonable fit to the relative occupancies in subsaturating glutamate at –80 mV (not shown) and +80 mV (Supplemental Figure S4.1 *F*), and it also slightly improved the fit in saturating glutamate (–80 mV not shown; +80 mV, Supplemental Figure 4.1 *E*). In saturating glutamate, the estimates of P_o were not affected by the addition of desensitization to the model (Supplemental Table S4.2), and the improvement in the fit was due to the increase in %C provided by the desensitized state. In subsaturating glutamate, however, the values of P_o

increased substantially, to the point of approaching those in saturating glutamate. Accordingly, almost all of the non-conducting time was provided by the desensitized state.

This model in some respects recapitulates my favored model, in which the channel switches between low- and high-affinity modes (Figure 4.7 *A*): in subsaturating glutamate at +80 mV, the channel spends ~70% of the time in either a very low open probability or a completely non-conducting mode, and the remainder of the time in a high open probability mode with P_o similar to that in saturating glutamate. However, several aspects of the independent-subunit-gating-plus-desensitization model are in conflict with well-established properties of desensitization in AMPA receptors. First, in order to properly fit the data, the extent of desensitization must be much greater in subsaturating than in saturating glutamate when in fact the opposite effect of agonist concentration on desensitization is seen in macroscopic currents (Robert and Howe, 2003). Second, the extent of desensitization is greater at +80 mV than at –80 mV, opposite the effect of membrane potential on desensitization in macroscopic currents (Raman and Trussell, 1995b).

The shut time distribution in subsaturating glutamate contained two exponential components, but the slow component (7.48 ms at –80 mV, 2.81 ms at +80 mV) was much too fast to be the result of desensitization. Finally, the rate of desensitization in the presence of CTZ is on the order of 1 s^{-1} for flip splice-variant receptors (Dr. James Howe, personal communication), and I applied glutamate in 200 ms pulses, so desensitization was unlikely to occur significantly during these brief applications. I conclude that desensitization is not an important factor in my experiments.

Supplemental Table S4.1. Comparison of open conductance levels for AMPA receptor single-channel currents from previously published reports.

Reference	Subtype	Agonist	G1 (pS)	G2 (pS)	G3 (pS)	G4 (pS)
Swanson et al., 1997	GluA4	100 μM glutamate	8	15	24	--
	GluA4/ GluA2(Q)	100 μM glutamate	8	17	26	--
Rosenmund et al., 1998	GluA3*	1 mM quisqualate	5	15	23	--
Derkach et al., 1999	GluA1	10 μM AMPA	9	14	21	28
Banke et al., 2000	GluA1	10 μM glutamate	5	14	20	--
Jin et al., 2003	GluA2(Q)	1 mM glutamate	6	11	18	--
Tomita et al., 2005	GluA4	10 mM glutamate	9	20	31	45
Zhang et al., 2008	GluA2(Q)	10 mM glutamate	7	15	23	36
Present study (-80 mV)	GluA2(Q)	5 mM glutamate	8	15	23	31

In the references by Swanson et al., Derkach et al., Banke et al., and Jin et al., single-channel currents were filtered at low frequencies (1-2 kHz) and idealized using time-course fitting (Colquhoun and Sigworth, 1995), except Derkach et al., who used a threshold-crossing method. Rosenmund et al. used a non-desensitizing chimera of GluA3 containing part of the ligand-binding domain of GluK2 and incubated the channels in a solution containing a saturating concentration of a high-affinity competitive antagonist before switching to a solution containing a saturating concentration of agonist. As antagonist molecules dissociated, the channels passed through three identifiable conductance levels of increasing conductance. The mean conductance of the open levels could be measured directly without idealization, and currents were filtered at 1-5 kHz. In the references by Tomita et al. and Zhang et al., single-channel currents were filtered at 2-4 kHz and idealized using the SKM algorithm (Qin, 2004). All studies were performed on recombinant channels in HEK cells at negative membrane potentials (–80 to –160 mV).

Supplemental Table S4.2. Effects of resolution on idealization of AMPA receptor single-channel currents.

	5 mM glutamate			
	-80 mV		+80 mV	
	td = 40 μs	td = 80 μs	td = 40 μs	td = 80 μs
τ1 (μs)	134 ± 24	148 ± 27	91 ± 9	107 ± 11
τ2 (μs)	188 ± 31	203 ± 25	89 ± 7	103 ± 8
τ3 (μs)	232 ± 36	250 ± 30	249 ± 42	295 ± 40
τ4 (μs)	114 ± 8	115 ± 10	217 ± 35	244 ± 37
%C	6 ± 3	7 ± 3	6 ± 2	6 ±2
%O1	18 ± 5	18 ± 5	4 ± 1	3 ±1
%O2	33 ± 4	33 ± 4	11 ± 2	10 ±2
%O3	36 ± 7	36 ± 7	46 ± 4	47 ±4
%O4	7 ± 2	6 ± 2	33 ± 5	34 ±5

	0.06 mM glutamate			
	-80 mV		+80 mV	
	td = 40 μs	td = 80 μs	td = 40 μs	td = 80 μs
τ1 (μs)	132 ± 17	131 ± 18	131 ± 10	139 ± 4
τ2 (μs)	181 ± 22	183 ± 16	104 ± 4	117 ± 6
τ3 (μs)	253 ± 46	255 ± 41	276 ± 30	299 ± 43
τ4 (μs)	140 ± 14	127 ± 16	206 ± 51	239 ± 57
%C	90 ± 1	90 ± 1	71 ± 5	71 ± 5
%O1	4 ± 0.4	4 ± 0.5	8 ± 0.2	8 ± 0.4
%O2	3 ± 0.6	3 ± 0.6	5 ± 0.8	4 ± 0.8
%O3	2 ± 0.4	2 ± 0.4	11 ± 3	10 ± 3
%O4	0.4 ± 0.2	0.4 ± 0.2	5 ± 2	6 ± 2
τ_{fast}, closed (ms)	0.42 ± 0.11	0.35 ± 0.09	0.46 ± 0.06	0.41 ± 0.05
τ_{slow}, closed (ms)	7.48 ± 1.14	6.87 ± 1.02	2.81 ± 0.16	2.90 ± 0.13
%τ_{fast}	37 ± 6	24 ± 8	39 ± 3	39 ± 3
%τ_{slow}	63 ± 6	76 ± 8	61 ± 3	61 ± 3
τ_{open}, highest level O1 (μs)	228 ± 25	244 ± 26	212 ± 4	232 ± 2
τ_{open}, highest level O2 (μs)	532 ± 63	574 ± 65	506 ± 17	556 ± 16
τ_{open}, highest level O3 (μs)	1201 ± 216	1245 ± 221	1168 ± 102	1267 ± 104
τ_{open}, highest level O4 (μs)	2263 ± 663	2359 ± 716	3346 ± 283	3456 ± 284

All parameters were determined from idealized records obtained from the SKM algorithm in QuB, using a dead time (td) of either 40 or 80 μs under otherwise identical

conditions (see Materials and Methods for details). The parameters compared are the mean lifetimes of each of the four open conductance levels (τ1-τ4) in 5 and 0.06 mM glutamate; the relative occupancies of the baseline conductance level (%C) and each of the four open conductance levels (O1-O4) in 5 and 0.06 mM glutamate; the time constants and relative areas of the fast and slow components of the shut time distributions (τ_{fast}, closed and τ_{slow}, closed) in 0.06 mM glutamate; and the mean lifetimes of open periods with each of the four open conductance levels as the highest conductance level reached (τ_{open}, highest level O1-O4) in 0.06 mM glutamate. All parameters are listed as mean ± SEM. *n* = 6 for 5 mM glutamate and *n* = 5 for 0.06 glutamate, except for the analysis of shut time distributions at –80 mV, for which *n* = 4 (see legend to Supplemental Figure S4.1).

Supplemental Table S4.3. Modeling the steady-state behavior of single AMPA receptor channels as a combination of independent subunit gating and desensitization.

	Subunit P_o	%non-conducting	%closed	%Ds	Plot
-80 mV, 5 mM glutamate	58%	3%	3%	--	Figure 4.2 *C*
	58%	5%	3%	2%	--
+80 mV, 5 mM glutamate	78%	0.2%	0.2%	--	Figure 4.5 *E*
	78%	5.2%	0.2%	5%	Supplemental Figure S4.1 *E*
-80 mV, 0.06 mM glutamate	2%	93%	93%	--	Figure 4.2 *D*
	39%	90%	2%	88%	--
+80 mV, 0.06 mM glutamate	6%	79%	79%	--	Figure 4.5 *F*
	62%	72.6%	0.6%	72%	Supplemental Figure S4.1 *F*

The relative occupancies of the baseline conductance level and each of the four open conductance levels were fit with either a binomial distribution (with relative occupancies determined by the individual subunit open probability (Subunit P_o)), or a model incorporating desensitization and independent subunit gating (with relative occupancies determined by the subunit open probability during non-desensitized periods and the relative amount of time spent in the desensitized state (%Ds), see Supplemental Discussion for details). For the binomial distribution the relative occupancy of the baseline conductance level (%non-conducting) consists entirely of closed, non-desensitized states (%non-conducting = %closed); for the model including desensitization the relative occupancy of the baseline conductance level is a combination of desensitized and closed, non-desensitized states (%non-conducting = %Ds + %closed). Examples of fits can be seen in Figure 4.2 *C-D* and Figure 4.5 *E-F* (pure binomial distribution), or Supplemental Figure S4.1 *E-F* (independent subunit gating and desensitization).

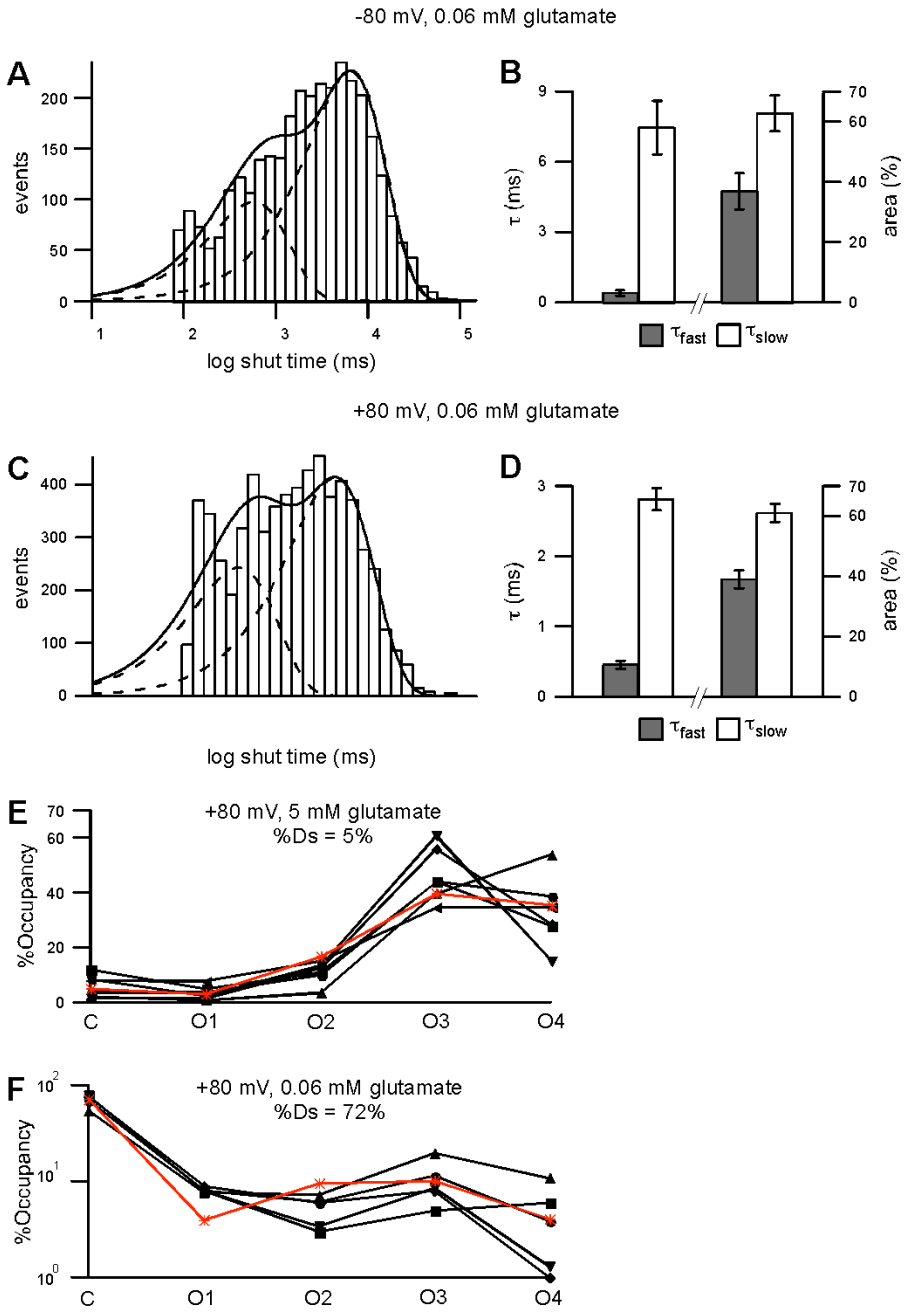

Supplemental Figure S4.1. Shut times of single AMPA receptor channels in subsaturating glutamate.

(A) Example shut time histogram for an outside-out patch containing a single GluA2(Q) channel in the presence of 0.06 mM glutamate at –80 mV, along with the probability density function for the best double exponential fit to the shut time distribution (*solid line)* and the individual exponential components of the pdf (*dashed lines*). The time constants for the two exponential components in this patch were 0.57 and 6.41 ms with relative areas of 30 and 70%. **(B)** Mean time constants and relative areas for the fast and slow components (τ_{fast} and τ_{slow}) of AMPA receptor single-channel shut time distributions in 0.06 mM glutamate at –80 mV. The mean time constants (± SEM) were 0.42 ± 0.11

and 7.48 ± 1.14 ms, with areas of 37 ± 6 and 63 ± 6% (*n* = 4). One patch had only a single exponential component of 5.64 ms apparent in its shut time distribution at –80 mV in 0.06 mM glutamate, and was not included in determining the mean values. **(C)** Same as (A) but the membrane potential was +80 mV. The time constants for the two exponential components were 0.29 and 2.67 ms with relative areas of 37 and 63%. **(D)** Same as (B) but for +80 mV. The mean time constants (± SEM) were 0.46 ± 0.06 and 2.81 ± 0.16 ms, with areas of 39 ± 3 and 61 ± 3% (*n* = 5). **(E)** Relative occupancies of the baseline conductance level (C) and each of the four open conductance levels (O1-O4) in response to 5 mM glutamate at +80 mV for each of six patches (*solid symbols and lines*, same data as shown in Figure 4.5), along with the relative occupancies predicted by a model incorporating desensitization and independent subunit gating (i.e, binomially distributed relative occupancies during non-desensitized periods, see Supplemental Discussion for details) that gave the best fit to the entire data set (**, red line*). The parameters that gave the best fit (± SD) were 5% desensitization (± 3%) with an individual subunit open probability of 78% (± 2%) during non-desensitized periods, giving relative occupancies of 5 (C), 3 (O1), 17 (O2), 40 (O3), and 35 (O4) %. **(F)** As in (E), but for currents in response to 0.06 mM glutamate and excluding one patch for which I did not obtain sufficient data (same data as shown in Figure 4.5), plotted on a logarithmic scale. The parameters that gave the best fit (± SD) were 72% desensitization (± 2%) with an individual subunit open probability of 62% (± 6%) during non-desensitized periods, giving relative occupancies of 72 (C), 4 (O1), 10 (O2), 10 (O3), and 4 (O4) %.

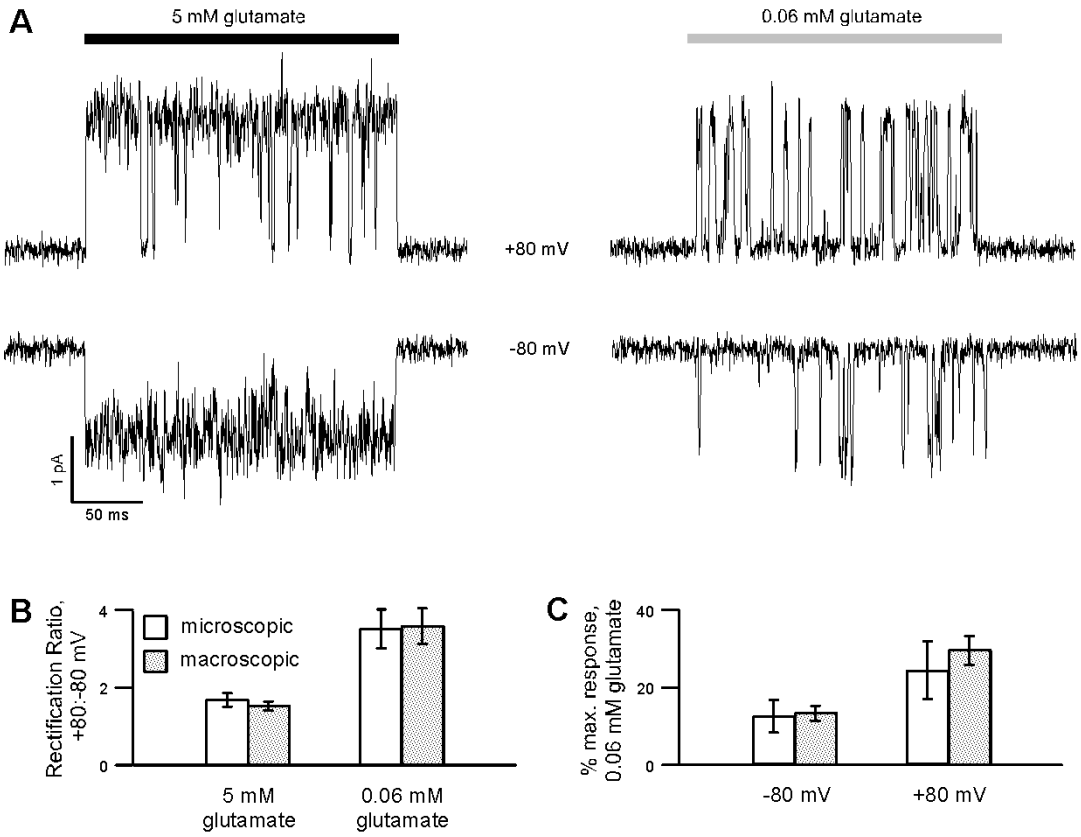

Supplemental Figure S4.2. Properties of microscopic AMPA receptor currents recapitulate those of macroscopic currents.

(A) Glutamate-activated currents from a HEK cell-derived outside-out patch containing a single GluA2(Q) receptor at –80 mV (*bottom*) and +80 mV (*top*) in response to 200 ms applications of 5 mM (*left*) or 0.06 mM (*right*) glutamate. Desensitization was blocked using CTZ. Currents are shown filtered at 1 kHz. **(B)** Mean ratios of current amplitudes (macroscopic currents, $n = 9$) or current integrals (microscopic currents, $n = 8$) at +80 to those at -80 mV, in response to 5 or 0.06 mM glutamate. Current integrals were determined after filtering at 5 kHz. Mean values (± SEM) were 1.51 ± 0.12 (macroscopic) and 1.66 ± 0.17 (microscopic) for 5 mM, and 3.57 ± 0.46 (macroscopic) and 3.50 ± 0.50 (microscopic) for 0.06 mM glutamate. **(C)** Mean current amplitudes (macroscopic currents, $n = 9$) or current integrals (microscopic currents, $n = 8$) in response to 0.06 mM glutamate, as fractions of the amplitude or integral in response to saturating (5 mM) glutamate, at –80 and +80 mV. Mean values (± SEM) were 13.2 ± 1.9 (macroscopic) and 12.1 ± 4.2 (microscopic) at –80 mV, and 29.4 ± 3.7 (macroscopic) and 24.0 ± 7.4 (microscopic) at +80 mV.

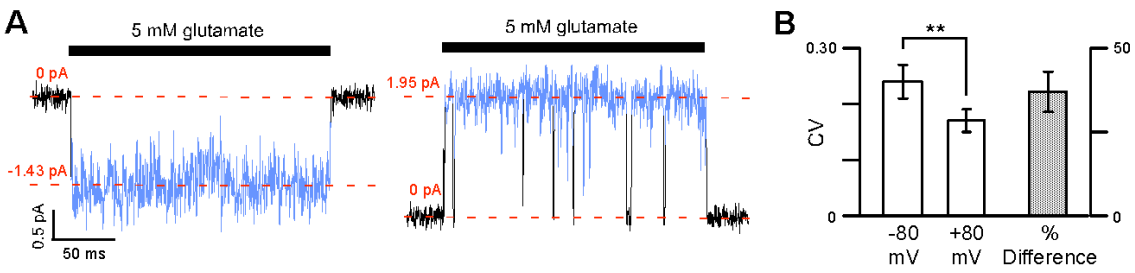

Supplemental Figure S4.3. AMPA receptor single-channel currents are noisier at negative than at positive potentials.

(A) Glutamate-activated currents from an outside-out patch containing a single GluA2(Q) channel at –80 (*left*) and +80 (*right*) mV. The record is shown sampled at 50 kHz and filtered at 1 kHz, the same sampling and filter frequencies used to analyze the noise. The points corresponding to the initial and final rise times of the glutamate activated current and to resolved closures in the presence of glutamate (along with the adjacent rise times) were excluded in determining the mean and coefficient of variation (CV) of the glutamate-activated currents (see Supplemental Materials and Methods for details). The points included in the analysis are shown in blue, with the baseline and mean open current levels indicated by the dashed lines. The mean and CV of the example currents were –1.43 pA and 0.19 (-80 mV), and 1.95 pA and 0.12 (+80 mV). **(B)** Mean CV values for open channel currents at –80 mV and +80 mV (*open bars, left axis*), and increase in CV values at –80 mV, relative to +80 mV. Mean CV values (± SEM), were 0.24 ± 0.03 (-80 mV) and 0.17 ± 0.02 (+80 mV) (n = 6). These values were statistically different (two-tailed t-test, $P < 0.05$ (**)). The mean increase in CV at –80 mV (±SEM) (% Difference, *solid bar, right axis*) was 37 ± 6%.

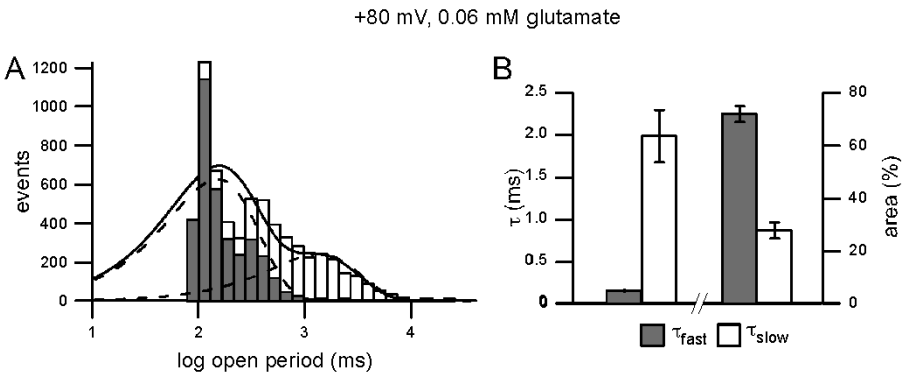

Supplemental Figure S4.4. Open periods of single AMPA receptor channels in subsaturating glutamate at +80 mV.

(A) Example open period histogram for an outside-out patch containing a single GluA2(Q) channel in the presence of 0.06 mM glutamate at +80 mV, along with the probability density function for the best double exponential fit to the shut open period distribution (*solid line)* and the individual exponential components of the pdf (*dashed lines*). The time constants for the two exponential components in this patch were 0.14 and 1.28 ms with relative areas of 72 and 28%. The histogram for open periods with O1 as the highest conductance level reached is shown in gray. **(B)** Mean time constants and relative areas for the fast and slow components (τ_{fast} and τ_{slow}) of AMPA receptor single-channel open period distributions in 0.06 mM glutamate at +80 mV. The mean time constants (± SEM) were 0.15 ± 0.01 and 1.99 ± 0.31 ms, with areas of 72 ± 3 and 28 ± 3% (n = 5).

CHAPTER 5: CONCLUDING REMARKS

One of the great challenges of ion channel physiology is interpreting the raw data of electrophysiological recordings in terms of specific changes in protein conformation. One example of this was seen in Chapter 3, where the exponential decay of macroscopic currents was interpreted in terms of a simple model of spermine block. The actual mechanism of spermine block is probably much more complicated than the single-site model used in my interpretation, but the electrical signal not contain enough information to draw more specific conclusions. Clearly the charge on D590 is important for the state-dependence of polyamine block, but the complexity of the block process made it difficult to develop a very "neat" model of this state-dependence based on electrophysiological data alone. Single-channel currents provide more detailed information than macroscopic recordings, but are still ambiguous to interpret. As seen in Chapter 4, subunit-independent gating is the best explanation for the multiple open conductance levels of AMPA receptors, but there is still no direct evidence that this is occurring.

In the future, combining electrophysiology with techniques responsive to other modalities will probably reduce some of this ambiguity. For example, patch-clamp recording has been performed simultaneously with optical recordings that report directly on conformational changes of the ion channel protein (e.g., Biskup et al., 2007; Pathak et al., 2007). Although this type of multimodal recording has only been implemented at the macroscopic level, it may eventually be possible (though extremely challenging) at the microscopic level as well. Single-channel recording, once the only technique available for observing conformational changes in single biological macromolecules, is now joined by other techniques such as single-molecule FRET, atomic force microscopy, and optical

tweezers. These new techniques should be viewed as potential complimentary partners for single channel recording, rather than as competitors.

Obviously, the availability of crystal structures also greatly reduces the ambiguity in interpreting ion channel current signals. This is particularly true if structures can be obtained for different functionally distinct conformations of the protein. Although there are no crystal structures for intact glutamate receptor proteins, these structures may become available in the near future. How might the information contained in these structures be applied to the issues addressed in this dissertation? Crystal structures are particularly useful as the basis for computational studies. For example, a high-resolution crystal structure of the AMPA receptor pore could be used in free-energy minimization studies to resolve the various non-covalent interactions between spermine and individual residues that contribute to binding affinity. This would only be a first step, however: spermine block must be understood in the context of its ability to permeate the channel, which requires a more dynamic approach. All-atom molecular dynamics studies on the time scale of spermine permeation are too computationally expensive to perform, but coarse-grained simulations have been used to study ion permeation (Berneche and Roux, 2003), so a similar approach could be applied to spermine. Permeant ions could be included in the simulation to determine their contribution to spermine block.

In Chapter 4, I describe single-channel recordings that suggest extensive interactions between the ligand-binding domains of AMPA receptor subunits. Determining the structural basis of these putative interactions also requires more structural information than is currently available. Crystal structures of isolated glutamate receptor ligand-binding domain dimers are abundantly available (Mayer, 2006), but the

paradigm of the ligand-binding domain dimer as functional unit, encouraged by these structures, is at odds with my results. The steep dependence of the receptor's affinity for glutamate on the number of occupied binding sites suggests strong interactions between all four ligand-binding domains. A structural interpretation of this result awaits crystallization of the intact tetrameric ligand-binding domain, at minimum, and possibly the associated amino-terminal domains and ion-channel linker regions in addition. Also, the intermediate protein conformations involved in the transition from the low- to the high-affinity mode are apparently very short-lived, since they cannot be resolved in single-channel recordings. The experimental investigation of such short-lived conformation is very difficult; indeed, "states" of kinetic models used to interpret electrophysiological data are, by definition, protein conformations long-lived enough to be detectable in electrophysiological recordings. One theoretical method developed specifically to study such short-lived conformations is rate-equilbrium free energy relationship (REFER) analysis (Zhou et al., 2005; Auerbach, 2007); however, application of this method requires detailed microscopic kinetic information for a large number of mutant channels with altered gating properties (Purohit et al., 2007), which would be very difficult to obtain for AMPA receptors. A perhaps better approach that may eventually be possible is dynamic simulations, of intermediate duration and structural resolution, of the entire ligand-binding domain.

In conclusion, the integration of electrophysiological recording with techniques responsive to other modalities, along with computational studies based on crystal structures, will greatly improve our understanding of glutamate receptors and ion channels in general. Hopefully, the many discoveries yet to be made will not only satisfy

our scientific curiosity, but will also improve understanding and treatment of central nervous system disorders that are a source of suffering for so many.

REFERENCES

Abele R, Keinanen K, Madden DR (2000) Agonist-induced isomerization in a glutamate receptor ligand-binding domain. A kinetic and mutagenetic analysis. J Biol Chem 275:21355-21363.

Antonov SM, Johnson JW, Lukomskaya NY, Potapyeva NN, Gmiro VE, Magazanik LG (1995) Novel adamantane derivatives act as blockers of open ligand-gated channels and as anticonvulsants. Mol Pharmacol 47:558-567.

Armstrong N, Gouaux E (2000) Mechanisms for activation and antagonism of an AMPA-sensitive glutamate receptor: crystal structures of the GluR2 ligand binding core. Neuron 28:165-181.

Armstrong N, Sun Y, Chen GQ, Gouaux E (1998) Structure of a glutamate-receptor ligand-binding core in complex with kainate. Nature 395:913-917.

Auerbach A (2007) How to turn the reaction coordinate into time. J Gen Physiol 130:543-546.

Auerbach A, Zhou Y (2005) Gating reaction mechanisms for NMDA receptor channels. J Neurosci 25:7914-7923.

Bahring R, Bowie D, Benveniste M, Mayer ML (1997) Permeation and block of rat GluR6 glutamate receptor channels by internal and external polyamines. J Physiol 502:575-589.

Banke TG, Traynelis SF (2003) Activation of NR1/NR2B NMDA receptors. Nat Neurosci 6:144-152.

Banke TG, Bowie D, Lee H, Huganir RL, Schousboe A, Traynelis SF (2000) Control of GluR1 AMPA receptor function by cAMP-dependent protein kinase. J Neurosci 20:89-102.

Benke TA, Luthi A, Isaac JT, Collingridge GL (1998) Modulation of AMPA receptor unitary conductance by synaptic activity. Nature 393:793-797.

Berneche S, Roux B (2003) A microscopic view of ion conduction through the K+ channel. Proc Natl Acad Sci U S A 100:8644-8648.

Berneche S, Roux B (2005) A gate in the selectivity filter of potassium channels. Structure 13:591-600.

Biskup C, Kusch J, Schulz E, Nache V, Schwede F, Lehmann F, Hagen V, Benndorf K (2007) Relating ligand binding to activation gating in CNGA2 channels. Nature 446:440-443.

Blanpied TA, Boeckman FA, Aizenman E, Johnson JW (1997) Trapping channel block of NMDA-activated responses by amantadine and memantine. J Neurophysiol 77:309-323.

Bowie D, Mayer ML (1995) Inward rectification of both AMPA and kainate subtype glutamate receptors generated by polyamine-mediated ion channel block. Neuron 15:453-462.

Bowie D, Lange GD, Mayer ML (1998) Activity-dependent modulation of glutamate receptors by polyamines. J Neurosci 18:8175-8185.

Burnashev N, Villarroel A, Sakmann B (1996) Dimensions and ion selectivity of recombinant AMPA and kainate receptor channels and their dependence on Q/R site residues. J Physiol 496 (Pt 1):165-173.
Burnashev N, Monyer H, Seeburg PH, Sakmann B (1992) Divalent ion permeability of AMPA receptor channels is dominated by the edited form of a single subunit. Neuron 8:189-198.
Burnashev N, Zhou Z, Neher E, Sakmann B (1995) Fractional calcium currents through recombinant GluR channels of the NMDA, AMPA and kainate receptor subtypes. J Physiol 485 (Pt 2):403-418.
Catterall WA (2000) From ionic currents to molecular mechanisms: the structure and function of voltage-gated sodium channels. Neuron 26:13-25.
Chang HR, Kuo CC (2008) The activation gate and gating mechanism of the NMDA receptor. J Neurosci 28:1546-1556.
Chapman ML, VanDongen AM (2005) K channel subconductance levels result from heteromeric pore conformations. J Gen Physiol 126:87-103.
Citri A, Malenka RC (2008) Synaptic plasticity: multiple forms, functions, and mechanisms. Neuropsychopharmacology 33:18-41.
Clarke RJ, Johnson JW (2008) Voltage-dependent gating of NR1/2B NMDA receptors. J Physiol 586:5727-5741.
Collingridge GL, Olsen RW, Peters J, Spedding M (2009) A nomenclature for ligand-gated ion channels. Neuropharmacology 56:2-5.
Colquhoun D, Hawkes AG (1995a) A Q-matrix cookbook: How to write only one program to calculate the single channel and macroscopic predictions for any kinetic mechanism. In: Single-Channel Recording (Sakmann B, Neher E, eds). New York, NY: Plenum Press.
Colquhoun D, Hawkes AG (1995b) The principals of the stochastic interpretation of ion-channel mechanisms. In: Single-Channel Recording (Sakmann B, Neher E, eds). New York, NY: Plenum Press.
Colquhoun D, Sigworth FJ (1995) Fitting and statistical analysis of single-channel records. In: Single-Channel Recording (Sakmann B, Neher E, eds), pp 483-587. New York, NY: Plenum Press.
Cordero-Morales JF, Cuello LG, Perozo E (2006a) Voltage-dependent gating at the KcsA selectivity filter. Nat Struct Mol Biol 13:319-322.
Cordero-Morales JF, Cuello LG, Zhao Y, Jogini V, Cortes DM, Roux B, Perozo E (2006b) Molecular determinants of gating at the potassium-channel selectivity filter. Nat Struct Mol Biol 13:311-318.
Cu C, Bahring R, Mayer ML (1998) The role of hydrophobic interactions in binding of polyamines to non NMDA receptor ion channels. Neuropharmacology 37:1381-1391.
Derkach V, Barria A, Soderling TR (1999) Ca2+/calmodulin-kinase II enhances channel conductance of alpha-amino-3-hydroxy-5-methyl-4-isoxazolepropionate type glutamate receptors. Proc Natl Acad Sci U S A 96:3269-3274.
Derkach VA, Oh MC, Guire ES, Soderling TR (2007) Regulatory mechanisms of AMPA receptors in synaptic plasticity. Nat Rev Neurosci 8:101-113.

Diamond JS (2005) Deriving the glutamate clearance time course from transporter currents in CA1 hippocampal astrocytes: transmitter uptake gets faster during development. J Neurosci 25:2906-2916.
Dingledine R, Hume RI, Heinemann SF (1992) Structural determinants of barium permeation and rectification in non-NMDA glutamate receptor channels. J Neurosci 12:4080-4087.
Dingledine R, Borges K, Bowie D, Traynelis SF (1999) The glutamate receptor ion channels. Pharmacol Rev 51:7-61.
Doyle DA, Morais Cabral J, Pfuetzner RA, Kuo A, Gulbis JM, Cohen SL, Chait BT, MacKinnon R (1998) The structure of the potassium channel: molecular basis of K^+ conduction and selectivity. Science 280:69-77.
Dutzler R, Campbell EB, MacKinnon R (2003) Gating the selectivity filter in ClC chloride channels. Science 300:108-112.
Ehlers MD, Heine M, Groc L, Lee MC, Choquet D (2007) Diffusional trapping of GluR1 AMPA receptors by input-specific synaptic activity. Neuron 54:447-460.
Erreger K, Chen PE, Wyllie DJ, Traynelis SF (2004) Glutamate receptor gating. Crit Rev Neurobiol 16:187-224.
Foster KA, Crowley JJ, Regehr WG (2005) The influence of multivesicular release and postsynaptic receptor saturation on transmission at granule cell to Purkinje cell synapses. J Neurosci 25:11655-11665.
Furukawa H, Singh SK, Mancusso R, Gouaux E (2005) Subunit arrangement and function in NMDA receptors. Nature 438:185-192.
Gebhardt C, Cull-Candy SG (2006) Influence of agonist concentration on AMPA and kainate channels in CA1 pyramidal cells in rat hippocampal slices. J Physiol 573:371-394.
Green WN, Andersen OS (1991) Surface charges and ion channel function. Annu Rev Physiol 53:341-359.
Hille B, Schwarz W (1978) Potassium channels as multi-ion single-file pores. J Gen Physiol 72:409-442.
Hodgkin AL, Keynes RD (1955) The potassium permeability of a giant nerve fibre. J Physiol 128:61-88.
Howe JR, Cull-Candy SG, Colquhoun D (1991) Currents through single glutamate receptor channels in outside-out patches from rat cerebellar granule cells. J Physiol 432:143-202.
Jin R, Banke TG, Mayer ML, Traynelis SF, Gouaux E (2003) Structural basis for partial agonist action at ionotropic glutamate receptors. Nat Neurosci 6:803-810.
Jin R, Clark S, Weeks AM, Dudman JT, Gouaux E, Partin KM (2005) Mechanism of positive allosteric modulators acting on AMPA receptors. J Neurosci 25:9027-9036.
Jones KS, VanDongen HM, VanDongen AM (2002) The NMDA receptor M3 segment is a conserved transduction element coupling ligand binding to channel opening. J Neurosci 22:2044-2053.

Kamboj SK, Swanson GT, Cull-Candy SG (1995) Intracellular spermine confers rectification on rat calcium-permeable AMPA and kainate receptors. J Physiol 486:297-303.
Kandel ER, Schwartz JH, Jessell TM (2000) Principles of Neural Science. New York, NY: McGraw-Hill.
Koh DS, Burnashev N, Jonas P (1995) Block of native Ca^{2+}-permeable AMPA receptors in rat brain by intracellular polyamines generates double rectification. J Physiol 486:305-312.
Kuner T, Beck C, Sakmann B, Seeburg PH (2001) Channel-lining residues of the AMPA receptor M2 segment: structural environment of the Q/R site and identification of the selectivity filter. J Neurosci 21:4162-4172.
Kussius CL, Popescu GK (2009) Kinetic basis of partial agonism at NMDA receptors. Nat Neurosci 12:1114-1120.
Lamsa KP, Heeroma JH, Somogyi P, Rusakov DA, Kullmann DM (2007) Anti-Hebbian long-term potentiation in the hippocampal feedback inhibitory circuit. Science 315:1262-1266.
Liao D, Hessler NA, Malinow R (1995) Activation of postsynaptically silent synapses during pairing-induced LTP in CA1 region of hippocampal slice. Nature 375:400-404.
Liu SQ, Cull-Candy SG (2000) Synaptic activity at calcium-permeable AMPA receptors induces a switch in receptor subtype. Nature 405:454-458.
Mahanty NK, Sah P (1998) Calcium-permeable AMPA receptors mediate long-term potentiation in interneurons in the amygdala. Nature 394:683-687.
Matulef K, Zagotta WN (2003) Cyclic nucleotide-gated ion channels. Annu Rev Cell Dev Biol 19:23-44.
Mayer ML (2006) Glutamate receptors at atomic resolution. Nature 440:456-462.
Mayer ML, Westbrook GL, Guthrie PB (1984) Voltage-dependent block by Mg2+ of NMDA responses in spinal cord neurones. Nature 309:261-263.
Nowak L, Bregestovski P, Ascher P, Herbet A, Prochiantz A (1984) Magnesium gates glutamate-activated channels in mouse central neurones. Nature 307:462-465.
Nowak LM, Wright JM (1992) Slow voltage-dependent changes in channel open-state probability underlie hysteresis of NMDA responses in Mg(2+)-free solutions. Neuron 8:181-187.
Oswald RE, Ahmed A, Fenwick MK, Loh AP (2007) Structure of glutamate receptors. Curr Drug Targets 8:573-582.
Panchenko VA, Glasser CR, Mayer ML (2001) Structural similarities between glutamate receptor channels and K^+ channels examined by scanning mutagenesis. J Gen Physiol 117:345-360.
Panchenko VA, Glasser CR, Partin KM, Mayer ML (1999) Amino acid substitutions in the pore of rat glutamate receptors at sites influencing block by polyamines. J Physiol 520:337-357.
Partin KM (2001) Domain interactions regulating ampa receptor desensitization. J Neurosci 21:1939-1948.

Partin KM, Fleck MW, Mayer ML (1996) AMPA receptor flip/flop mutants affecting deactivation, desensitization, and modulation by cyclothiazide, aniracetam, and thiocyanate. J Neurosci 16:6634-6647.
Partin KM, Patneau DK, Winters CA, Mayer ML, Buonanno A (1993) Selective modulation of desensitization at AMPA versus kainate receptors by cyclothiazide and concanavalin A. Neuron 11:1069-1082.
Pathak MM, Yarov-Yarovoy V, Agarwal G, Roux B, Barth P, Kohout S, Tombola F, Isacoff EY (2007) Closing in on the resting state of the Shaker K(+) channel. Neuron 56:124-140.
Plant K, Pelkey KA, Bortolotto ZA, Morita D, Terashima A, McBain CJ, Collingridge GL, Isaac JT (2006) Transient incorporation of native GluR2-lacking AMPA receptors during hippocampal long-term potentiation. Nat Neurosci 9:602-604.
Popescu G, Auerbach A (2003) Modal gating of NMDA receptors and the shape of their synaptic response. Nat Neurosci 6:476-483.
Priel A, Kolleker A, Ayalon G, Gillor M, Osten P, Stern-Bach Y (2005) Stargazin reduces desensitization and slows deactivation of the AMPA-type glutamate receptors. J Neurosci 25:2682-2686.
Purohit P, Mitra A, Auerbach A (2007) A stepwise mechanism for acetylcholine receptor channel gating. Nature 446:930-933.
Qian A, Johnson JW (2002) Channel gating of NMDA receptors. Physiol Behav 77:577-582.
Qin F (2004) Restoration of single-channel currents using the segmental k-means method based on hidden Markov modeling. Biophys J 86:1488-1501.
Raman IM, Trussell LO (1995a) The mechanism of alpha-amino-3-hydroxy-5-methyl-4-isoxazolepropionate receptor desensitization after removal of glutamate. Biophys J 68:137-146.
Raman IM, Trussell LO (1995b) Concentration-jump analysis of voltage-dependent conductances activated by glutamate and kainate in neurons of the avian cochlear nucleus. Biophys J 69:1868-1879.
Robert A, Howe JR (2003) How AMPA receptor desensitization depends on receptor occupancy. J Neurosci 23:847-858.
Rosenmund C, Stern-Bach Y, Stevens CF (1998) The tetrameric structure of a glutamate receptor channel. Science 280:1596-1599.
Rozov A, Burnashev N (1999) Polyamine-dependent facilitation of postsynaptic AMPA receptors counteracts paired-pulse depression. Nature 401:594-598.
Rozov A, Zilberter Y, Wollmuth LP, Burnashev N (1998) Facilitation of currents through rat Ca^{2+}-permeable AMPA receptor channels by activity-dependent relief from polyamine block. J Physiol 511:361-377.
Schwenk J, Harmel N, Zolles G, Bildl W, Kulik A, Heimrich B, Chisaka O, Jonas P, Schulte U, Fakler B, Klocker N (2009) Functional proteomics identify cornichon proteins as auxiliary subunits of AMPA receptors. Science 323:1313-1319.

Sheng M, Kim MJ (2002) Postsynaptic signaling and plasticity mechanisms. Science 298:776-780.
Sheng M, Hoogenraad CC (2007) The postsynaptic architecture of excitatory synapses: a more quantitative view. Annu Rev Biochem 76:823-847.
Shin J, Shen F, Huguenard JR (2005) Polyamines modulate AMPA receptor-dependent synaptic responses in immature layer V pyramidal neurons. J Neurophysiol 93:2634-2643.
Smith TC, Howe JR (2000) Concentration-dependent substate behavior of native AMPA receptors. Nat Neurosci 3:992-997.
Smith TC, Wang LY, Howe JR (2000) Heterogeneous conductance levels of native AMPA receptors. J Neurosci 20:2073-2085.
Sobolevsky AI, Koshelev SG, Khodorov BI (1999) Probing of NMDA channels with fast blockers. J Neurosci 19:10611-10626.
Sobolevsky AI, Beck C, Wollmuth LP (2002) Molecular rearrangements of the extracellular vestibule in NMDAR channels during gating. Neuron 33:75-85.
Sobolevsky AI, Yelshansky MV, Wollmuth LP (2003) Different gating mechanisms in glutamate receptor and K^+ channels. J Neurosci 23:7559-7568.
Sommer B, Kohler M, Sprengel R, Seeburg PH (1991) RNA editing in brain controls a determinant of ion flow in glutamate-gated channels. Cell 67:11-19.
Soto D, Coombs ID, Kelly L, Farrant M, Cull-Candy SG (2007) Stargazin attenuates intracellular polyamine block of calcium-permeable AMPA receptors. Nat Neurosci 10:1260-1267.
Stern-Bach Y, Russo S, Neuman M, Rosenmund C (1998) A point mutation in the glutamate binding site blocks desensitization of AMPA receptors. Neuron 21:907-918.
Sun Y, Olson R, Horning M, Armstrong N, Mayer M, Gouaux E (2002) Mechanism of glutamate receptor desensitization. Nature 417:245-253.
Swanson GT, Gereau RWt, Green T, Heinemann SF (1997) Identification of amino acid residues that control functional behavior in GluR5 and GluR6 kainate receptors. Neuron 19:913-926.
Tomita S, Adesnik H, Sekiguchi M, Zhang W, Wada K, Howe JR, Nicoll RA, Bredt DS (2005) Stargazin modulates AMPA receptor gating and trafficking by distinct domains. Nature 435:1052-1058.
Tour O, Parnas H, Parnas I (1998) Depolarization increases the single-channel conductance and the open probability of crayfish glutamate channels. Biophys J 74:1767-1778.
Venkatachalam K, Montell C (2007) TRP channels. Annu Rev Biochem 76:387-417.
Watanabe S, Kusama-Eguchi K, Kobayashi H, Igarashi K (1991) Estimation of polyamine binding to macromolecules and ATP in bovine lymphocytes and rat liver. J Biol Chem 266:20803-20809.

Weston MC, Gertler C, Mayer ML, Rosenmund C (2006) Interdomain interactions in AMPA and kainate receptors regulate affinity for glutamate. J Neurosci 26:7650-7658.
Wollmuth LP, Sobolevsky AI (2004) Structure and gating of the glutamate receptor ion channel. Trends Neurosci 27:321-328.
Wyllie DJ, Traynelis SF, Cull-Candy SG (1993) Evidence for more than one type of non-NMDA receptor in outside-out patches from cerebellar granule cells of the rat. J Physiol 463:193-226.
Yellen G (2002) The voltage-gated potassium channels and their relatives. Nature 419:35-42.
Zhang W, Cho Y, Lolis E, Howe JR (2008) Structural and single-channel results indicate that the rates of ligand binding domain closing and opening directly impact AMPA receptor gating. J Neurosci 28:932-943.
Zhou Y, Pearson JE, Auerbach A (2005) Phi-value analysis of a linear, sequential reaction mechanism: theory and application to ion channel gating. Biophys J 89:3680-3685.
Zucker RS, Regehr WG (2002) Short-term synaptic plasticity. Annu Rev Physiol 64:355-405.